1-1-2005

The effect of retained austenite on the distortion in carburized SAE 8620 steel.

Haitao (Lily) He
University of Windsor

THE EFFECT OF RETAINED AUSTENITE ON THE DISTORTION IN CARBURIZED SAE 8620 STEEL

by

Haitao (Lily) He

A Thesis
Submitted to the Faculty of Graduate Studies and Research
through Engineering Materials
in Partial Fulfillment of the Requirements for the
Degree of Master of Applied Science at the
University of Windsor

Windsor, Ontario, Canada

2005

Your file Votre référence
ISBN: 978-0-494-57630-4
Our file Notre référence
ISBN: 978-0-494-57630-4

ABSTRACT

The effects of retained austenite and other metallurgical parameters on the dimensional stability of carburized SAE 8620 steel have been investigated. The purpose is to find the optimum amount of retained austenite (RA) in SAE 8620 steel that is typically used in the carburized condition for powertrain applications in the automotive industry.

A specially designed specimen, known as a Navy C-ring has been used for this study. The SAE 8620 steel was first normalized prior to machining the Navy C-ring specimens. The C-ring specimens were then heat treated by carburizing at one of two temperatures (6hrs at 1700°F & 4hrs at 1750°F) at four levels of carbon potential (0.9, 1.0, 1.1, 1.2) followed by quenching and tempering at one of two temperatures (300°F & 350°F). For every combination of heat treatment conditions, the distortion of the C-ring was evaluated by dimensional measurements of the ID, OD and gap width. XRD techniques were used to determine both the residual stress and the retained austenite. The retained austenite value for the as-carburized samples was also evaluated using an optical metallographic technique. Hardness profiles from the surface to the core were determined for the as-carburized samples using microhardness measurements. The carbon contents at the surface were measured using optical emission spectroscopy (OES).

The amount of retained austenite and the residual stress increase with increasing carburizing temperature and carbon potential. The amount of retained austenite and the residual stress decrease with increasing tempering temperature. However, there is not a

large change when the tempering temperature is increased from 300°F to350°F. Distortion is influenced both by the amount of retained austenite and the magnitude of the residual stress. With increasing retained austenite / residual stress, the distortion becomes more serious. Based on the distortion data (OD, ID & Flatness) for the quenched and tempered specimens, the optimum amount of retained austenite was about 25%.

TO MY FATHER

ACKNOWLEDGEMENTS

First I would like to acknowledge Dr. D. O. Northwood for his supervision, encouragement and patience. I would also like to acknowledge Dr. Xichen Sun for his technical suggestions and support particularly with respect to access to experimental facilities. The laboratory help of Mr. J. W. Robinson is also much appreciated.

Secondly I would like to thank all staff and students of the Engineering Materials Group for their support and friendship during my studies.

Finally I would like to express my sincere thanks to my mother, my husband, Xu Wang, and my son, Chee-Chee, for their selfless love and support.

TABLE OF CONTENTS

LIST OF TABLES

APPENDIX

LIST OF FIGURES

Chapter 2

Chapter 3

Chapter 4

CHAPTER 5

CHAPTER 6

APPENDIX

CHAPTER 1 INTRODUCTION

Distortion issues where components exhibit geometric changes during heat treatment have been key issues leading to quality problems. In the automotive industry there is a need to improve gear precision for reduction of gear noise levels. In the bearing industry, efforts are being made to decrease the distortion in order to shorten the finish-grinding times [1]. Furthermore, distortion has a large influence on the production costs. In Europe, these distortion-related costs have been quantified as being around 4% of total sales for the industry producing power engineering components (e.g. gears & rolling bearings). If this figure were applied to the world-wide production of bearings, the cost would be more than 1 billion USD per year [2].

Therefore, distortion issues are becoming increasingly important in today's automotive industry. An understanding of the preventive measures necessary to control distortion will allow for greater dimensional accuracy and precision, while reducing tolerance limits, which will then lead to a reduction in contact noise levels for components such as gears, and a considerable reduction in manufacturing costs.

The effects of retained austenite and other metallurgical parameters on the distortion of carburized SAE 8620 steel have been investigated. The purpose is to find the optimum amount of retained austenite (RA) in SAE 8620 steel that is typically used in the carburized condition for powertrain applications in the automotive industry.

A specially designed specimen, known as a Navy C-ring has been used for this study. The SAE 8620 steel was first normalized prior to machining the Navy C-ring specimens. The C-ring specimens were then heat treated by carburizing at one of two

temperatures (6 hours at 1700°F & 4 hours at 1750°F) at four levels of carbon potential (0.9, 1.0, 1.1, 1.2) followed by quenching and tempering at one of two temperatures (300°F & 350°F) for 1 hour.

For every combination of heat treatment conditions, the distortion of the C-ring specimen was evaluated by dimensional measurements of the OD (outside diameter), gap width, flatness, thickness, ID (inside diameter), roundness and cylindricity using a PRISMO coordinate measuring machine (CMM). XRD techniques were used to determine both the residual stress and the retained austenite. The retained austenite value for the as-carburized samples was also evaluated using an optical metallographic technique. In the current study, the amount of retained austenite varied from 4.0% to 43.5% and was associated with different heat treatment schedules. Hardness profiles (from the surface to the core) were determined for the as-carburized samples. Micro-hardness testing system was used to obtain microhardness values which were converted to Rockwell C Hardness (HRC) values in all cases. The carbon contents at the surface were measured using optical emission spectroscopy (OES) in selected specimens.

The relationships between the distortion, retained austenite and residual stress are complex. Higher levels of retained austenite generally lead to higher levels of residual stress but these higher levels of residual stress do not necessarily lead to a lower level of distortion in the as-carburized condition.

CHAPTER 2 LITERATURE REVIEW

This literature review covers all aspects of the thesis topic: the effect of retained austenite on the distortion in carburized SAE 8620 steel. First some basic definitions, principles and measurement techniques are introduced relating to carburized SAE 8620 steel, retained austenite, residual stress and distortion in heat treatment. Data are then presented on the profiles for retained austenite, residual stress and hardness for steels in the carburized condition. Finally the relationships between these three parameters and their influence on distortion are reviewed in detail.

2.1 Carburized SAE 8620 Steel

In general, the carburizing process is conducted on those low-carbon steels that rely on a surface layer, or case, of high hardness to provide a level of strength and wear resistance not obtainable from the core metal. The initial carbon content in most steels used for carburizing is the range of 0.10 to 0.30% [3]. In the automotive industry, carburized SAE 8620 steel is typically used for differential ring gears, camshafts and transmission gears for its excellent carburizing response with good hardenability for most section sizes [3, 4].

2.1.1 Carburizing

Carburizing is a case-hardening process in which carbon is diffused into the surface layers of a steel part at a temperature below its melting point and above its A_3 critical temperature (Figure 2.1) [5], at which austenite, with its high solubility for carbon,

is the stable crystal structure. In Figure 2.1, the A_1 critical temperature is the temperature (1340°F / 727°C) at which the first phase change occurs on heating. At the A_3 temperature, the last of the proeutectoid ferrite has been absorbed into the austenite. At the Acm temperature all of the proeutectoid cementite has been dissolved and austenite of the same carbon content as the steel is formed [6]. Hardening is accomplished when the high-carbon surface layer is quenched to form martensite. The resulting gradient in carbon content from surface to core causes a gradient in hardness, producing a high-carbon martensitic case on the material, usually a low-carbon steel with good wear and fatigue resistance, superimposed on a tough, low-carbon steel core [7, 8]. In gas carburizing, the source of carbon is a carbon-rich furnace atmosphere produced either from gaseous hydrocarbons, for example, methane (CH_4), propane (C_3H_3), and butane (C_4H_{10}), or from vaporized hydrocarbon liquids [7, 8]. Steels for case hardening usually have base-carbon contents of about 0.2% [3, 7]. Compositions of some typical case-hardening steels are given in Table 2.1 [3].

In general, two different terms are used to specify case depth for carburized parts. One is known as "case depth to 0.40% C", which means the distance from the surface at which a 0.40% C content is obtained. The other is called "effective case depth to Rockwell C 50", which means the distance from the surface providing a minimum hardness reading of Rockwell C 50 [9].

Harris [9] has developed a formula for the effects of time and temperature on case depth for normal carburizing:

$$\text{Case depth } D = \frac{31.6\sqrt{t}}{10^{(6700/T)}} \qquad \textbf{Eq. 2.1 [9]}$$

where case depth is in inches; t is the time at temperature in hours; and T is the absolute temperature in degrees Rankine (°F + 460).

For a specific carburizing temperature, the relationship becomes simply:

$$\text{Case depth} = K\sqrt{t} \qquad \textbf{Eq. 2.2 [9]}$$

$$= 0.025\sqrt{t} \quad \text{for } 1700\,°F / 927\,°C$$

$$= 0.021\sqrt{t} \quad \text{for } 1650\,°F / 899\,°C$$

$$= 0.018\sqrt{t} \quad \text{for } 1600\,°F / 871\,°C$$

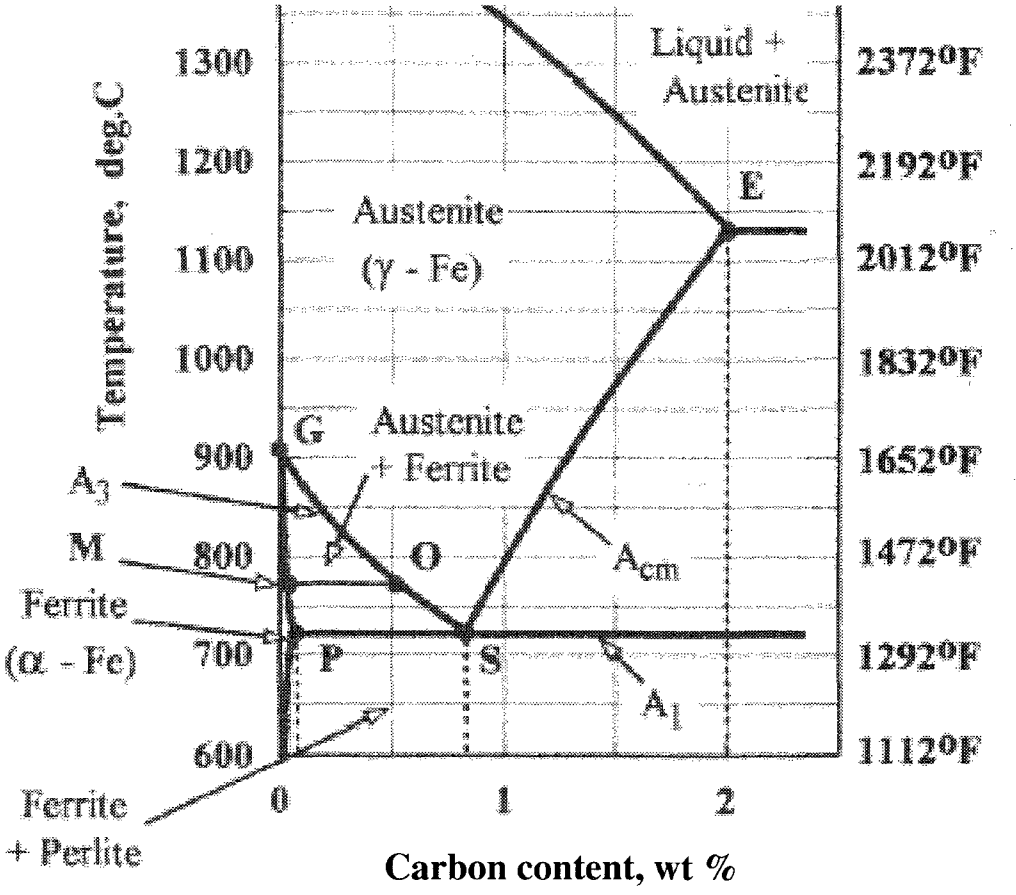

Fig. 2.1 The lower left-hand part of the iron-iron carbide equilibrium diagram showing the A_1, A_3 and Acm temperatures [5].

Table 2.1 Compositions of case-hardening steels [3]

Steel	Composition, %							
	C	Mn	P	S	Si	Ni	Cr	Mo
Carbon steels								
1010	0.08–0.13	0.30–0.60	0.040 max	0.050 max	...	...	...	...
1012 mod	0.10–0.15	0.30–0.60	0.040 max	0.050 max	...	0.30	0.30	...
1018	0.15–0.20	0.60–0.90	0.040 max	0.050 max	...	...	...	...
1020	0.17–0.23	0.30–0.60	0.040 max	0.050 max	...	...	...	...
1039	0.37–0.44	0.70–1.00	0.040 max	0.050 max	...	...	...	...
Resulfurized steels								
1113	0.13 max	0.70–1.00	0.07–0.12	0.24–0.33	...	...	...	...
1117	0.14–0.20	1.00–1.30	0.040 max	0.08–0.13	...	...	...	...
Alloy steels								
3310	0.08–0.13	0.45–0.60	0.025 max	0.025 max	0.20–0.35	3.25–3.75	1.40–1.75	...
4118	0.18–0.23	0.70–0.90	0.035 max	0.040 max	0.20–0.35	...	0.40–0.60	0.08–0.15
4140	0.38–0.43	0.75–1.00	0.035 max	0.040 max	0.20–0.35	...	0.80–1.10	0.15–0.25
4320	0.17–0.22	0.45–0.65	0.035 max	0.040 max	0.20–0.35	1.65–2.00	0.40–0.60	0.20–0.30
4620	0.17–0.22	0.45–0.65	0.035 max	0.040 max	0.20–0.35	1.65–2.00	...	0.20–0.30
8617	0.15–0.20	0.70–0.90	0.035 max	0.040 max	0.20–0.35	0.40–0.70	0.40–0.60	0.15–0.25
8620	0.18–0.23	0.70–0.90	0.035 max	0.040 max	0.20–0.35	0.40–0.70	0.40–0.60	0.15–0.25
8720	0.18–0.23	0.70–0.90	0.035 max	0.040 max	0.20–0.35	0.40–0.70	0.40–0.60	0.20–0.30
8822	0.20–0.25	0.75–1.00	0.035 max	0.040 max	0.20–0.35	0.40–0.70	0.40–0.60	0.30–0.40
9310	0.08–0.13	0.45–0.65	0.025 max	0.025 max	0.20–0.35	3.00–3.50	1.00–1.40	0.08–0.15
AMS 6470(a)	0.38–0.43	0.50–0.70	0.040 max	0.040 max	0.20–0.40	...	1.40–1.80	0.30–0.40
Nitralloy 125(b)	0.20–0.30	0.40–0.70	...	...	0.20–0.40	...	0.90–1.40	0.15–0.25
Nitralloy 1.35(b)	0.30–0.40	0.40–0.70	...	...	0.20–0.40	...	0.90–1.40	0.15–0.25
Nitralloy N(b)	0.20–0.27	0.40–0.70	...	...	0.20–0.40	3.25–3.75	1.00–1.50	0.20–0.30
Tool steel								
H13(c)	0.35	...	...	...	...	...	5.0	1.50
Maraging steel								
18% Ni (300 CVM)(d)	0.03 max	0.10 max	0.010 max	0.010 max	0.10 max	18.5	...	4.8

(a) AMS 6470 also contains 0.90 to 1.35% Al. (b) These steels also contain 0.85 to 1.20% Al. (c) H13 steel also contains 1.0% V. (d) This steel also contains 0.10% Al, 0.60% Ti, 9.0% Co, 0.003% B, 0.02% Zr, and 0.05% Ca.

2.1.2 Properties & Applications

From Table 2.1 we can see SAE 8620 steel is a hardenable low alloy steel which is usually used for carburizing to develop a case-hardened part [10]. In the automotive industry, carburized SAE 8620 steel is typically used for differential ring gears, camshafts

and transmission gears which are usually moderate section sizes, requiring medium hardenability, strength and shock resistance [4].

Selection of the hardening treatment is mainly dependent upon the properties required in both the case and core [4]. For a SAE 8620 steel, the approximate critical temperatures are as follows; A_1 (Figure 2.1): 1350°F / 732°C and A_3 (Figure 2.1):1525°F 829°C [10]. Usually, most carburizing treatments take place above the A_3 temperature (Figure 2.1) where both absorption and diffusion are quite rapid and grain growth is not too severe. In practice, SAE 8620 steel is generally heated at 1700°F / 927°C in the carburizing process [7]. Sometimes, for certain deep-case requirements, the carburizing temperature can be raised to 1750°F / 954°C, or even 1800°F / 982°C. After carburizing, SAE 8620 steels are usually quenched directly from the carburizing temperature [9].

2.2 Retained Austenite

High carbon and carburized low carbon steels such as carburized SAE 8620 steel always contain retained austenite to varying degrees in the as-hardened and also in the tempered microstructures [11].

2.2.1 Origin of retained austenite

In hardenable steels, austenite is stable at temperatures above the A_3 and Acm (Figure 2.1) phase boundaries, but is unstable below these temperatures. On quenching from the austenite-stable area, austenite transforms to martensite which usually forms at a characteristic temperature named M_s and continues to form with decreasing temperature until M_f, the temperature of 100% transformation is reached. However, in many hardenable steels such as plain carbon and low alloy steels with carbon contents more

than 0.5%, the M_f temperature is below room temperature, so that a considerable quantity of untransformed austenite may be retained at room temperature in these steels [12-22].

From the isothermal transformation diagram (I-T diagram) of SAE 8620 (Figure 2.2), we can see the Ms (750°F/400°C), M_{50} (700°F /370°C) and M_{90} (670°F/350°C) temperatures for SAE 8620 steel [23]. These particular percentages of martensite (50 in M_{50} & 90 in M_{90}) have no special meaning and are used only to convey some idea of the progress of transformation of austenite to martensite as cooling continues below Ms. Because measurement becomes increasingly less reliable with greater percentages of martensite, the temperature for 90% martensite is often chosen rather than that for some higher percentage. Although the Ms (750°F/400°C), M_{50} (700°F /370°C) and M_{90} (670°F/350°C) temperatures are well above room temperature, the steel may retain an appreciable percentage of austenite after carburizing [11, 22]. The precise amount is dependent upon several complex factors (see section 2.2.2).

Quenching is usually followed by tempering, which will generally reduce the amount of retained austenite (RA) [21, 24-28]. Tempering reduces the amount of RA in steels by promoting the following changes in the as-quenched microstructure: (1) From 180°F / 82°C to 400°F / 204°C, the supersaturated carbon in α iron will be partially relieved and precipitated throughout the martensite with a loss of tetragonality: RA remains unchanged; (2) From 400°F / 204°C to 550°F / 288°C, RA transforms to bainite. The complete transformation is not accomplished unless the steel is held at the tempering temperature for sufficient time. The transformation of the austenite increases the hardness of the steel; (3) From 550°F / 288°C to 750°F /399°C, the very fine carbide particles congregate and form larger carbide particles. As a result, there is a pronounced softening of the steel which accompanies this change [7].

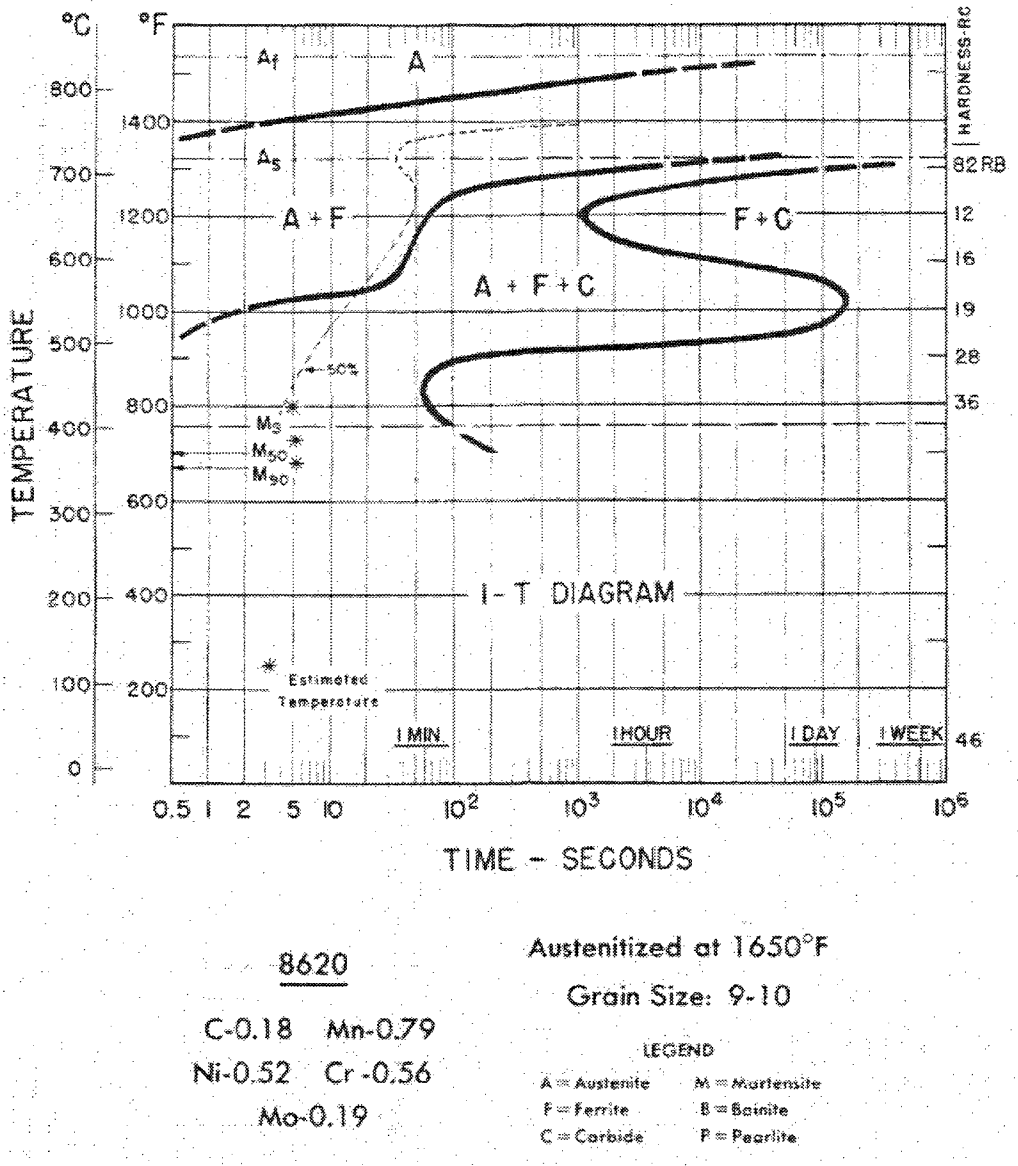

Fig. 2.2 Isothermal diagram of SAE 8620 steel [23]

2.2.2 Range of retained austenite

The quantity of retained austenite depends on the austenitizing temperature, chemical composition, especially the carbon content, cooling rate and final temperature of the quenching process [21].

High carbon and carburized low carbon steels such as used for bearings, gears, and cold work tool steels always contain retained austenite in varying degrees in the as-hardened and the tempered microstructures. Retained austenite exists in the as-hardened microstructures of all plain carbon and alloyed steels containing more than about 0.5% C [11, 21].

As to the presence of retained austenite, Grosch and Schwarz [22] point out that the case-microstructure of carburized steels always consists of plate martensite and retained austenite for case-carbon contents higher than 0.6%. The amount of retained austenite is mainly determined by the carbon content: for steels of the same carbon content, the effect of the content of the other alloying elements is also noticeable [22].

The martensite finish temperature, M_f, of plain carbon and low alloy steels with carbon contents more than about 0.5%, is below room temperature. That is why austenite that contains more than 0.5% carbon in solid solution does not completely transform into martensite when quenched to room temperature [22].

2.2.3 Retained Austenite Profile and Hardness Profile in Carburized Condition

Grosch and Schwarz [22] examined the retained austenite profiles of three carburized steels with different nickel contents (15CrNi6, 14NiCr14, 14NiCr18) in the as-quenched condition and the results are shown in Figure 2.3. Using an enriching gas with nitrogen and methyl alcohol with propane, ground cylindrical specimens, 10mm long and

25mm diameter, were first control carburized to a case carbon content of 0.85%, and were then direct quenched into oil at 60°C. Half of the quenched specimens were tempered for 1 hour at 180 °C in a muffle furnace. The final case-depth was between 0.95 and 1.1mm. From Figure 2.3, we can see that the highest values of retained austenite are present at a distance of 0.05-0.1mm from the surface. In the area beyond the carburizing depth, there was no measurable amount of retained austenite. Tempering (180 °C/1h) was found to have only a small effect on the retained austenite profiles. The effect of tempering on the maximum amount of retained austenite is shown in Figure 2.4 [22].

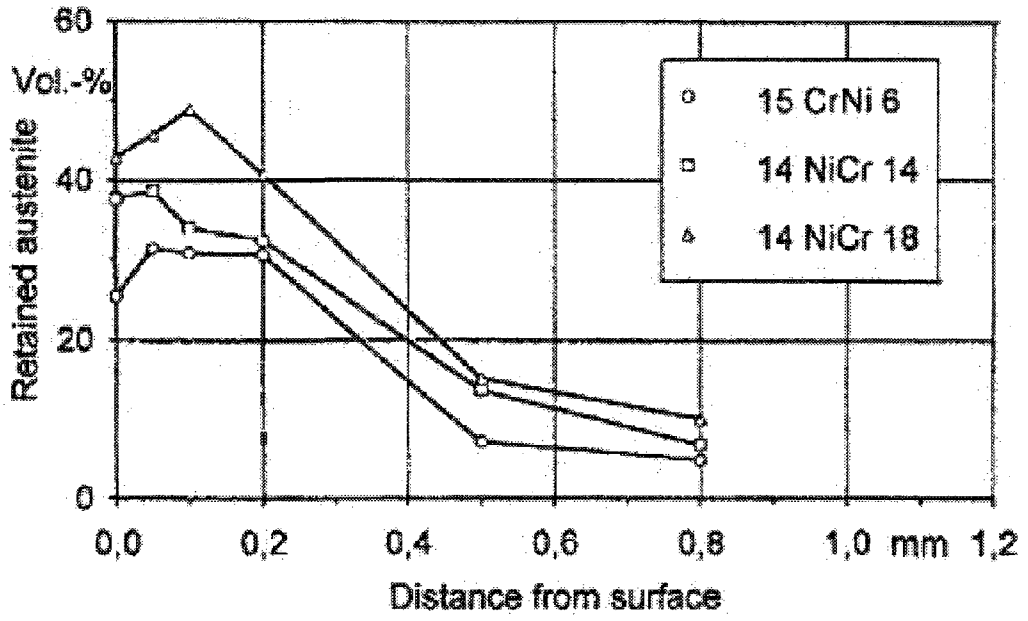

Fig. 2.3 Retained austenite profiles in Cr-Ni steels, as-quenched into oil at 60°C [22]

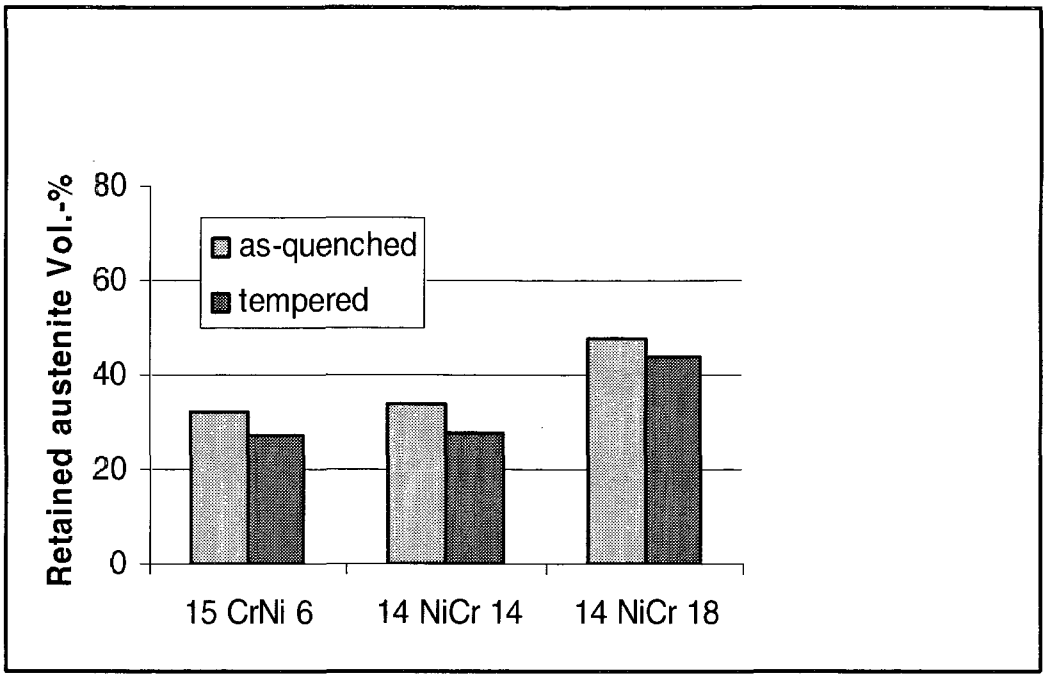

Fig. 2.4 Maximum amount of retained austenite in as-quenched and quenched-and-tempered Cr-Ni steels [22]

As well as amount of retained austenite, the hardness profiles were determined by Grosch and Schwarz [22]. The hardness profiles of the as-quenched microstructure are determined by the amount of both the harder martensitic, and the softer austenitic, phases. Typical hardness profiles obtained by Grosch and Schwarz are shown in Figure 2.5; HV1 means Vickers hardness using 1Kg force load. The first hardness indentation could only be placed at a distance of about 50 μm from the surface, i.e. in the area of the highest amount of retained austenite. This leads to the lower hardness values found in this area. With increasing distance from the surface, both the amount of the retained austenite and the carbon content become smaller, which explains the observed hardness maximum at a distance of about 0.4 mm (15CrNi6) to 0.5 mm (14NiCr14 and 14NiCr18) from the surface. For distances greater than about 0.8 mm from the surface, the amount of retained

austenite is very small, and the hardness profiles of the different steels become almost superimposed [22].

As shown in Figure 2.6 [9], for same steel, the hardness is higher at quenching condition than any of tempering condition. The hardness of a carburized case decrease as the tempering temperature increases. The hardness profiles for the four steels are similar: the peak hardness happens at the surface or a small distance from surface. After the peak hardness, hardness becomes smaller with the increase of distance from surface. The data in Figure 2.6 are from specimens carburized and quenched directly from 1700°F / 927°C. For the convenience of hardness comparisons of different steels or same steel at different distance from surface, Rockwell C hardness values shown were converted from Rockwell A for the surface hardness measurements and from Vickers for hardness traverses taken at the midlength of the sectioned specimen 3 in. long. Each plotted point is the average of two specimens.

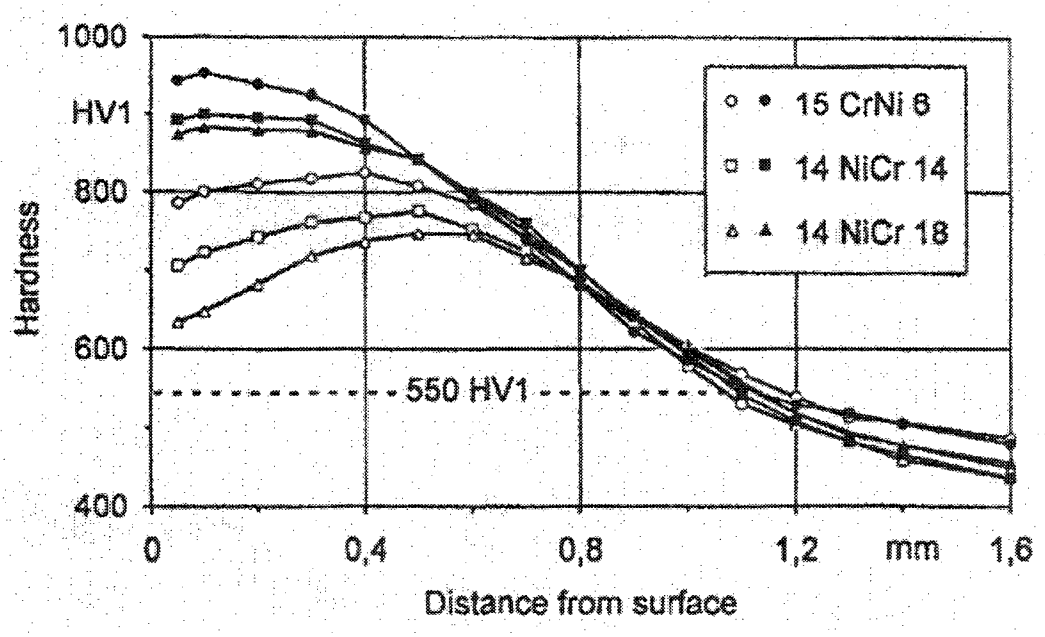

Fig. 2.5 Hardness profiles of as-quenched Cr-Ni steels. Open symbols: as-quenched into oil at 60°C. Full symbols: deep cooled [22]

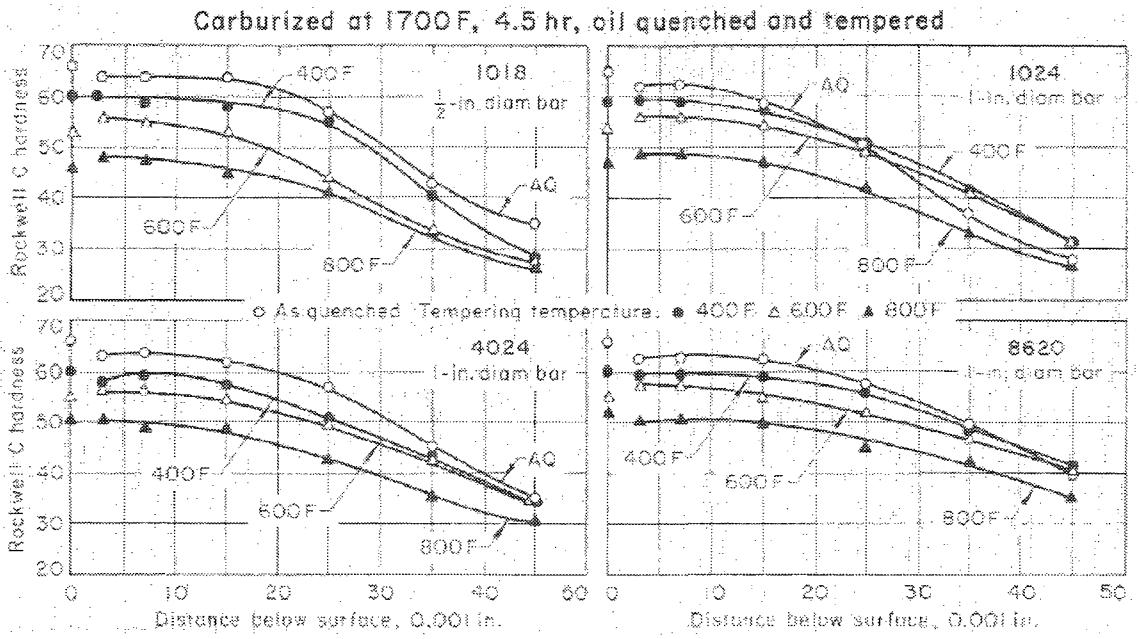

Fig. 2.6 Effect of tempering on hardness in carburized cases [9]

Spice and Matlock [29] conducted similar work to Grosch & Schwarz [22] on retained austenite profiles. They used an SAE 8620 steel in their study. A commercial carburizing process was used. Samples were carburized at 893°C (1640°F) for 380 minutes with a carbon potential of 1.27 at the beginning and 1.14 during the soak. The samples were then oil quenched to 121°C (250°F) and then tempered at 149°C (300°F) for 1 hour. The retained austenite profiles are shown in Figure 2.7. It can be readily seen that the retained austenite content is lower at the surface than at depths up to 0.25 mm from the surface [29].

Lee and Ho [30] also examined the profile of retained austenite in carburized SAE 8620 steel. It was shown that the amount of retained austenite increased as the thickness of the hardened layer increased.

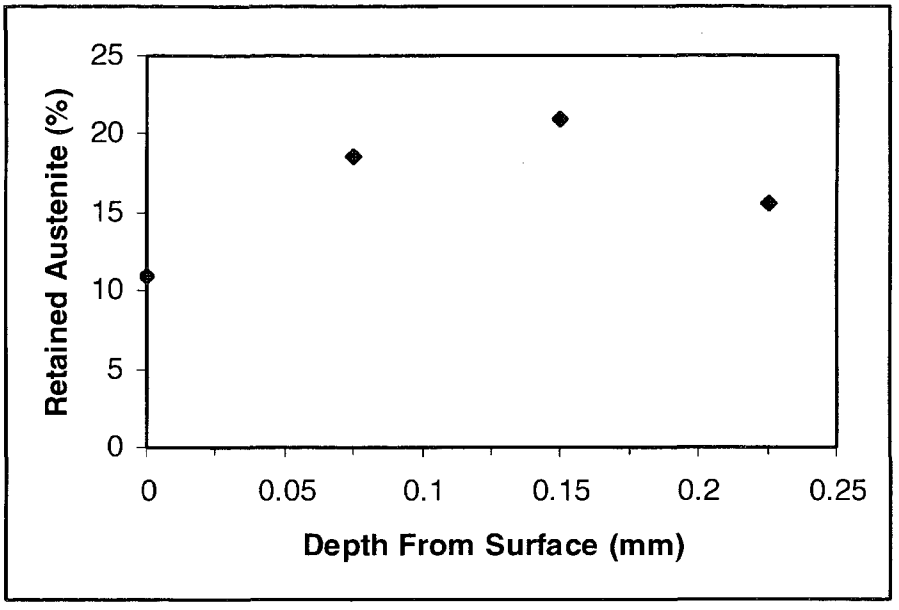

Fig 2.7 Retained austenite profiles of carburized SAE 8620 steel specimens [29].

2.2.4 Techniques for Measurement of Retained Austenite

Many different techniques having been successfully applied to the measurement of the amount of retained austenite in martensitic and ferritic microstructures.

If the austenite content is high (more than 15%), quantitative optical microscopy is generally considered to be a reliable and satisfactory method [31-36]. However, if the retained austenite content is below about 15%, optical microscopy becomes unsatisfactory in many steels due to etching and resolution difficulties [11], although instances of measurements as low as 2 percent have been reported [11].

Currently, an x-ray diffraction technique is considered to be the most accurate retained-austenite-measurement method. It is independent of external calibration and is reliable in measuring low austenite contents ($\geq$2%). In practice, accurate results can be obtained quickly using either recorded traces of the diffraction pattern or electronic scan-counting of peak intensities obtained from the specimen [11].

Other important techniques that have been used in the past for retained austenite measurement have included electrical resistivity [31, 37, 38], magnetic permeability [32, 39], and thermal analysis [33]. However, all of these techniques were predominantly used for the measurement of the austenite present during transformation than that retained in the final microstructure. In conjunction with a calibration using x-ray or optical methods, several of these techniques can provide reliable measurements of the amount of retained austenite, but they are usually too cumbersome to use [11]. Figures 2.8 & 2.9 show a comparison of retained austenite measurements made by metallographic point counting, magnetic susceptibility measurements and an x-ray diffraction method [40]. It can be readily seen that there are differences in the measurements made using these three methods.

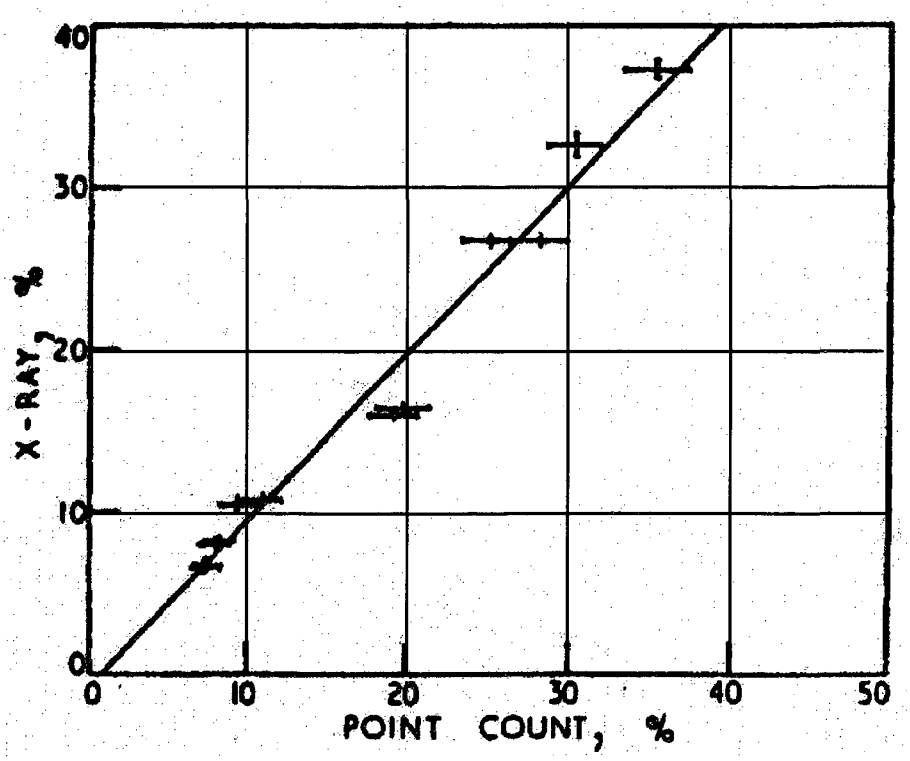

Fig. 2.8 Comparison of retained austenite measurements made by metallographic point counting and x-ray method [40]

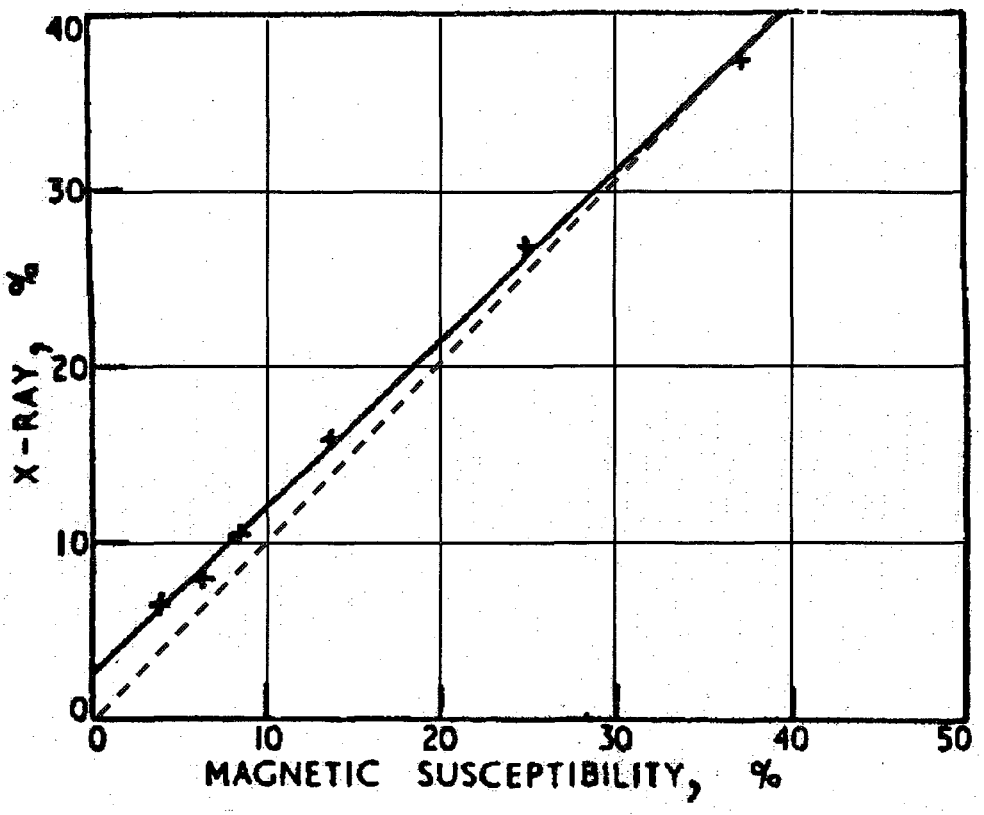

Fig. 2.9 Comparison of retained austenite measurements made by magnetic susceptibility and x-ray method [40]

(1) Principles of retained austenite measurement by x-ray diffraction

The irradiation of x-rays on a crystalline substance produces a characteristic diffraction pattern which is determined by the crystal structure of all phases existing within that substance [35, 39, 41-50]. Peaks of varying height correspond to diffraction of the x-ray energy from various (hkl) planes in the crystal structure of each phase. Peaks are observed in the diffraction pattern at discete 2θ angles. The specific 2θ locations of the peaks are determined by the "d" spacings of the planes and the wavelength of the x-ray radiation used. Cr, Mo and Cu x-radiation are generally employed in x-ray measurements of retained austenite. More diffraction (hkl) peaks can be seen with the shorter wavelength Cu and Mo radiations than with the longer wavelength Cr radiation. This can

be predicted from Braggs' Law, Equation 2.3, which detains the relationship between the x-ray wavelength (λ), the interplanar spacing (d) and the diffraction angle (θ) [11].

$$n\lambda = 2d\sin\theta \qquad \textbf{Eq. 2.3 [11]}$$

The relative volume fractions of martensite and austenite can be quantitatively determined from x-ray diffraction charts because the x-ray intensity diffracted from each phase is proportional to the volume fraction of that phase. Furthermore if x-rays cannot pass through the sample due to its infinite thickness and the phase contains a completely random arrangement of crystals, the diffracted intensity from any single (hkl) plane within that phase is also proportional to the volume fraction of that phase. Thus in random specimens, diffracted intensity measurements can be conducted on only one austenite (A) and one martensite (M) diffraction peak (hkl) to accurately establish the volume fraction of each phase. However, if preferred orientation (P.O.) exists within the specimen, intensity measurements may have to be made on a number of austenite and martensite peaks so as to obtain an accurate result by averaging [51].

(2) Typical x-ray procedure for measurement of retained austenite

In practice the procedure for measuring retained austenite by x-ray diffraction generally involves the following six steps (1) selection of the radiation, (2) running of the diffraction pattern, (3) selection of the optimum M and A peaks for comparison of the diffracted intensities, (4) actual measurement of the diffracted intensities under each selected peak, (5) a comparison of two austenite line or peak intensities to obtain the degree of preferred orientation (P.O.) or texture if present in the specimen, and (6) employment of the proper equations to convert the measured intensity values to volume fractions of austenite [11].

For specimens with random or low P. O. (1.2-1.8), the following two equations, Equations 2.4 and 2.5, can be used to convert the measured intensity values to volume fractions of austenite. I_A^{hkl}, I_M^{hkl} and I_C^{hkl} are integrated intensities measured for a single preselected austenite, martensite and carbide line respectively. The factors R_A^{hkl}, R_M^{hkl} and R_C^{hkl} are theoretical intensity values for the same (hkl) planes. V_C is the carbide volume measured or estimated optically.

$$\text{Volume Fraction} = \text{VA} = \frac{I_A^{hkl}/R_A^{hkl}}{I_A^{hkl}/R_A^{hkl} + I_M^{hkl}/R_M^{hkl} + I_C^{hkl}/R_C^{hkl}} \qquad \textbf{Eq. 2.4 [11]}$$

$$\text{Volume Fraction} = \text{VA} = \frac{1 - V_C}{1 + (R_A^{hkl}/R_M^{hkl})(I_M^{hkl}/I_A^{hkl})} \qquad \textbf{Eq. 2.5 [11]}$$

Equations 2.4 and 2.5 above may be successfully used to measure retained austenite in hardened and in tempered steels because in either of these conditions the majority of steels do not show any appreciable amount of preferred orientation. Therefore, accurate results may be obtained easily from intensity measurements of only one austenite and one martensite reflection [11].

2.3 Residual Stress

2.3.1 Origin of residual stress

The residual stress may be defined as the self-equilibrating internal or locked-in stress remaining within a body with no applied (external) force, external constraint, or temperature gradient [52-54]. These residual stresses must be balanced near the surface or

in the body of a material, i.e., negative (compressive) in one region and positive (tensile) in another [52]. Residual stresses may be generated by variations in stress, temperature, and chemical species within the body [52]. In heat-treated materials, residual stresses may be generated by a variation in temperature (thermal gradient) alone or a combination with a change in chemical species [52].

When a steel part is quenched from the austenitizing temperature to room temperature, residual stresses are produced due to a combination of a thermal gradient and a phase transformation-induced volume expansion: austenite transforms to martensite or other products [55]. Table 2.2 shows the changes in volume during transformation of austenite into different phases [56, 57].

Table 2.2 Changes in volume during the phase transformations of austenite into different phases (Source: Ref 57)

Transformation	Change in volume, %, as a function of carbon content (wt % C)
Spheroidized pearlite → austenite	-4.64 + 2.21 x (% C)
Austenite → Martensite	4.64 – 0.53 x (% C)
Austenite → lower bainite	4.64 – 1.43 x (% C)
Austenite → upper bainite	4.64 – 2.21 x (% C)

The stress generated by a thermal gradient alone during cooling can be calculated using Equation 2.6:

$$\sigma_{th} = E \cdot \Delta T \cdot \alpha \qquad \textbf{Eq. 2.6 [52]}$$

where σ_{th} is the thermal stress, E is the modulus of elastidity, and α is the thermal coefficient of expansion of the material [52].

As for the stress induced from the volume change, there is no general equation that can be used.

2.3.2 Residual stress pattern of carburized and quenched steel

After carburizing and quenching, the microstructure of the core first transforms to ferrite and pearlite at a high temperature (1100°F / 593°C to 1300°F / 704°C) with an accompanying stress relaxation. Later, the microstructure of the case transforms to martensite at a lower temperature (less than 570°F / 299°C) with an accompanying volume expansion but no stress relaxation. Therefore, a residual compressive stress is generated in the case and the stress at the surface is a maximum [52].

However, in actual practice, the maximum compressive stress happens at some distance away from the surface (Figure 2.10 & 2.11) due to the presence of the soft retained austenite at the surface [52, 58]. The peak compressive stress takes place at 50 to 60% of the total case depth corresponding to about the 0.5 to 0.6% carbon level which produces both a low retained austenite content and a martensite hardness around the maximum [59]. The position of the peak for the compressive stress depends on the quenching parameters, the case depth, the steel hardenability [60, 61]. The compressive stress converts into a tensile stress at a position which is at, or near, the case-core interface [52].

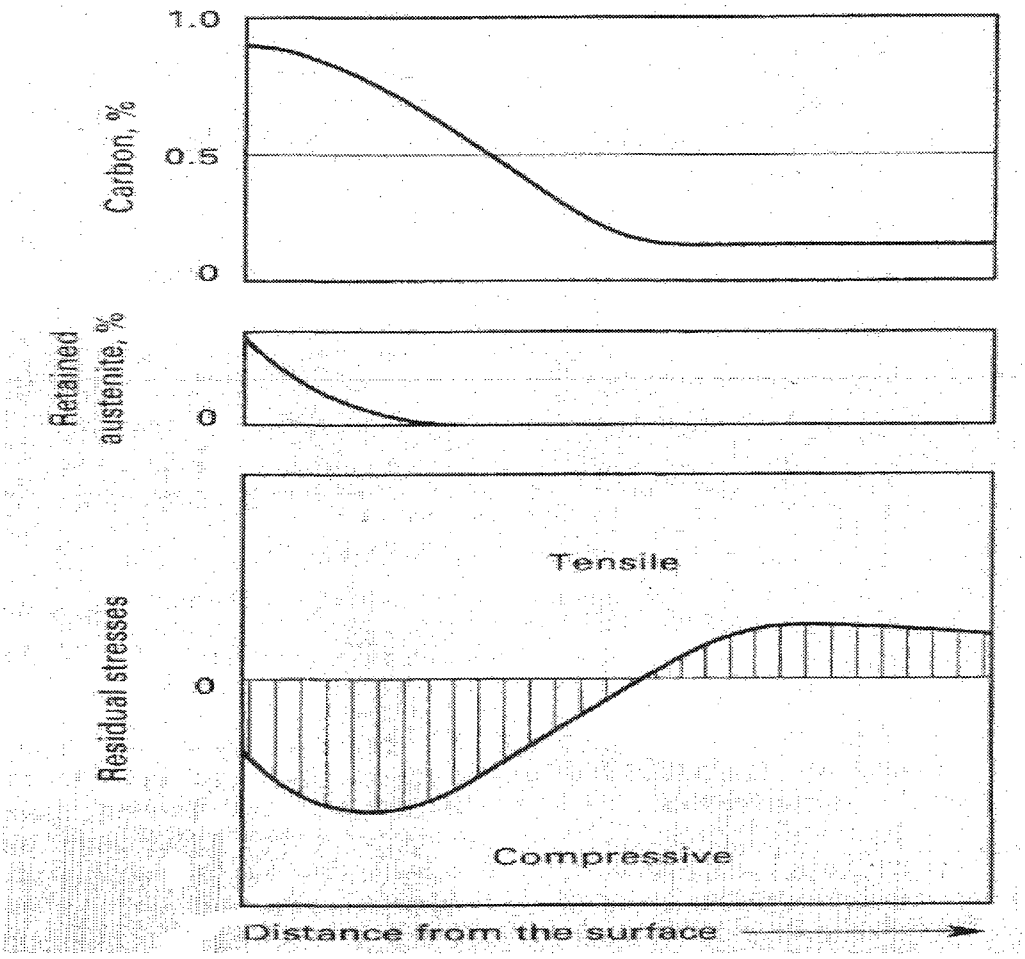

Fig. 2.10 Relationship between carbon content, retained austenite, and residual stress pattern. It shows the development of peak compressive stress some distance away from the surface [52]

Spice and Matlock [29] measured the residual stress profiles in specimens made of SAE 8620 steel and the results are shown in Figure 2.12. In general, the surface layer shows a compressive residual tangential stress. With increasing of distance from surface, the compressive residual tangential stress increased to a maximum at a depth that corresponded approximately to the 0.50% carbon level. The compressive stress changed to a tensile stress in the uncarburized core [62].

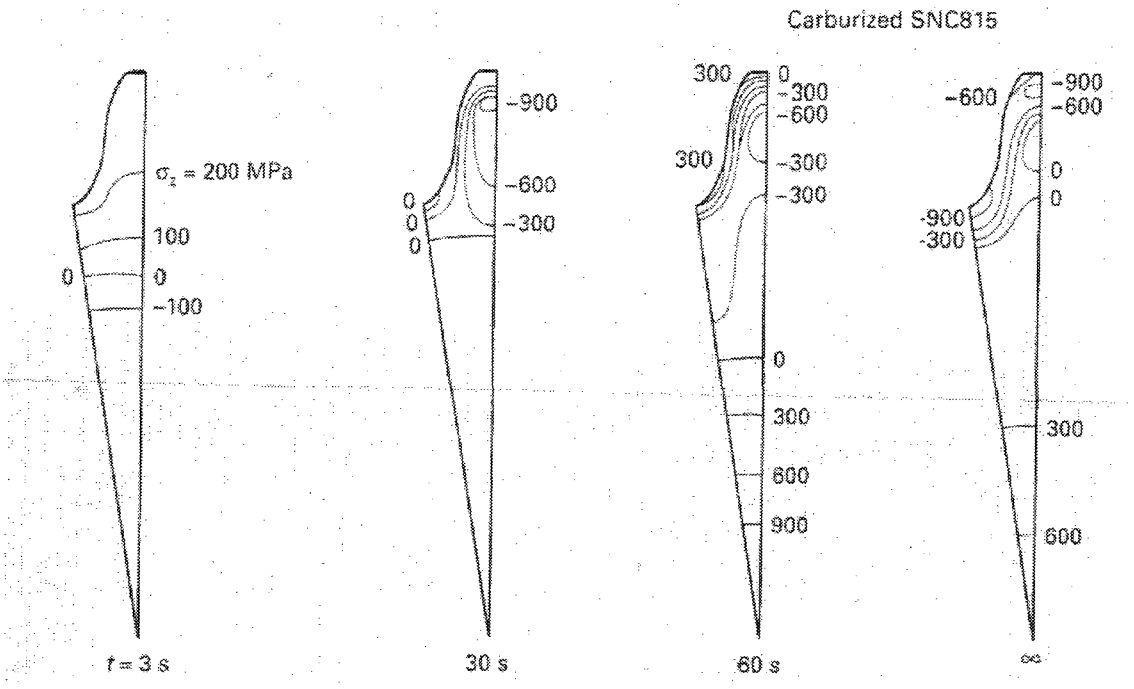

Fig. 2.11 Axial stress distribution (given in Mpa) in carburized gear during quenching [52].

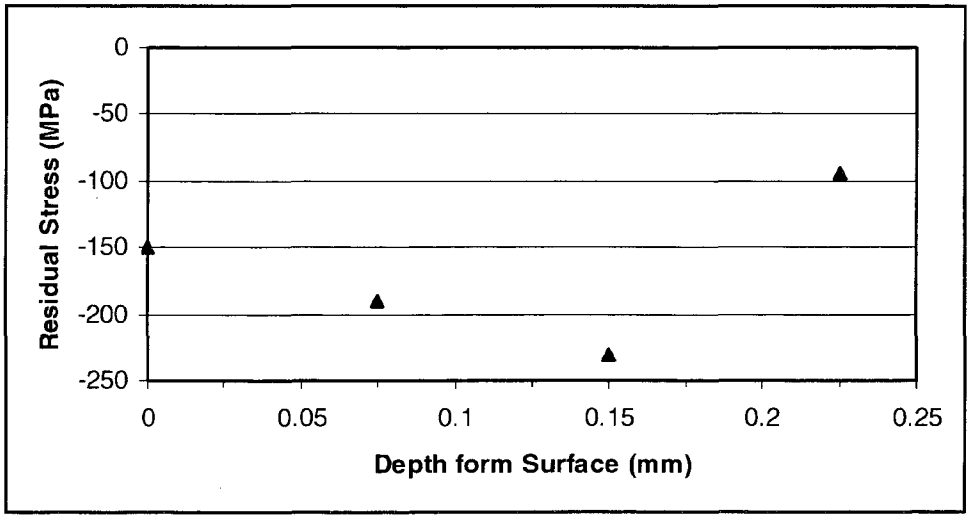

Fig. 2.12. Residual stress profiles in carburized SAE 8620 steel [29].

2.3.3 Residual stress measurement by x-ray diffraction

Residual stress, like all other forms of stress, is determined by strain measurement. If a mechanical method is employed, strain is measured by electrical resistance strain gages, or by measuring changes in the geometry of the specimen. In the x-ray diffraction (XRD) method, the strain is determined by measuring the change of separation (d-spacing) between planes of atoms in the grains of the material [63, 64].

The most commonly used technique in XRD is to measure two strain vectors at different angles to the surface (Fig. 2.13b and c), and then calculate a third vector lying in the surface (Fig. 2.13a). In practice, the specimen is measured normally, and then titled away from this position, about the diffractometer axis. Then the d-spacing measurement is conducted in some grains at $\psi = 0$ (Fig. 2.13b), and then the spacing of the same type of planes, but in other grains, at $\psi \neq 0$, eg 45° (Fig. 2.13c).

If a change of d-spacing exists, the magnitude of the residual elastic strain (ε) can be calculated from Equation 2.7 [64].

$$\varepsilon = \frac{d_i - d_0}{d_0} = \frac{\Delta d}{d} \qquad \textbf{Eq. 2.7}$$

These elastic strains are usually converted to stresses using isotropic elastic theory, Equation 2.8 [64]. where σ is the residual stress, E is Young's Modulus and ν is Ratio.

$$\varepsilon = \frac{\sigma}{E}(1+\nu)\sin^2\psi \qquad \textbf{Eq. 2.8}$$

Equation 2.9 comes from Equation 2.7 and 2.8.

$$\frac{\Delta d}{d} = \sigma \frac{(1+\nu)}{E} \sin^2 \psi \qquad \textbf{Eq. 2.9}$$

Thus a plot of $\Delta d/d$ vs. $\sin^2 \psi$ will be a straight line with a slope $\sigma(1+\nu)/E$

Alternatively, because

$$\frac{\Delta d}{d} = -\cot\theta \Delta\theta = \frac{2\Delta\theta}{2\tan\theta} \qquad \textbf{Eq. 2.10}$$

by differentiating Equation 2.10, Equation 2.11 is obtained. Where, $2\Delta\theta$ is the angular difference in Bragg angle.

$$2\Delta\theta = [2\sigma \frac{1+\nu}{E} \tan\theta] \sin^2 \psi \qquad \textbf{Eq. 2.11}$$

and a plot of 2θ vs. $\sin^2 \psi$ will be a straight line with a slope $[2\sigma(1+\nu)\tan\theta / E]$, where θ is in radians. Provided that E and ν are known, the stress can then be calculated [64].

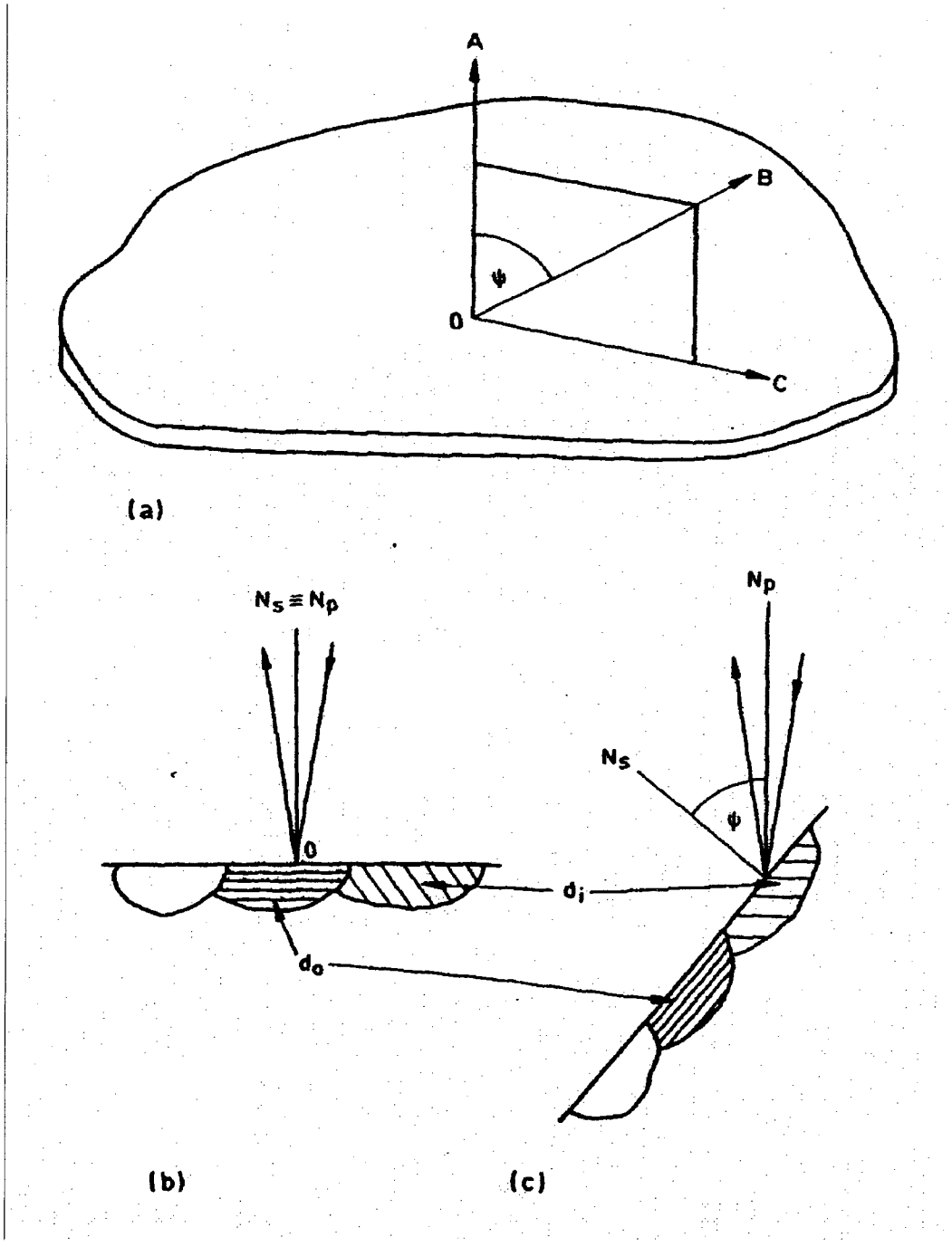

Fig. 2.13 (a) Direction of strain vectors in relation to specimen surface. A and B are two strain vectors at different angles to the surface, and C is the third vector lying in the surface; (b) and (c) orientation of specimen relative to the x-ray beam for measuring d_0(b) and d_i(c). (Ns=normal to specimen surface; Np=normal to reflecting planes) [64].

2.4 Distortion in Heat Treatment

Distortion is mostly attributed to the heat treatment. Generally, both size (volume) and shape distortion occur during a heat-treatment process cycle. In practice, the shape distortion in either water- or oil-hardening steels is usually more significant than the size distortion and is more noticeable due to its unpredictability [65].

2.4.1 Types of Distortion

Distortion can be defined as an irreversible, and usually unpredictable, dimensional change in the component during processing from heat treatment and from temperature variations and loading in service. The term dimensional change is used to denote changes in both size and shape [66].

Reversible changes are produced by applying a stress in the elastic range, or by temperature variations which neither induce stresses above the elastic limit, nor cause changes in the metallurgical structure. Irreversible changes are generated by stresses in excess of the elastic limit or by changes in the metallurgical structure (for example, phase transformations). These dimensional changes sometimes can be corrected by heat treatment such as tempering, annealing or cold treatment.

During heat - treatment operations, distortion can be classified into two types: size distortion and shape distortion. Size distortion is the net change in volume after heat treatment which is produced by a phase transformation. Shape distortion or warpage is a change in geometrical form and is revealed by changes such as curving, bending, twisting, and / or nonsymmetrical dimensional change without any volume change [67, 68]. Generally, both types of distortion occur during a heat-treatment process cycle. In

practice, shape distortion in water- or oil-hardening steels is usually more significant than size distortion and is more noticeable due to its unpredictability.

2.4.2 Distortion Caused by Changes in Metallurgical Structure

There are many factors which influence distortion. Of these factors, the ones resulting from transformation during heating and cooling generate internal stresses / strains which can lead to localized deformation and general part distortion [69-71].

(1) Austenitizing

Austenitizing is the process of forming austenite by heating a ferrous alloy above the transformation range. In this process, thermal expansion occurs continuously until the temperature A_{C1} is reached, where the steel contracts with the transformation of body-centered cubic (bcc) ferrite to face-centered cubic (fcc) austenite. The volume of contraction is related to the increased carbon content in the steel (Table 2.2) [52].

(2) Hardening

When cooled from the austenitizing temperature, steels experience a transformation-induced expansion which depends on two factors: carbon content in the austenite and the phases to which austenite transforms. The magnitude of the expansion increases with a decrease in the carbon content in the austenite. The volume increase is a maximum if the austenite transforms to martensite, intermediate with lower bainite, and is minimum with upper bainite and pearlite (Table 2.2). During quenching, the steel contracts up to the Ms temperature, then expands during martensitic transformation. Finally, thermal contraction occurs with further cooling to room temperature [52].

During such transformations at stresses lower than the yield stress for the phases present, plastic deformation (distortion) occurs [72]. The quenching operation (hardening) has a much greater influence on distortion than the heating process (austenitizing) (Table 2.2).

(3) Tempering

The martensite formed in the quenching operation is exceedingly brittle, highly stressed and dimensionally unstable [7]. Consequently, cracking and distortion are likely to occur after quenching. Therefore, quenching is usually followed by tempering to relieve stresses and allow the arrested reaction of cementite precipitation. Tempering reduces the volume of martensite but not sufficiently to completely equalize the prior volume increase during the quenching process [52].

2.4.3 Factors That Influence Distortion of Carburized Parts

There are many factors which influence the distortion of a carburized component. In general, they may be put into two categories: heat treat process-related variables (pretreatment, load arrangement, process selection and technique, quench considerations, and equipment design) and component-related variables (material chemistry, hardenability, part geometry, design considerations, and steel quality) [69, 71, 73, 74].

Of these factors, the ones resulting from transformation during heating and cooling generate internal stresses / strains which can lead to localized deformation and general part distortion [69-71].

Part geometry, steel production methods, and steel quality are important as well. The geometry of a part has a great influence on the post heat treatment distortion results. Steel production methods and steel quality also play a significant role [69]. Grain size has

some effect on the dimensional change of a part. During quenching, the volume increase of a fine-grained shallow-hardening steel is less than a coarse-grained deep-hardening steel of the same composition [52].

2.4.4 Control of Distortion of Carburized parts

The following are some methods to minimize and /or control the amount and type of distortion and to make the dimensional and the metallurgical changes predictable [69].

(1) Normalizing Prior to Machining & Carburizing

Normalizing is performed by heating a material above the upper critical temperature and then typically air cooling outside the furnace to relieve the residual stresses and to aid dimensional stability. In a normalized material, the areas of the microstructure that contain about 0.8 percent carbon are pearlitic, while the areas of low carbon are ferritic. After normalizing, the steel becomes very machinable and relieves any residual stresses present from the steel making and forging processes that could cause later distortion during carburizing [69].

Normalizing is a first step in the heat treatment process to present a homogenous microstructure to the carburizing process. To reduce overall part distortion, it is highly undesirable to normalize parts such as gears during the carburizing cycle because ferritic areas do not transform to the same hardness and stress levels as the pearlitic areas in this condition, which will result in serious distortion.

A prior normalizing cycle removes the problems associated with pearlite and ferrite segregation and results in much less distortion. For gears, normalizing is usually conducted by holding the material "at temperature" for two hours minimum, or one hour

per inch of section thickness. The temperature used in normalizing should be the same or higher than the carburizing temperature that is used later [69].

(2) Quenching

The quenching process plays a key role in control of distortion [69, 74, 75]. After carburizing, components can be directly quenched, or be slow cooled, reheated, and then quenched, to cause hardening to occur accompanied by a volume expansion (4.64% minus 0.53 times the percentage of carbon). In general, the method of direct quenching yields somewhat less distortion due to fewer phase changes taking place in the part [69, 74].

Quenching severity also has a large influence on distortion: i.e. faster cooling rate will cause greater danger of distortion [52]. To control distortion, milder quenching such as oil quenching, polymer quenching and martempering are used instead of water quenching. Milder quenchants generate slower and more uniform cooling in the parts, which greatly decreases the potential distortion. Martempering is an interrupted quench from the austenitizing temperature of steels. Through delaying the cooling just above the martensitic transformation temperature for a period of time, the temperature of the piece equilibrates. Thus, martempering has the function of minimizing the distortion, cracking and residual stress [76]

Oil quenching has been used for a long time for its unique ability to cool a part, and to be readily controlled. It is popular for its excellent performance results and stability over a broad range of operating conditions. In general, oil quenching is used when the hardenability of the steel is high enough to achieve the desired mechanical and metallurgical properties [69].

2.5 The Effect of Residual Stress on Distortion

It is well known that residual stresses are always accompanied by the changes in the shape and the size of parts, which greatly increases the tendency towards distortion. Another major effect of the residual stress is with respect to the resistance to crack initiation: a residual compressive stress is beneficial but a residual tensile stress is harmful [52].

Stress relieving is performed to avoid distortion in heat treatment and to avoid cracking caused by the combination of residual stress and the thermal stress.

Quenching is usually followed by tempering which is generally considered effective in relieving stresses induced by quenching in addition to lowering hardness to within a specified range, or meeting certain mechanical property requirements. Table 2.3 shows a summary of the maximum residual stresses in surface-treated steels [40]. From Table 2.3, we can see that tempering can significantly reduce the residual stress level. Usually, tempering is done by holding at a relatively low temperature (about 300°F / 149°C) to retain 50 to 60% of the residual stress in the quenched condition. A higher tempering temperature (~1110°F / 600°C) is sometimes applied to mechanically deformed parts (such as hot-rolled bars) or components with tensile surface residual stresses.

Table 2.3 A Summary of the Maximum Residual Stresses in Surface Heat-Treated Steels [40]

Steel	Heat treatment	Residual stress (longitudinal)	
		Mpa	ksi
832M13	Carburized at 970 °C (1780 °F) to 1 mm (0.04 in.) case with 0.8% surface carbon		
	Direct-quenched	280	40.5
	Direct-quenched, -80 °C (-110 °F) subzero treatment	340	49
	Direct-quenched, -90 °C (-130 °F) subzero treatment, tempered	200	29
805A20	Carburized and quenched	240-340(a)	35.0-49.0
805A20	Carburized to 1.1-1.5 mm (0.043-0.06 in.) case at 920 °C (1690 °F), direct oil quench, no temper	190-230	27.5-33.5
805A17		400	58
805A17	Carburized to 1.1-1.5 mm (0.043-0.06 in.) case at 920 °C (1690 °F), direct oil quench,tempered 150 °C (300 °F)	150-200	22-29
897M39	Nitrided to case depth of about 0.5 mm (0.02 in.)	400-600	58.0-87.0
905M39 Cold-rolled steel		800-1000	116.0-145.0
	Induction hardened, untempered	1000	145
	Induction hardened, tempered 200 °C (390 °F)	650	94
	Induction hardened, tempered 300 °C (570 °F)	350	51
	Induction hardened, tempered 400 °C (750 °F)	170	24.5

(a) Immediately sub-surface, that is, 0.05 mm (0.002 in.). Source: Ref 40

2.6 The Effect of Retained Austenite on Distortion and other Properties

The influence of retained austenite can be positive or negative depending on which aspect / property is of concern.

Some of the most significant positive effects are:

1. It improves the contact fatigue life in carburized or uncarburized high carbon gears and bearings [8, 24, 77-87].
2. It improves the bending fatigue resistance of the same steels [88]. However, there is a maximum R.A. content above which the bending fatigue resistance decreases (e.g. for SAE 8620 steel, the maximum R. A. content is about 50%) [89].
3. It improves impact fatigue strength of carburized steels (e.g. Fe-0.18C-2Ni-0.78Mo-0.33Mn-0.08Cr-0.04Si; Fe-0.2C-2.08Ni-0.82Mo-0.47Mn-0.03Si; Fe-0.18C-1.03Mo-0.67Cr-0.37Mn-0.22Ni-0.032Nb-0.03Si; Fe-0.21C-1.01Mo-0.63Cr-0.46Mn-0.03Si, and JIS SCM420, SCr420, and SNCM420) [88, 90].
4. It improves ductility and fracture toughness at high strength levels in standard high strength steels [91-93].
5. It improves the corrosion resistance of tool steels [94].

The important negative effects of retained austenite in hardened microstructures are:

1. It may cause an unwanted dimensional increase in finished gears, bearings and tools and gages during service if such items are subjected to temperatures at which the retained austenite can transform isothermally [14-20, 24, 95-97].
2. It increases the susceptibility to burning and heat checking in grinding operations [20].

2.6.1 The Effect of Retained Austenite on Dimensional Stability

As discussed, retained austenite can have a negative effect on dimensional stability [14-20, 24, 95-97]. The transformation of austenite is always associated with an increase in volume that is unacceptable for precision components. Grosch & Schwarz [22] have suggested that where accurate dimensions are required, the microstructure of carburized components should therefore contain as little retained austenite as possible [22]. Grosch and Schwarz also point out that microstructures with a high hardness and a low amount of retained austenite resulting in a high stability with respect to dimensional changes, can be produced by deep cooling even with high carbon and alloying contents [22]. In their tests, some carburized specimens were deep cooled in liguid nitrogen for 30 minutes directly after quenching and stored at -40°C. McCarthy [98] found that the amount of retained austenite had a very significant effect on dimensional stability. Reitz and Pendray [99] in their research on cryoprocessing, which is the process of cooling a material to extremely low temperatures, found that it generated enhanced mechanical and physical properties. Their research showed that the improvements which occured in the dimensional stability and the hardness were due to a reduction in the amount of retained austenite [99]. Grinberg, Arkhangel'skij and Tikhonova [100] showed that the presence of 30% retained austenite in the structure was the main reason for the dimensional instability of 25Kh17N2B-Sh steel parts after a finish heat treatment. Transformation of this retained austenite in the process of service, or long-time storage, can lead to considerable dimensional changes [100]; Vetters and Schissler [101] studied the effect of the amount of retained austenite on the machining parameters of austempered spheroidal cast-iron. They showed that under the influence of temperature and any externally applied loads, the unstable retained austenite with a lower carbon content transforms into martensite. Within

the retained austenite, tensile stresses were generated, which leads to local distortion [101].

The papers cited above [22, 98-101] focus on the relationship between retained austenite and dimensional stability; less retained austenite generally leads to better dimensional stability. An increase in the stability of the retained austenite with respect to the martensite transformation results in a smaller distortion in service. Therefore, the amount of the retained austenite should be minimized in these precision parts, especially if they are liable to be subjected to temperatures at which the retained austenite can transform isothermally to other phases.

For some parts, however, the main concern is the relationship between the amount of retained austenite and the distortion immediately after heat treatment (quenching and tempering) instead of in later service. Fujio and Yamada have pointed out that the distortion of gears caused by through-hardening is related not only to the hardenability of the steel but also to the presence of retained austenite [102]. Prokhorov, Shabalina and Drizhkov found that the deformation of welded strips of ST3 steel is controlled both by the retained austenite transformation-induced expansion and the ageing of the ferrite [103]. According to Fujio and Yamada [102] and Prokhorov et al [103], retained austenite has a harmful effect on distortion or dimensional stability right after heat treatment, but there is little detailed data given in either paper.

2.7 Summary of Relationships between Heat Treatment Processing Parameters, Retained Austenite, Residual Stresses and Distortion

In the carburizing process, heat treatment parameters have a significant influence on retained austenite, residual stresses and distortion [21, 55, 69, 71, 73, 74]. Austenite induced-transformations generate internal stresses / strains induced by volumetric

changes and lead to localized deformation and general part distortion [69-71]. Therefore, retained austenite can have a negative effect on dimensional stability [14-20, 24, 95-97]. The relationships between heat treatment processing parameters, retained austenite, residual stress and distortion can be summarized as follows:

1. The quantity of retained austenite is determined by the carburizing temperature, chemical composition, especially the carbon content, cooling rate and final temperature of quenching process [21]. Tempering generally reduces the amount of retained austenite by promoting austenitic transformations [7].
2. Residual stresses are produced due to a combination of a thermal gradient and a phase transformation-induced volume expansion: austenite transforms to martensite or other products [55].
3. There are many factors which influence the distortion of a carburized component. In general, they may be put into two categories: heat treatment process-related variables (pretreatment, load arrangement, process selection and technique, quench considerations, and equipment design) and component-related variables (material chemistry, hardenability, part geometry, design considerations, and steel quality) [69, 71, 73, 74].
4. Residual stresses are always accompanied by the changes in the shape and the size of parts, which greatly increases the tendency towards distortion [52]. Tempering is effective in relieving stresses induced by quenching [52].
5. As discussed in 2.6.1, there is no detailed data on the relationship between retained austenite and distortion right after carburizing. Therefore, the effect of retained austenite on the distortion immediately after quenching or quenching and tempering is still, to some extent, unknown.

CHAPTER 3 EXPERIMENTAL DETAILS

In this study, the effects of retained austenite and other metallurgical parameters on distortion of carburized SAE8620 steel have been investigated through an experimental program. The purpose is to find the optimum amount of retained austenite (RA) to minimize distortion in a SAE 8620 steel that is typically used in the carburized condition for powertrain applications in the automotive industry.

3.1 Material

SAE 8620 steel was used in this study. This is a hardenable chromium, molybdenum, nickel low alloy steel often used for carburizing to develop a case-hardened part. This case-hardening will result in good wear characteristics. In the carburized condition this alloy is used for differential ring gears, camshafts and transmission gears in automotive industry.

The steel was received in the form of a hot-rolled bar. The composition of the as-received SAE 8620 steel used in the current study is given in Table 3.1.

3.2 Pre-Heat Treatment, Carburizing and General Overview of Processing

The as-received material was first normalized at 1750°F (954°C) for 4 hours, and then air cooled outside the furnace to minimize any induced stress present and to aid dimensional stability [69]. Figure 3.1 shows the microstructures of the SAE 8620 hot rolled bar both before and after normalizing: before normalizing, needle-like ferrite and pearlite with a somewhat non-uniform distribution of the phases. after normalizing, ferrite

and fine pearlite distributed uniformly. This homogeneous ferrite and pearlite microstructure after normalizing can help improve machinability and eliminate growth in parts during subsequent hardening, thus minimizing any finish grinding that may be required [69]. The normalized steel was then machined into Navy C-ring specimens, the dimensions of which are given in Figure 3.2. Four different measurements, the outer diameter, inner diameter, thickness, and the gap width were used to gauge the amount of distortion. Additional measurements of flatness, cylindricity and roundness were also made and were incorporated into the criteria for the relative distortion of the Navy C-ring test specimens. The distortion associated with the heat treatment is measured by the change in dimensions of these seven parameters after heat-treating and quenching.

The C-ring specimens were then heat treated by carburizing at one of two temperatures (6hrs at 1700°F / 927 °C & 4hrs at 1750°F / 954 °C) at four levels of carbon potential (0.9, 1.0, 1.1, 1.2) followed by oil quenching or oil quenching and tempering at one of two temperatures (300°F / 149 °C & 350°F / 177 °C). For the convenience of this study, the heat treatment processes have been classified into 7 cycles, namely: (1) carburizing at 1700°F / 927 °C for 6 hours at 0.9% carbon potential (C1); (2) carburizing at 1700°F / 927 °C for 6 hours at 1.0% carbon potential (C2); (3) carburizing at 1700°F / 927 °C for 6 hours at 1.1% carbon potential (C3); (4) carburizing at 1750°F / 954 °C for 4 hours at 0.9% carbon potential (C4); (5) carburizing at 1750°F / 954 °C for 4 hours at 1.0% carbon potential (C5); (6) carburizing at 1750°F / 954 °C for 4 hours at 1.1% carbon potential (C6); (7) carburizing at 1750°F / 954 °C for 4 hours at 1.2% carbon potential (C7). In each cycle, three samples were quenched and tempered at one of the two temperatures (300°F / 149 °C & 350°F / 177 °C). The heat treatment schedules are given in Table 3.2.

All the carburizing treatments were performed in a 75 KW sealed quench furnace (Figure 3.3). An endothermic atmosphere was employed in this carburizing furnace. Carburizing was done using a propane-enriched gas under carbon potentials varying from 0.9 to 1.2%. The carbon potential was monitored and controlled using an oxygen probe during the gas carburizing. Each carburizing schedule included two stages, namely a boost stage and a diffusion stage. In the boost stage, the specimens on the loading rack were exposed to propane-enriched gas. Then, in the diffusion stage, the carburizing chamber was exposed to nitrogen gas to allow the diffusion to occur. The boost and diffusion cycle was repeated during each carburizing period.

For the oil quenching, the temperature of the oil was maintained at 156°F / 70°C while the cell pressure above the oil bath was maintained at 700 millibars. The duration of the oil quench was 15 minutes for all specimens.

Table 3.1 Chemical composition of as-received SAE 8620 steel

Composition	Weight Percent (%)
C	0.200
Cr	0.500
Mn	0.820
Mo	0.200
Ni	0.460
P	0.008
Si	0.200
S	0.200
Cu	0.200
Al	0.270

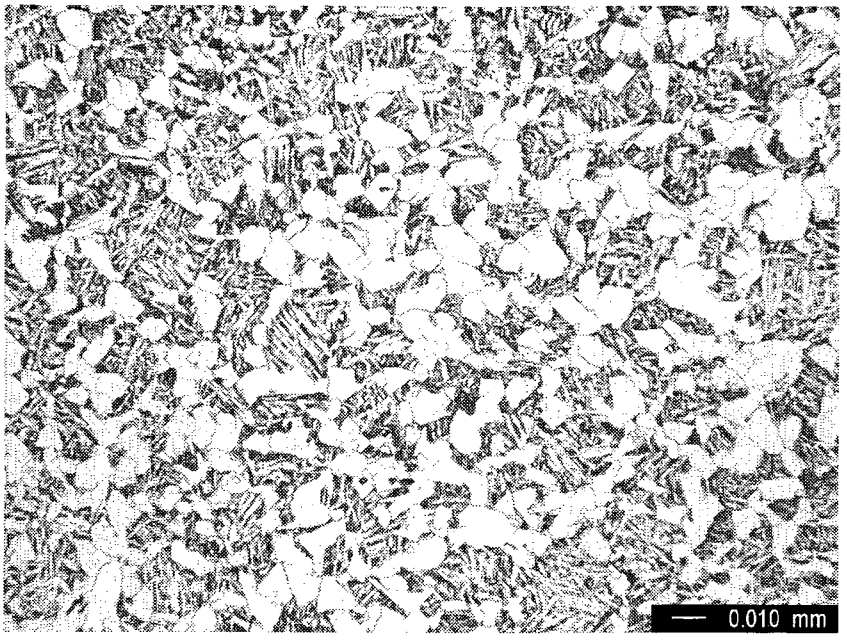

(a)

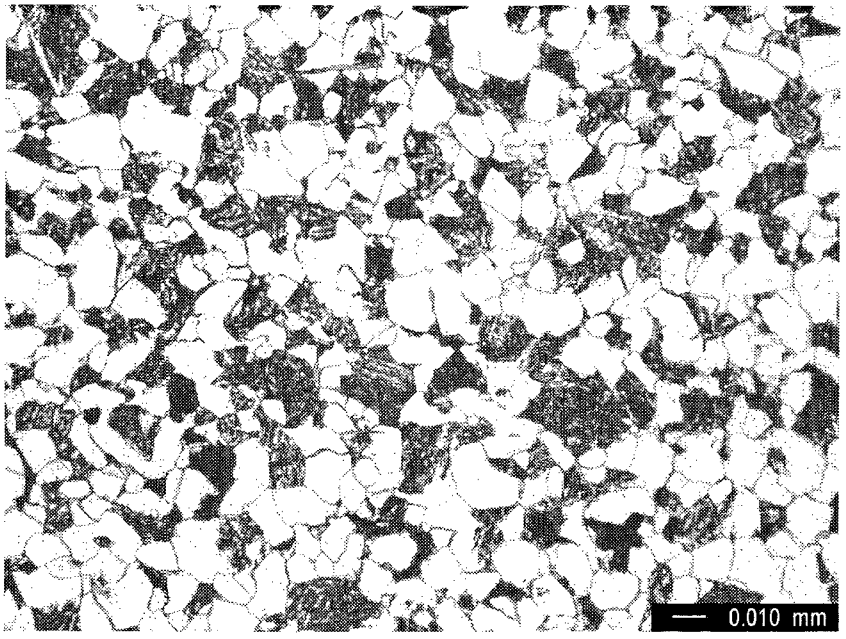

(b)

Fig. 3.1 SAE 8620 hot rolled bar before and after normalizing. (a) As-received microstructure showing needle-like ferrite and pearlite; (b) Normalized at 1750°F/4hrs microstructure showing ferrite and pearlite

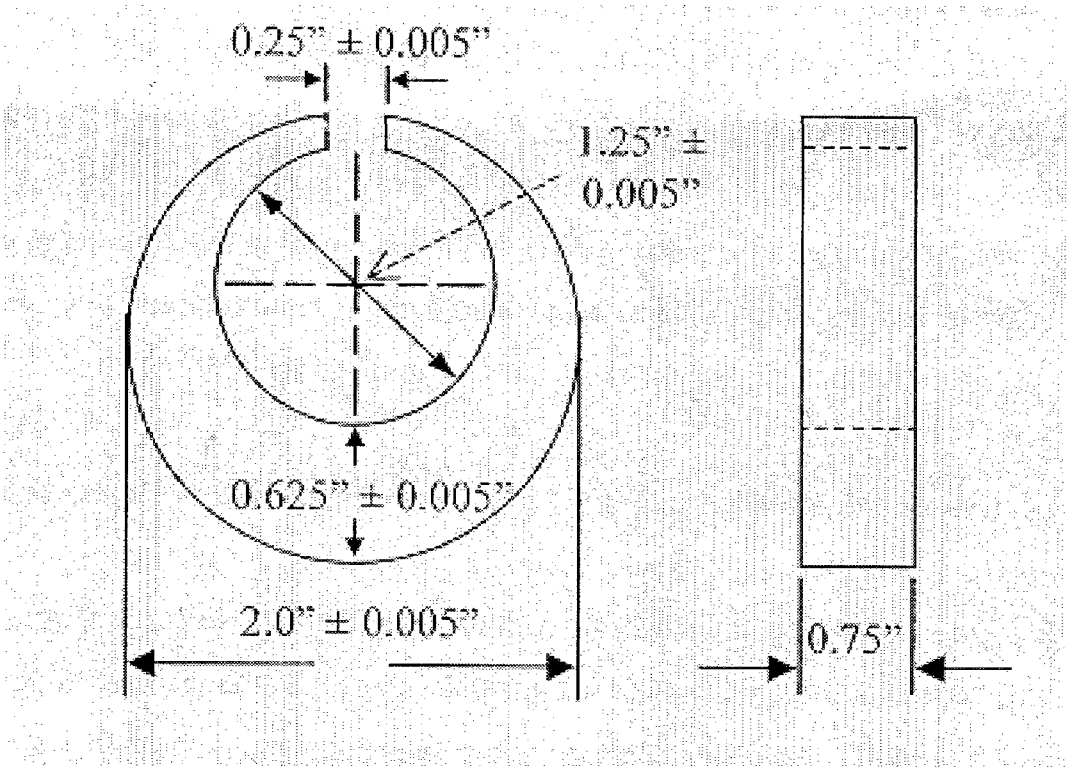

Fig. 3.2 The dimensions of Navy C-ring specimen.

Table 3.2 SAE 8620 Navy C –Ring heat treatment matrix

Normalizing Process (Temperature/Time)	Carburizing Process (Temperature/Time)	Carbon Potential (%)	Tempering Process (Temperature/Time)
1750 °F/4 hours (954 °C/4 hours)	1700 °F/6 hours (927 °C/6 hours)	0.9	RT*
			300 °F/1 hour (149 °C/1 hour)
			350 °F/1 hour (177 °C/1 hour)
		1.0	RT
			300 °F/1 hour (149 °C/1 hour)
			350 °F/1 hour (177 °C/1 hour)
		1.1	RT
			300 °F/1 hour (149 °C/1 hour)
			350 °F/1 hour (177 °C/1 hour)
	1750 °F/4 hours (954 °C/4 hours)	0.9	RT
			300 °F/1 hour (149 °C/1 hour)
			350 °F/1 hour (177 °C/1 hour)
		1.0	RT
			300 °F/1 hour (149 °C/1 hour)
			350 °F/1 hour (177 °C/1 hour)
		1.1	RT
			300 °F/1 hour (149 °C/1 hour)
			350 °F/1 hour (177 °C/1 hour)
		1.2	RT
			300 °F/1 hour (149 °C/1 hour)
			350 °F/1 hour (177 °C/1 hour)

* After carburizing, the samples were quenched to room temperature with no further tempering.

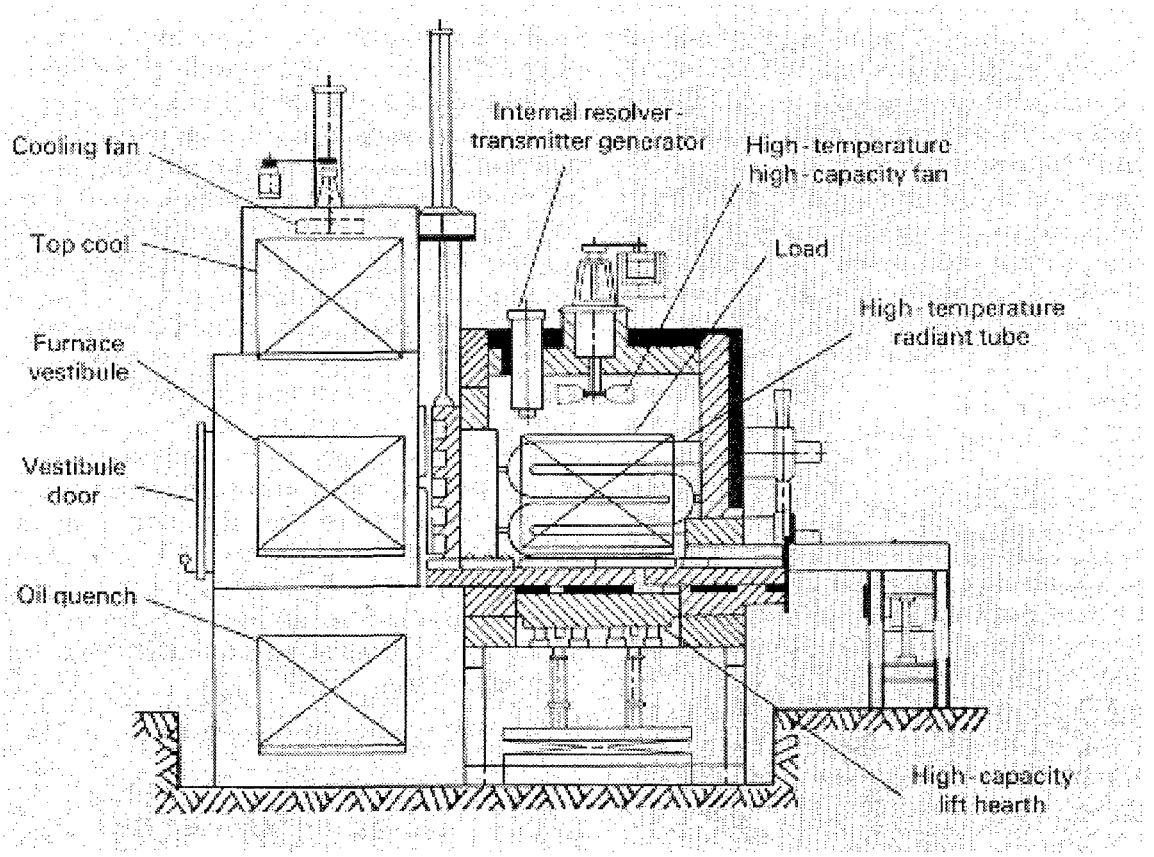

Fig.3.3 Carburizing furnace

3.3 Material Characterization Techniques

Metallographic preparation was conducted before the observation by scanning electron microscopy (SEM) and Optical Microscopy (OM). All specimens were sectioned, mounted, wet ground on silicon carbide papers of 240, 320, 400 and 600 grit followed by polishing on 1.0 micron and 0.5 micron alumina wheels, and then etched in 3% Nital.

3.3.1 Scanning Electron Microscopy

Scanning electron microscopy (SEM) was used to characterize the microstructures of the 6 specimens carburized at 1.0% carbon potential at two different carburizing temperatures (1700°F(927 °C) / 6hrs and 1750°F (954 °C) / 4hrs) followed by quenching or tempering at two different temperatures (300°F (149 °C) / 1 hr and 350°F (177 °C) / 1hr).

After metallographic preparation, the six specimens were coated in POLARON SC502 Sputter Coater and then placed in the SEM for the microstructural observations. A JEOL - JSM - 5800 LV Scanning Electron Microscope was used at magnifications ranging from 50× to 300,000×. The accelerating voltage was 15KV and the images were recorded on 9.5×12.5cm sheet film at 5000× magnification.

3.3.2 Optical Microscopy

After metallographic preparation, all specimens were placed under the optical microscope for the microstructural observations. A ZEISS AXIOVERT 25 optical microscope with EXWARE HAD digital color video camera attached was used at magnifications ranging from 50× to 1000×. In the resultant black-and-white micrographs

with 1000× magnification, retained austenite appears as a white phase and martensite as a dark phase.

3.3.3 X-ray Diffraction

X-ray diffraction techniques were used for both the retained austenite and the residual stress determinations. Measurements of the volume percent of retained austenite were made at the surface of each specimen. The residual stress that was measured was the hoop stress which is the stress tangent to the circumference also known as "circumferential stress" and "tangential stress [104].

A Bruker D8 Discover X-Ray Diffraction System, Figure 3.4, was used in this study. This unit is enclosed in a lead radiation-protection cabinet. The XYZ stage could be fixed at the center for mapping or auto-change samples.

Four peaks were examined to determine the percentage of retained austenite. The peaks evaluated are the (200) and (211) martensite peaks and the (220) and (311) austenite peaks. The set up for the XRD scan was over a range of 60° to 105° (2θ) with a step size of 0.025 degrees (2θ) and a 5 seconds time per step. A 1.54 $\overset{o}{A}$ CuKα radiation source was used with a generator voltage of 45KV and a generator current at 40A. The x-ray beam size was 0.2mm diameter.

The (211) martensite peak was examined to determine the value of residual stress of each specimen at four different ψ values (0°, 10°, 20° and 30°) while 2θ was fixed at 156°. A CrKα radiation source was used whose wave length was 2.23 $\overset{o}{A}$.

3.3.4 Optical Metallography

An optical metallographic technique was also used to determine the amount of retained austenite. In this method, a standard chart for estimating the amount of retained austenite is required and x-ray measurements are used as reference [11]. Through a process of comparing the optical photomicrographs to the standard chart [11], the amount of retained austenite was determined.

3.3.5 Hardness Measurement

The hardnesses were determined using a MT-90ASW Micro-hardness Tester (seen Figure 3.5) which was equipped with a square-based diamond pyramid (Vickers) indenter. The load is variable from 10 grams to 1,000 grams. In the present work, 1,000 grams for 10 seconds was applied to all specimens. After the heat treatment cycle was finished, specimens were cross-sectioned, mounted, polished on 1.0 micron and 0.5 micron alumina wheels. The Vickers / Diamond Pyramid hardness profile was measured across the carburized region into the core of each specimen. Hardness transverses were measured at three different locations of the cross sections, and the final hardness values represent an average from the three locations. The Vickers / Diamond Pyramid hardness value was then converted to a Rockwell C hardness (HRC) number by referring to Table 3.3 [6] because the HRC value is the typical industry-standard for hardness measurement of carburized parts.

The effective case depths were determined to be the depth at which the Rockwell hardness value was equivalent to 50HRC [9].

3.3.6 Optical Emission Spectroscopy

Among the various elemental analysis techniques for iron and steel, Optical Emission Spectroscopy (OES) is widely used because of its simplicity [105]. In this study, the surface elemental composition of selected C-ring specimens were measured using ARL (Applied Research Laboratories) Metal Analyzer 3460.

3.4 Dimensional Measurements

A PRISMO (Carl Zeiss IMT Company) coordinate measuring machine (CMM), Figure 3.6, was used to measure the distortion of the specimens to a precision of 1μm. Contact scans of the C-ring surfaces were conducted to determine seven parameters for each specimen: flatness, cylindricity, roundness, outer diameter, inner diameter, thickness, and the gap width of each specimen. The dimensional measurements of each C-ring obtained from the CMM provide a set of points referred to as a point cloud in the computer. The analysis of C-ring features was determined with the "Imageware Surface" scanning software through calculating the deviation between the actual dimensions and nominal dimensions for the as-machined and the heat treated specimens.

Figure 3.4 shows the measurement locations of each Navy C-ring specimen for the seven parameters. For each sample, before and after heat treatment, the flatness of the numbered surface was measured. About 2500 points were chosen on this surface and the flatness was the deviation between the highest point and the lowest point [106] (Figure 3.8); OD was measured at one location; Cylindricity was measured at three different locations on which about 4000 points were scanned [107, 108] (Figure 3.9). Two locations (so called top and bottom) were chosen for the gap width measurements. Three different measurement locations (top, middle and bottom) were chosen when measuring

ID and thickness. The roundness of each ID was determined through scanning about 880 points on each measured ID circle (Figure 3.10). Quantitatively, the degree of roundness was expressed by the dimension of out-of-roundness, that is, the deviation from the ideal form [109].

3.5 Summary of Experimental Procedures & Measurements

This study involved the following experimental procedures: 3D measurements using a Coordinate Measuring Machine (CMM), heat treatment, Scanning Electron Microscopy (SEM), X-Ray Diffraction (XRD), micro-hardness, Optical Emission Spectroscopy (OES). Figure 3.11 is a schematic flowchart of all experimental procedures conducted in this study.

Table 3.3 Hardness Conversion Numbers for Steel [6]

Rockwell C Hardness Number	Vickers Hardness Number (Kg/mm^2)	Rockwell C Hardness Number	Vickers Hardness Number (Kg/mm^2)
68	940		
67	900	—	—
66	865		
65	832		
64	800	49	498
63	772	48	484
62	746	47	471
61	720	46	458
60	697	45	446
59	674	44	434
58	653	43	423
57	633	42	412
56	613	41	402
55	595	40	392
54	577	39	382
53	560	38	372
52	544	37	363
51	528	36	354
50	513	35	345

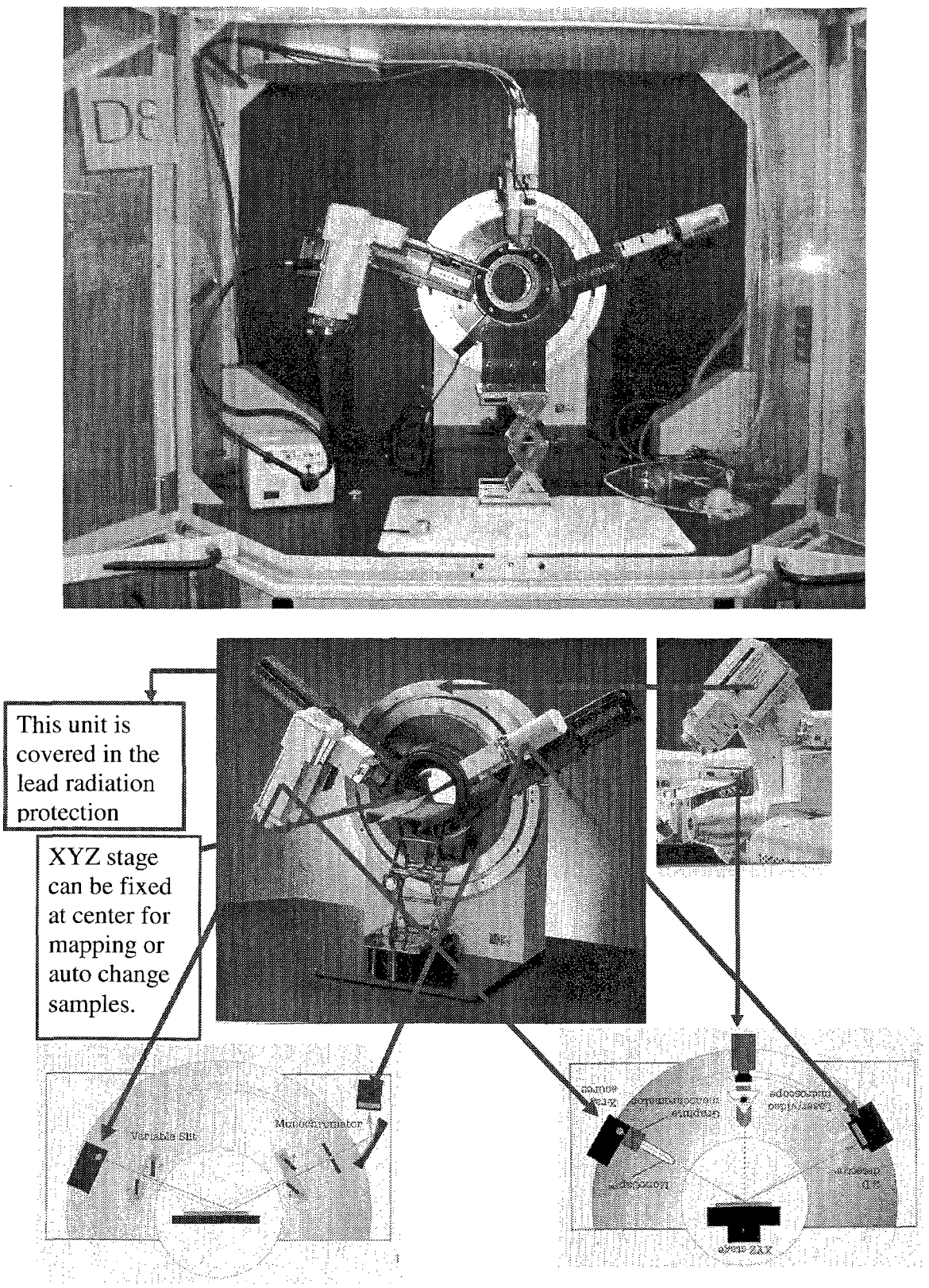

Fig. 3.4 Brucker D8 Discover X-Ray Diffraction System

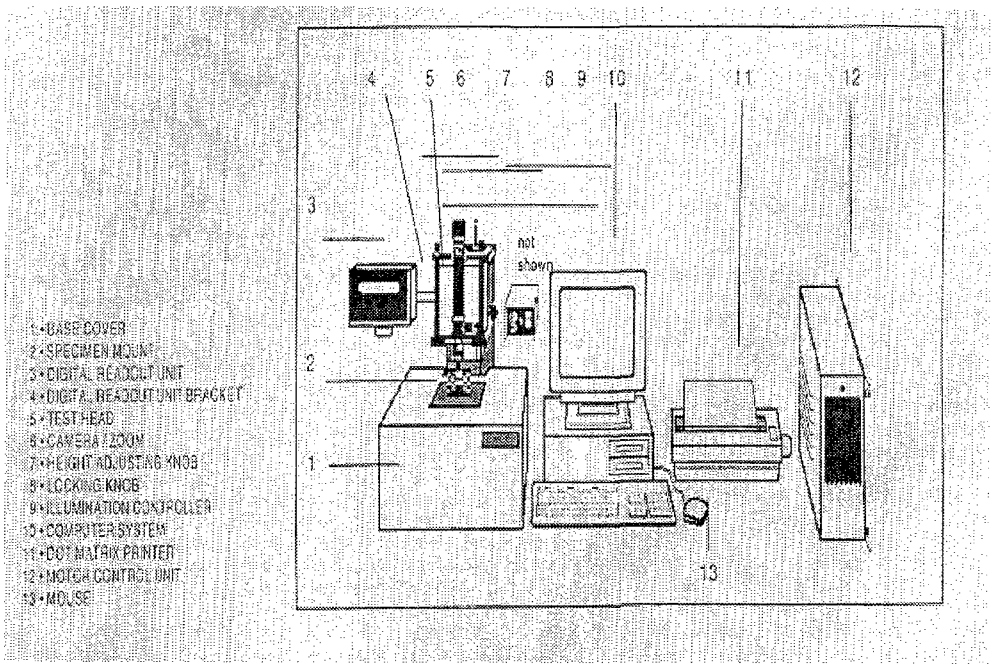

Fig. 3.5 Schematic diagram of MT-90ASW micro-hardness testing system and principle of operation.

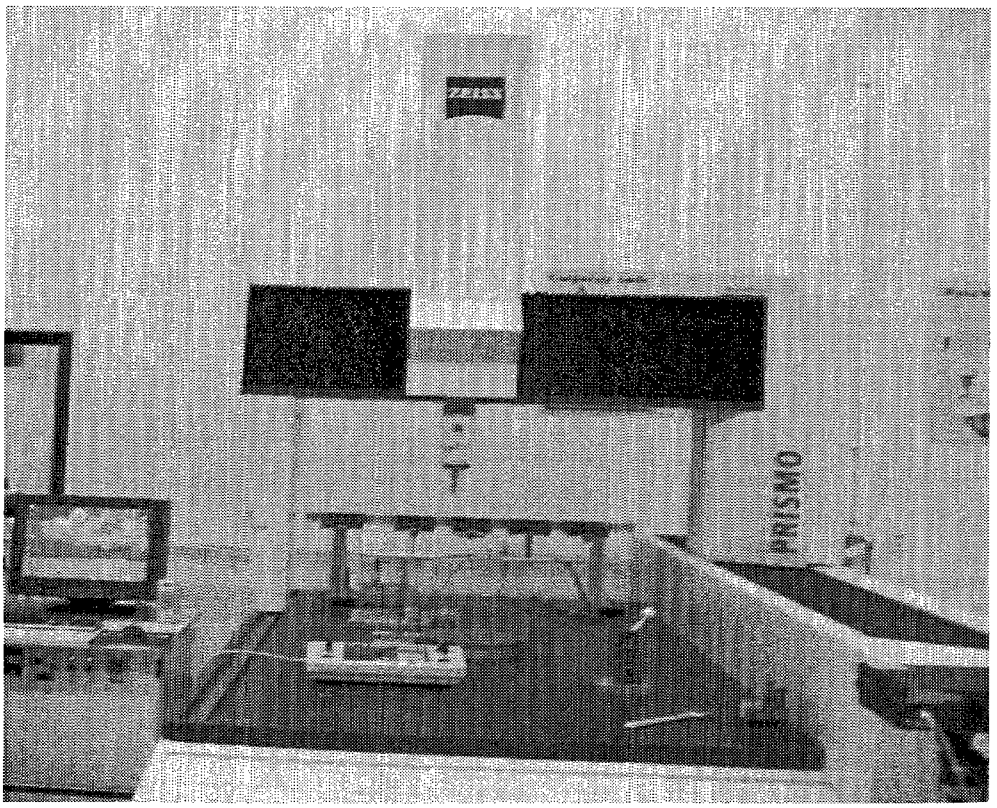

Fig. 3.6 PRISMO Coordinate Measuring Machine (CMM)

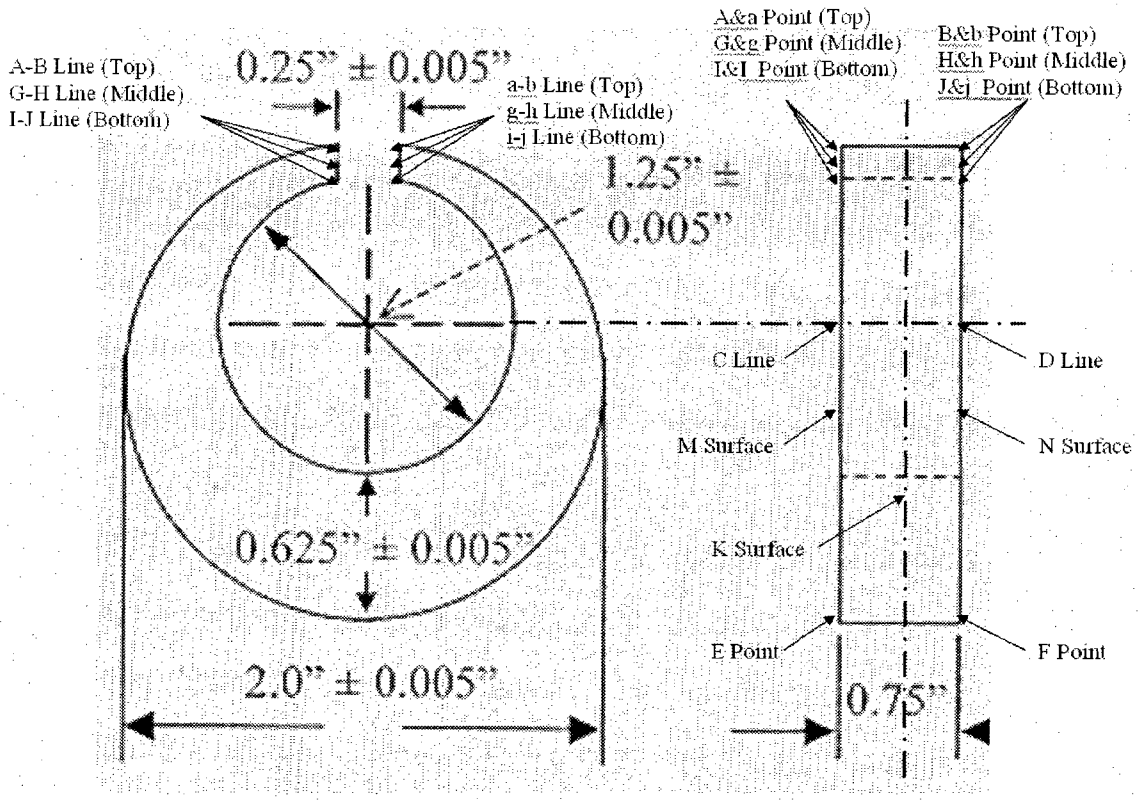

Measurement report shows:

1. Flatness_Numbered Side (N surface flatness)
2. Diameter_OD (Outside Diameter)
3. Cylindricity_OD (Outside Cylindricity)
4. Diameter_ID-1 (Inside Diameter at M Surface)
5. Roundness_ID-1 (Inside Roundness at M Surface)
6. Diameter_ID-2 (Inside Diameter at K Surface)
7. Roundness_ID-2 (Inside Roundness at K Surface)
8. Diameter_ID-3 (Inside Diameter at N Surface)
9. Roundness_ID-3 (Inside Roundness at N Surface)
10. Thickness_1 (Thickness between A Point to B Point)
11. Thickness_2 (Thickness between C Line to D Line)
12. Thickness_3 (Thickness between E Point to F Point)
13. Dis_Gap_Top (Gap Between A-B Line to a-b Line)
14. Dis_Gap_Middle (Gap Between G-H Line to g-h Line)
15. Dis_Gap_Bottom (Gap Between I-J Line to i-j Line)

Fig. 3.7 CMM measurement positions for each Navy C-ring specimen

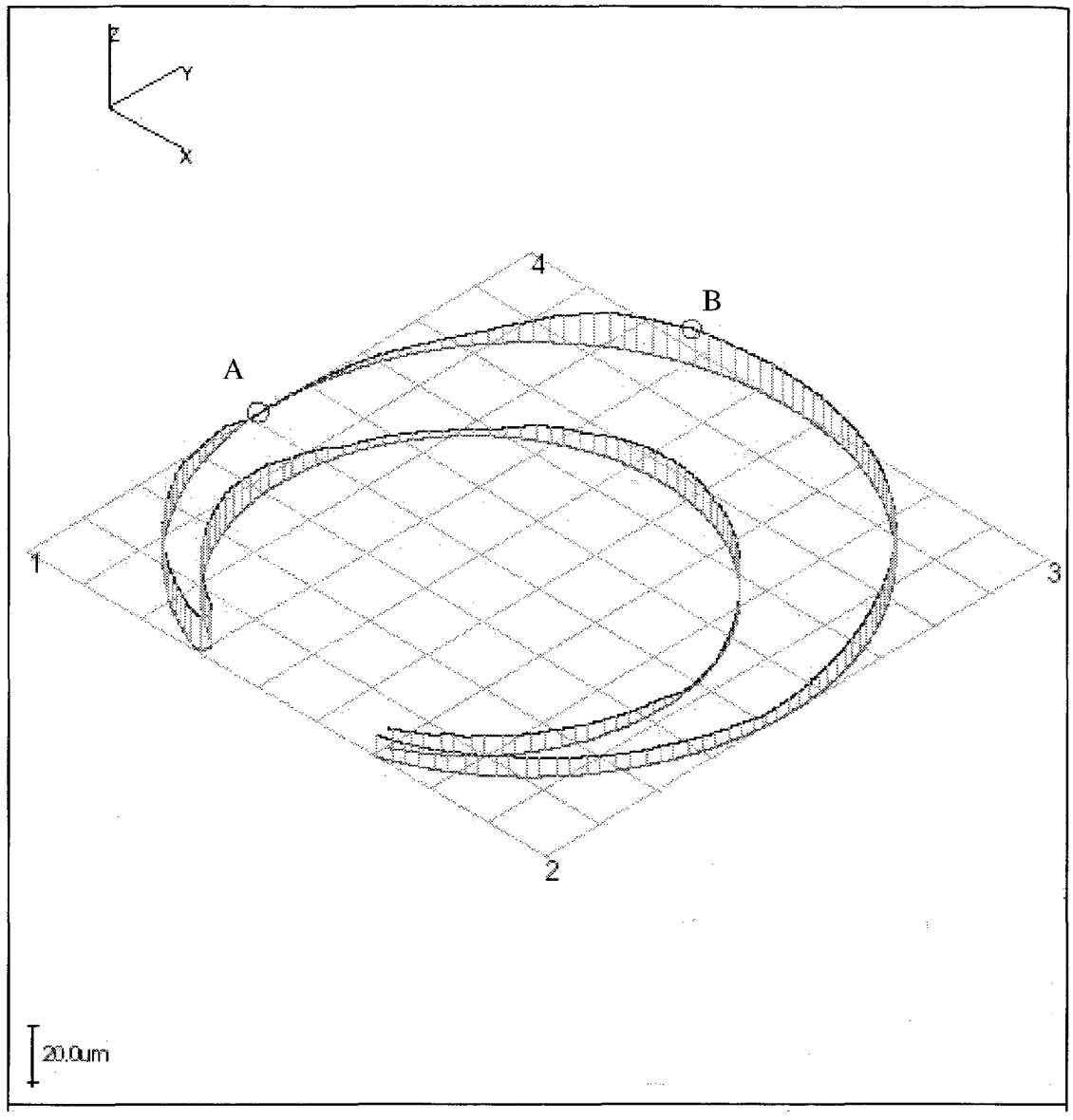

Fig. 3.8 Example plot of flatness measurements using CMM. The 'A' spot is the maximum deviation spot towards the surface '1234' and the 'B' spot is the maximum deviation spot away from the surface '1234'.

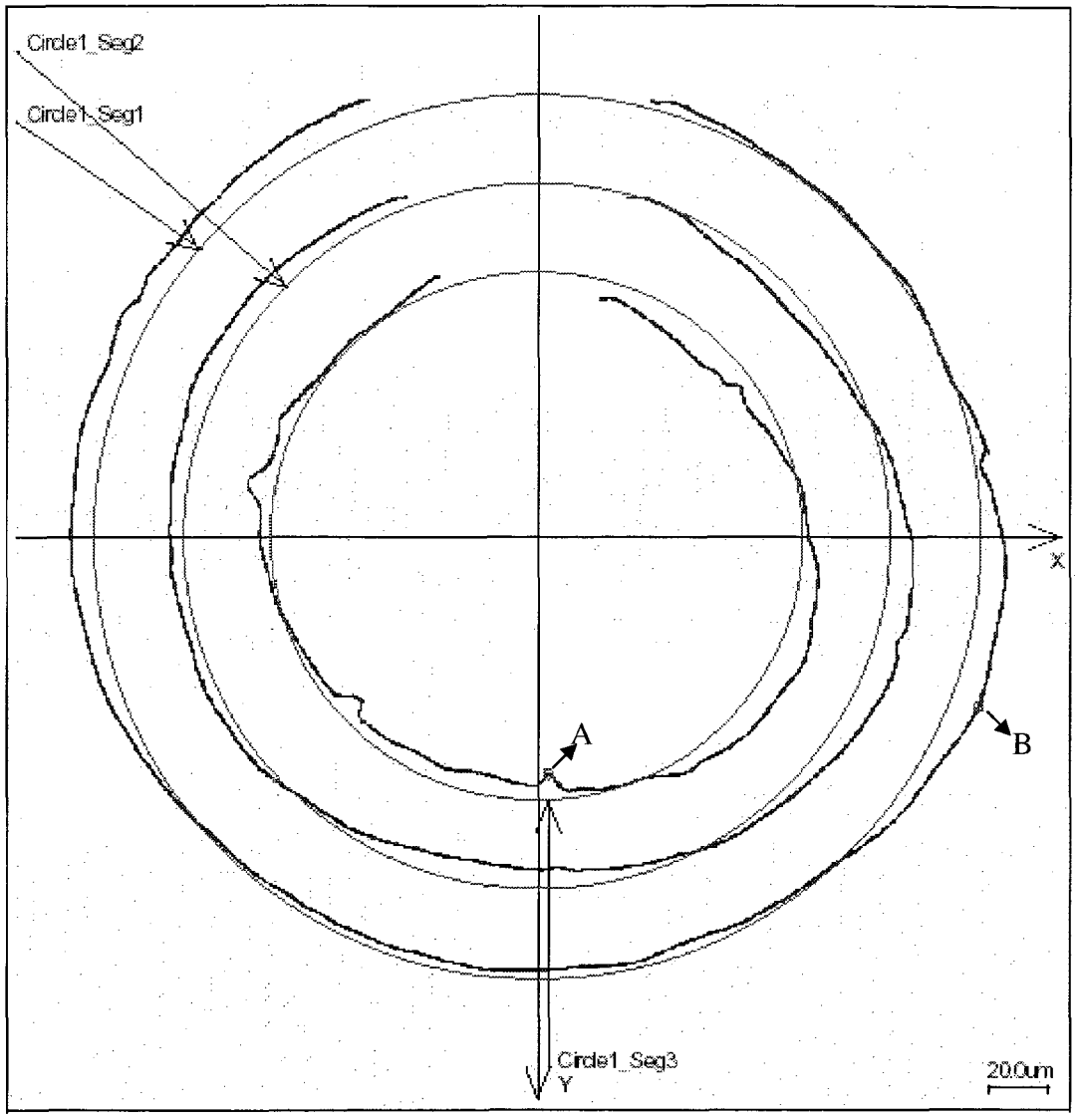

Fig. 3.9 Example plot of cylindricity measurements using CMM. The 'A' spot is the maximum deviation spot towards the center of the three circles and the 'B' spot is the maximum deviation spot away from the centre of the three cycles.

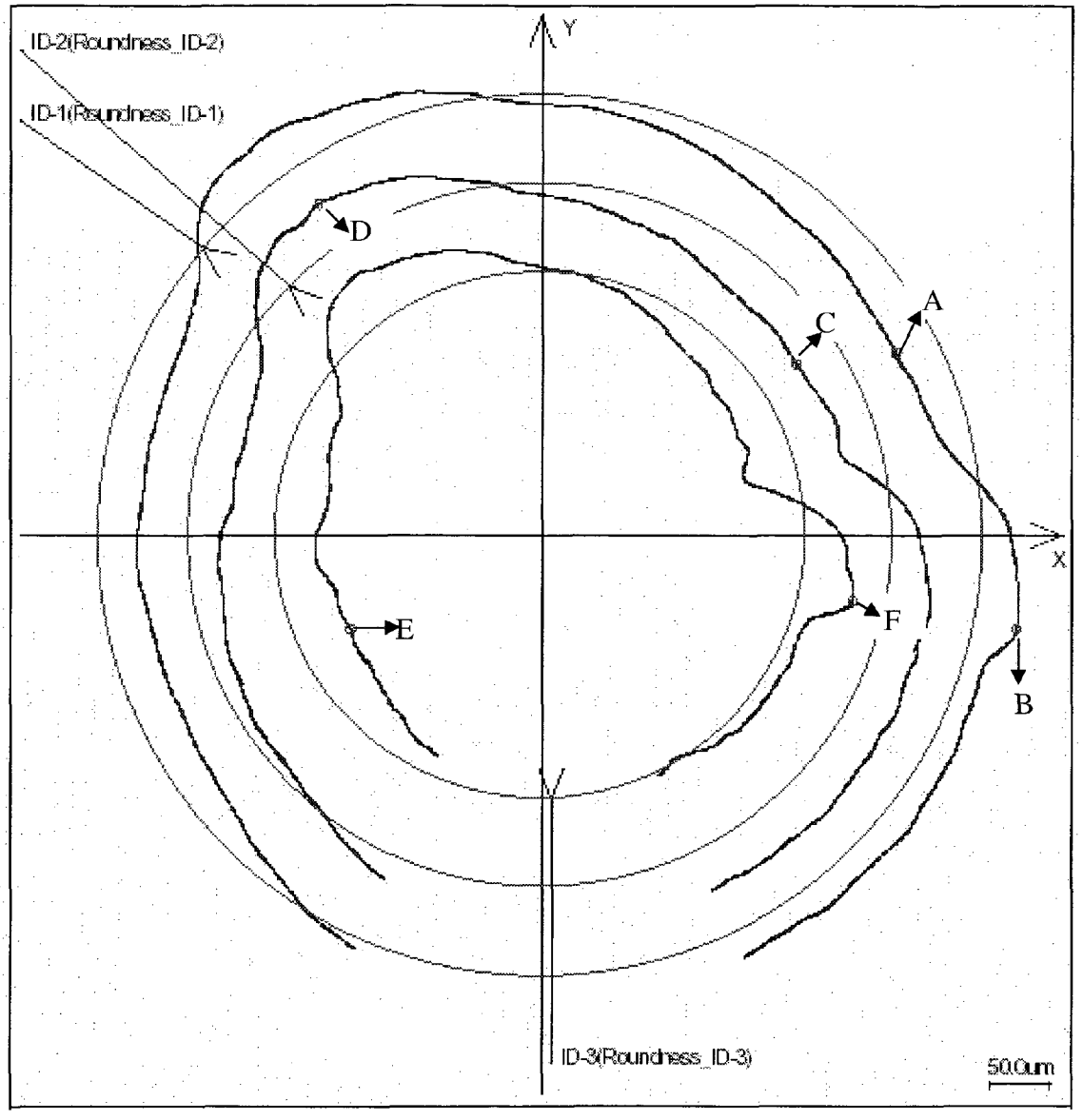

Fig. 3.10 Example plot of roundness measurements using CMM. The 'A' and 'B' are the maximum deviation spots for ID-1 towards and away from the center of the circles. The 'C' and 'D' are the maximum deviation spots for ID-2 towards and away from the center of the circles. The 'E' and 'F' are the maximum deviation spots for ID-3 towards and away from the center of the circles.

Fig. 3.11 Schematic flowchart of all experimental procedures

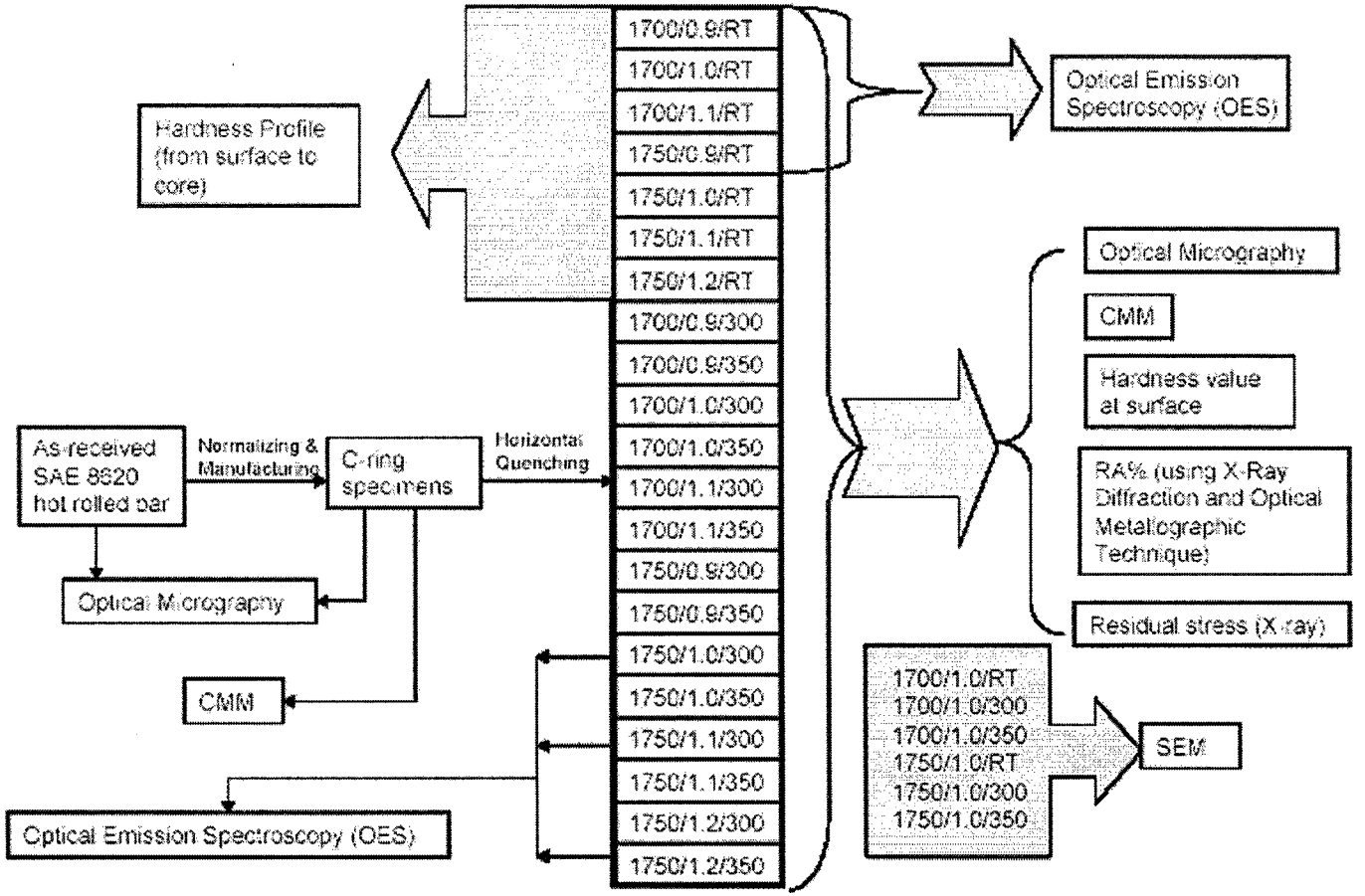

CHAPTER 4 THE EFFECT OF RETAINED AUSTENITE ON OD, GAP AND FLATNESS DISTORTION OF SAE 8620 STEEL

In this chapter, the correlations between the following four factors are discussed: heat treatment process parameters, retained austenite, residual stress and the distortion values for OD, gap width and flatness. The optimum retained austenite and residual stress for the reduction of the distortion for OD, gap width and flatness are discussed separately. Finally, the optimum retained austenite and residual stress for the reduction of the average distortion (combined distortion factor incorporating OD, gap width and flatness) are detailed.

4.1 Distortion

The distortion values for OD, gap width and flatness of C-ring samples are summarized in Table 4.1. Table 4.1 also lists the average distortion of OD, gap width and flatness which is based on their absolute values and calculated according to equation 4.1:

Average Distortion (%) = [Σ (Absolute value of OD, Gap Width & Flatness distortion)] / 3----------Eq.4.1

Figure 4.1 (a) show example plots of the flatness distortion for three heat treatment conditions, i.e. as-machined, as-quenched (1750/1.2/RT) and as-quenched & tempered (1750/1.2/350). From Figure 4.1 (a) we can see that the highest spot and the lowest spot (the red small cycles in the figure) do not stay in same place after quenching. The carburizing and quenching process (1750/1.2/RT) creates both a new high spot and a new low spot which remain in place during tempering but undergo reductions in magnitude. However, this is not the usual behaviour. For most heat treatment processes, the high and low spots usually "walk" to different positions after tempering (see Figure

4.1 (b)). In very few instances in this study, do the positions of the high / low spots stay the same after tempering.

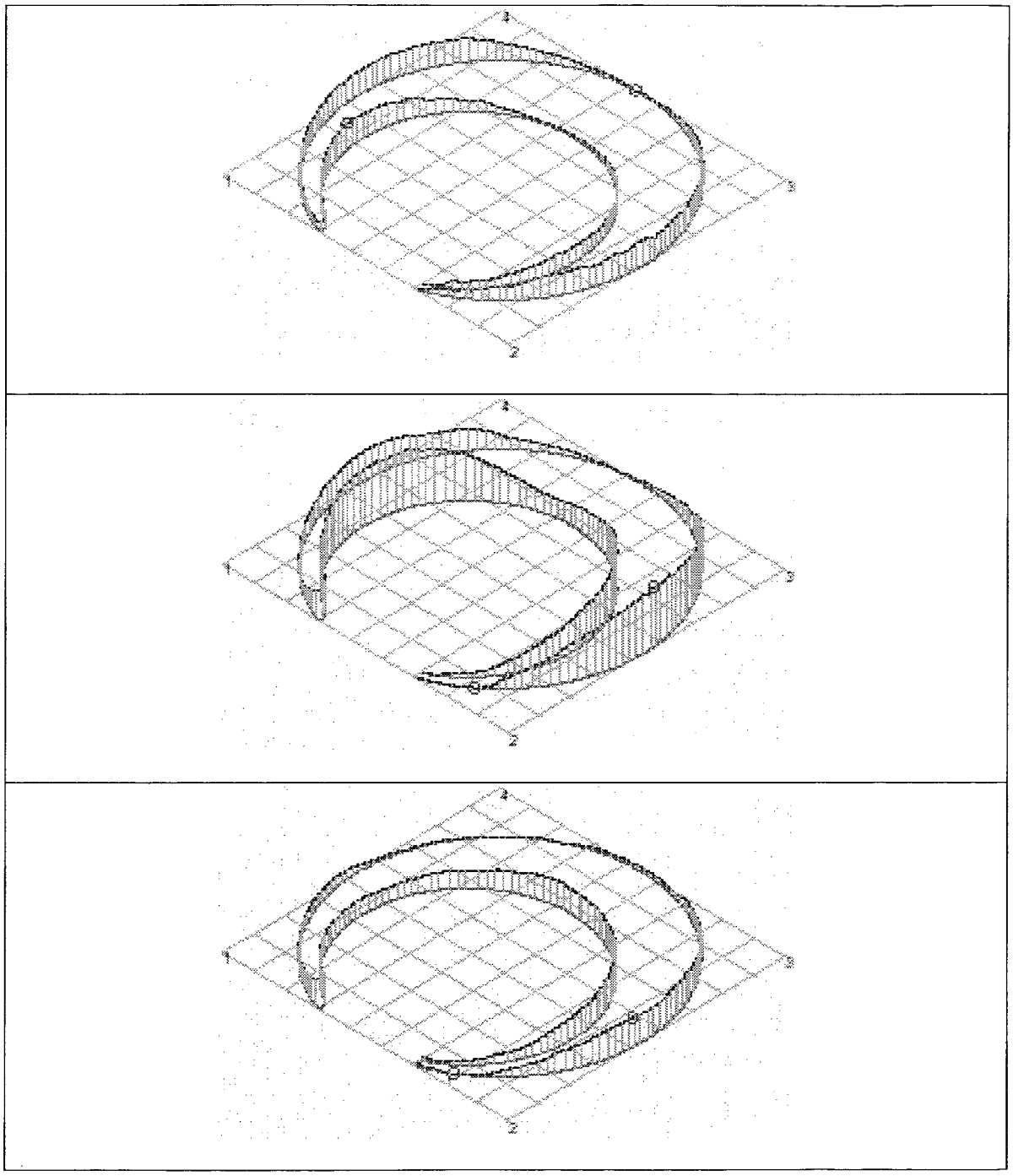

Fig. 4.1 (a) One example plot of flatness distortion at three conditions showing the high and low spots remaining in place during tempering: as-machined (top), as-quenched (1750/1.2/RT) (middle) and as-quenched & tempered (1750/1.2/350) (bottom).

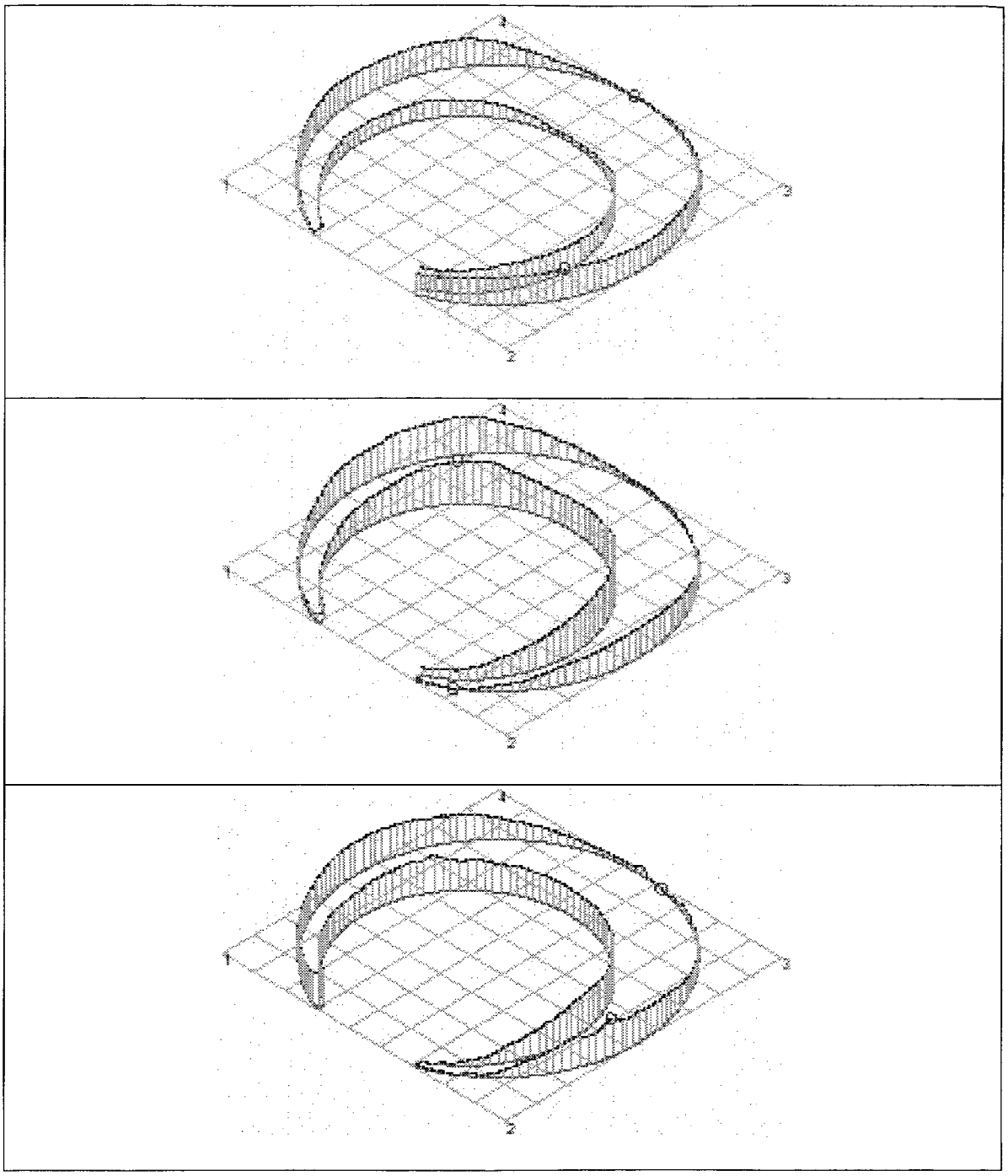

Fig. 4.1 (b) One example plot of flatness distortion at three conditions showing the high and low spots walking during tempering: as-machined (top), as-quenched (1700/1.1/RT) (middle) and as-quenched & tempered (1700/1.1/300) (bottom).

The relationship between the OD distortion and process cycle is shown in Figure 4.2. Figure 4.3 shows the gap width distortion vs. process cycle. Figure 4.4 shows the flatness distortion vs. process cycle. Figure 4.5 shows the average distortion vs. heat treatment process cycle. From Figs 4.2, 4.3, and 4.4, we can see that there is distortion after carburizing and quenching / tempering. The OD and gap are both enlarged. This is due to the phase, and associated volume, change from austenite to martensite. Also from Figs 4.2, 4.3, and 4.4, it can be seen that tempering can reduce the distortion to a significant degree. Tempering helps eliminate the elastic deformation through relieving the internal stresses that arise from retained austenite. It is also clear from Figs 4.3 and 4.4 that the distortion becomes more significant with increasing carburizing temperature and carbon potential. From Figure 4.5 we can see the optimum heat treatment for reduced distortion is 1750/1.1/350, i.e. carburized at 1750°F for 4 hours at 1.1% carbon potential, oil quenched and then tempered at 350°F for 1 hour.

4.2 Retained austenite and residual stress

The results for retained austenite and residual stresses are given in Table 4.2. Based on the data in Table 4.2, we obtain Fig. 4.6 which shows the relationship between retained austenite, residual stresses and process cycle.

From Fig. 4.6, we can see that an increase in carburizing temperature gives rise to an increase in the amount of retained austenite. Also, with increasing carbon potential, the amount of retained austenite increases. Compared to the quenched condition, the amount of retained austenite is reduced after tempering. With increased tempering temperature (300°F to 350°F), the amount of retained austenite is decreased but not significantly.

For residual stresses, the situation is very similar to that for retained austenite, i.e. with increasing carburizing temperature and carbon potential, the residual stress increases. Tempering reduces the residual stress. As the tempering temperature is increased from 300°F to 350°F, the residual stress decreases but not significantly.

The other general feature that can be seen in Fig. 4.6 is that an increase in retained austenite tends to give rise to an increase in residual stress.

4.3 Distortion vs. retained austenite and residual stress

Tables 4.3, 4.4 and 4.5 show the distortion of OD, gap width and flatness vs. retained austenite and residual stresses after quenching. The distortion values are ranked from low to high. From Tables 4.3, 4.4 and 4.5, we can see the lowest values of distortion of the OD, gap width and flatness all occur at 1700/0.9/RT, 8.5% retained austenite (X-ray measurement) and -429.0 MPa residual stress. From Tables 4.4, 4.5 and Figure 4.7 (a) which is constructed based on the data in Table 4.4, we can also see that the distortion of gap width and flatness becomes increasingly serious with increasing values of retained austenite and residual stress.

Tables 4.6, 4.7 and 4.8 show the distortion of OD, gap width and flatness vs. retained austenite and residual stresses after 300°F/1hr tempering. The distortion values are ranked from low to high. From Table 4.6, we can see the smallest OD distortion happens at 1750/1.1/300, 29.5% retained austenite (X-ray measurement) and -888.0 MPa residual stress. As for the gap distortion, the smallest distortion, Table 4.7, occurs for 1700/0.9/300, 4.0% retained austenite, -370.0 MPa residual stress. Finally, the smallest flatness distortion, Table 4.8, occurs for 1750/0.9/300, 20.0% retained austenite and -645.5 MPa residual stress.

Tables 4.9, 4.10 and 4.11 give the distortion values vs. retained austenite and residual stress after 350°F/1hr tempering. From Table 4.9, it can be found for OD distortion the lowest distortion is for 1750/0.9/350, 18.5% retained austenite and -620.5 MPa residual stress. For the gap distortion, Table 4.10, the lowest distortion is for 1700/0.9/350, 4.0% retained austenite and -360.0MPa residual stress. For flatness, Table 4.11, the lowest distortion is for 1750/1.1/350, 26.0% retained austenite and -840.5 MPa residual stress.

Based on the data in Tables 4.7 and 4.10, Figure 4.7 (b) is constructed showing the gap distortion generally becoming severe with increasing retained austenite after quenching and quenching and tempering at 300°F or 350°F for 1hour.

Table 4.12 summarizes the lowest distortion values for quenched and quenched and tempered (300°F and 350°F) samples. From Table 4.12 we can see the lowest OD distortion occurs for 1750/1.1/300 (carburized at 1750°F for 4 hours at 1.1% carbon potential, oil quenched and then quenched at 300°F for 1 hour), 29.5% retained austenite and -888.0Mpa residual stress. For the gap width distortion, the lowest distortion is for 1700/0.9/300 (carburized at 1700°F for 6 hours at 0.9% carbon potential, oil quenched and then tempered at 300°F for 1 hour), 4.0% retained austenite and -370.0MPa residual stress; For the flatness distortion, the lowest distortion is for 1750/1.1/350 (carburized at 1750°F for 4 hours at 1.1% carbon potential, oil quenched and tempered at 350°F for 1 hour), 26.0% retained austenite and -840.5MPa residual stress. As discussed before, from Figure 4.5 it can been seen that the optimum heat treatment condition is 1750/1.1/350 (carburized at 1750°F for 4 hours at 1.1% carbon potential, oil quenched and then tempered at 350°F for 1 hour), 26.0% retained austenite and -840.5MPa residual stress.

Table 4.1 Distortion values for Navy-C ring specimens subjected to various heat treatments.

Cycle No.	Carburizing Temp. (°F) /Carbon Potential (%) /Tempering Temp. (°F)	OD Distortion (%)	Gap Width Distortion (%)			Flatness Distortion (%) *	Average Distortion of OD,Gap Width & Flatness (%) **
			Top	Bottom	Average		
C1	1700/0.9/RT	0.071	1.70	1.79	1.75	20.5	7.44
	1700/0.9/300	0.027	0.13	0.27	0.20	3.9	1.38
	1700/0.9/350	0.019	0.33	0.37	0.35	2.3	0.89
C2	1700/1.0/RT	0.079	1.99	1.97	1.98	31.4	11.15
	1700/1.0/300	0.033	0.59	0.63	0.61	2.2	0.95
	1700/1.0/350	0.014	0.57	0.66	0.62	4.7	1.78
C3	1700/1.1/RT	0.146	2.56	2.51	2.54	42.3	14.99
	1700/1.1/300	0.030	0.65	0.66	0.66	2.1	0.93
	1700/1.1/350	0.015	0.66	0.68	0.67	4.8	1.83
C4	1750/0.9/RT	0.096	2.23	2.27	2.25	62.9	21.75
	1750/0.9/300	0.027	0.47	0.46	0.47	1.1	0.53
	1750/0.9/350	0.012	0.43	0.49	0.46	3.3	1.26
C5	1750/1.0/RT	0.123	2.97	2.99	2.98	110.1	37.73
	1750/1.0/300	0.041	0.60	0.56	0.58	-8.3	2.97
	1750/1.0/350	0.013	0.61	0.64	0.63	1.2	0.61
C6	1750/1.1/RT	0.101	3.11	3.09	3.10	125.2	42.80
	1750/1.1/300	0.010	0.81	0.77	0.79	1.8	0.87
	1750/1.1/350	0.012	0.85	0.88	0.87	-0.6	0.49
C7	1750/1.2/RT	0.102	3.15	3.08	3.12	188.5	63.91
	1750/1.2/300	0.042	0.88	0.91	0.90	26.2	9.05
	1750/1.2/350	0.018	0.90	0.93	0.92	10.3	3.74

$$*\text{Flatness Distortion}(\%) = \frac{\text{deviation(of flatness)after heat treatment} - \text{deviation(of flatness)beforeheat treatment}}{\text{deviation(of flatness)beforeheat treatment}} \times 100\%$$

** Average Distortion of OD, Gap Width & Flatness (%) = [Σ (Absolute value of OD, Gap Width & Flatness distortion)] / 3

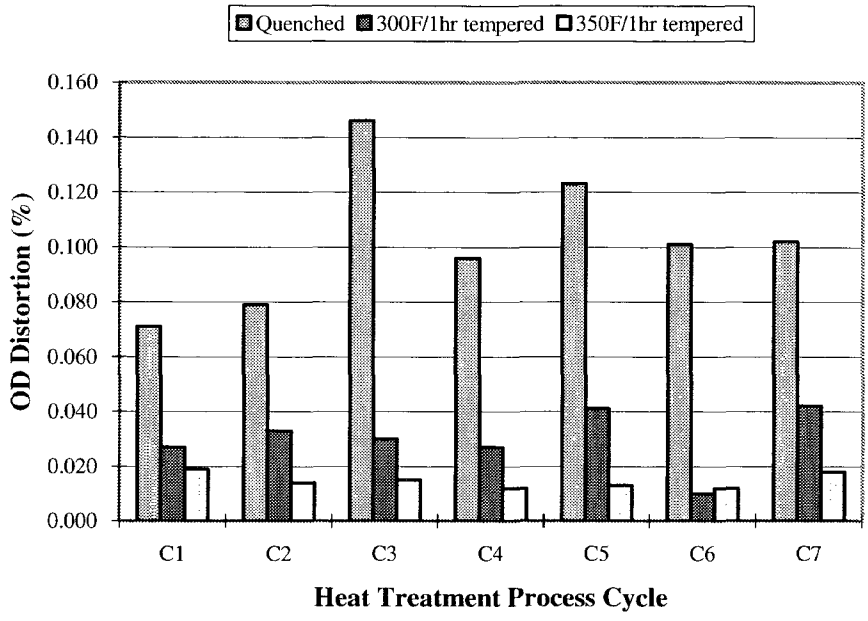

Fig. 4.2 OD distortion vs. heat treatment process cycle

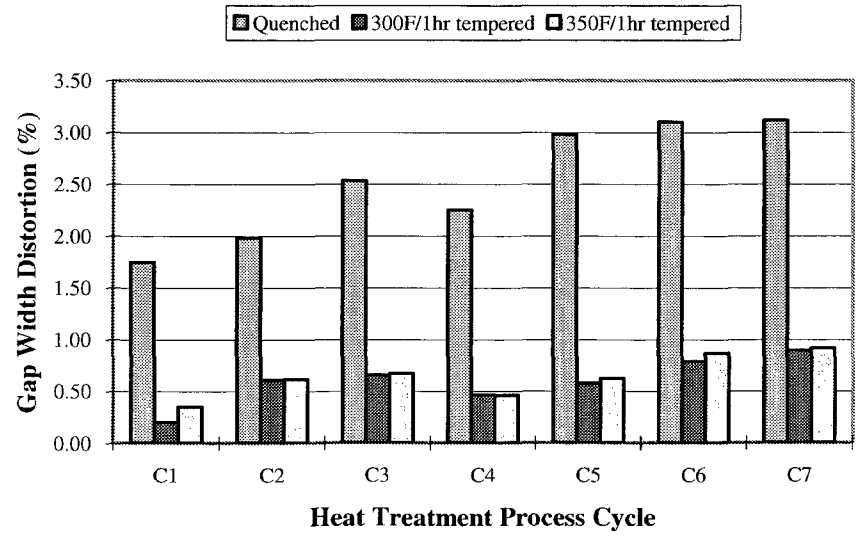

Fig. 4.3 Gap width distortion vs. heat treatment process cycle.

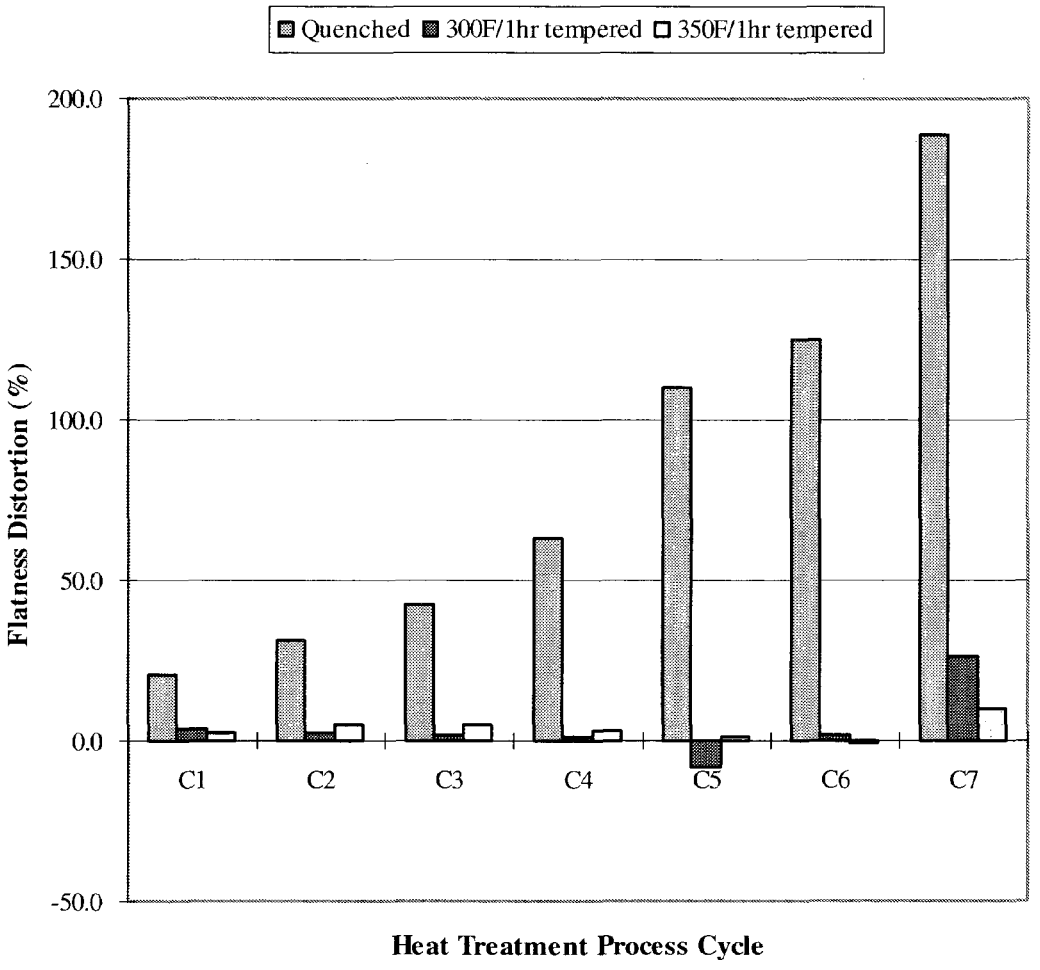

Fig. 4.4 Flatness distortion vs. heat treatment process cycle.

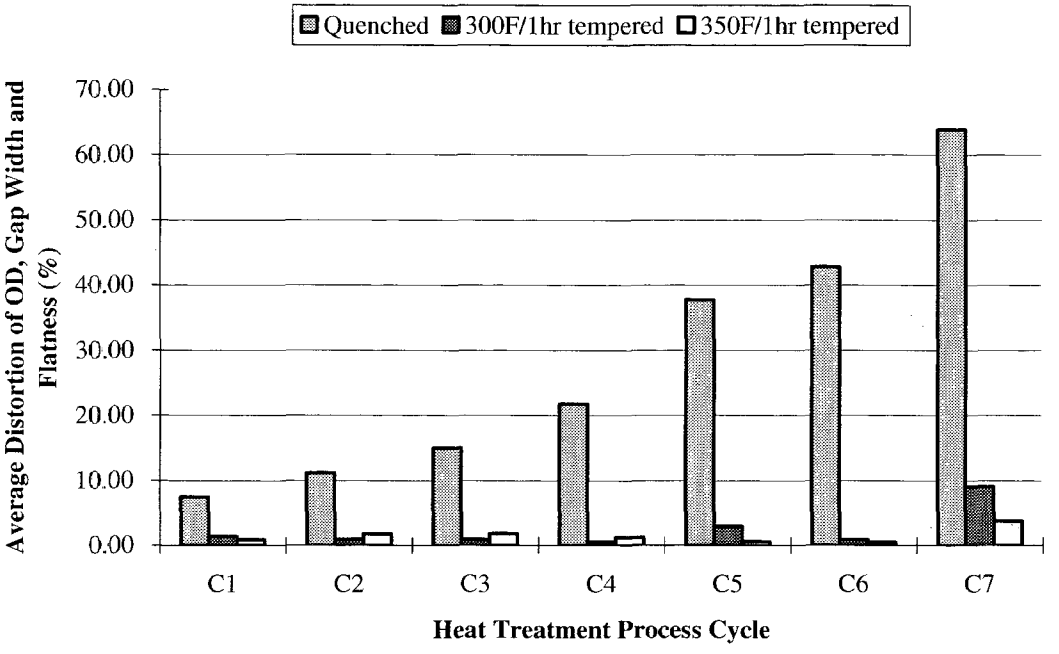

(a)

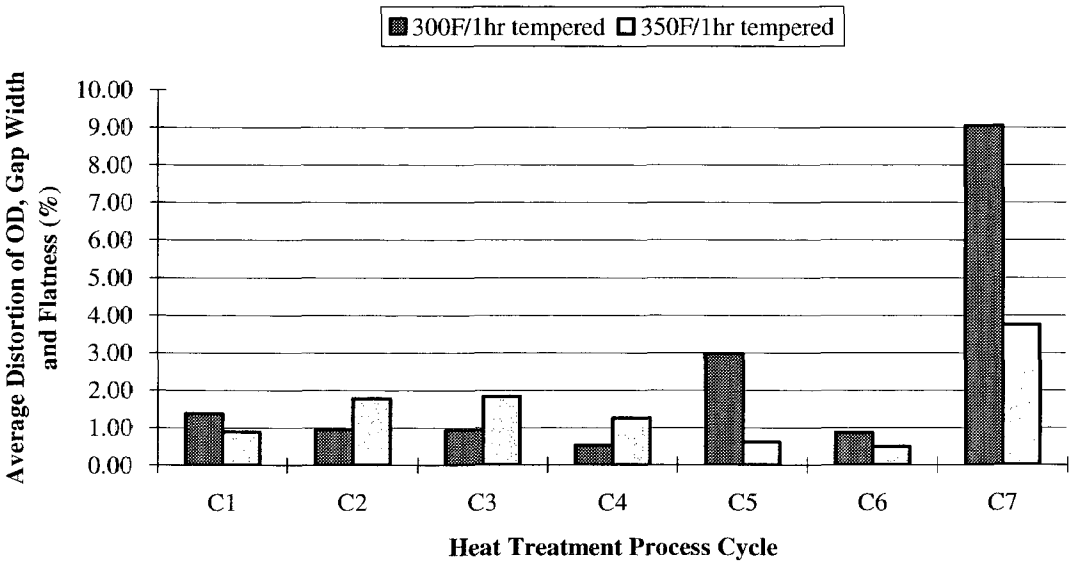

(b)

Fig. 4.5 Average distortion of OD, gap width and flatness vs. heat treatment process cycle. **(a)** In quenched & quenched and tempered condition. **(b)** In quenched and tempered condition.

Table 4.2 Retained austenite and residual stresses in Navy C-ring specimens subjected to various heat treatment condition.

Cycle No.	Carburizing Temperature(°F) /Carbon Potential (%) /Tempering Temperature (°F)	RA-M* (%)	RA-X* (%)	RS-X* (MPa)
	1700/0.9/RT	10	8.5	-429.0
	1700/0.9/300	5	4.0	-370.0
C1	1700/0.9/350	5	4.0	-360.0
	1700/1.0/RT	15	17.5	-625.5
	1700/1.0/300	10	12.5	-559.5
C2	1700/1.0/350	10	10.0	-542.3
	1700/1.1/RT	20	22.5	-700.5
	1700/1.1/300	15	20.1	-645.5
C3	1700/1.1/350	15	17.5	-633.5
	1750/0.9/RT	20	21.4	-650.5
	1750/0.9/300	15	20.0	-645.5
C4	1750/0.9/350	15	18.5	-620.5
	1750/1.0/RT	25	28.6	-822.5
	1750/1.0/300	20	25.0	-800.5
C5	1750/1.0/350	20	23.2	-816.5
	1750/1.1/RT	30	33.5	-901.0
	1750/1.1/300	25	29.5	-888.0
C6	1750/1.1/350	25	26.0	-840.5
	1750/1.2/RT	40	43.5	-900.5
	1750/1.2/300	40	40.0	-874.5
C7	1750/1.2/350	35	36.5	-866.3

* RA-M: restained austenite is measured using an optical metallographic technique.
RA-X: retained austenite is measured using a X-ray diffraction technique.
RS-X: residual stresses are measured by a X-ray diffraction technique.

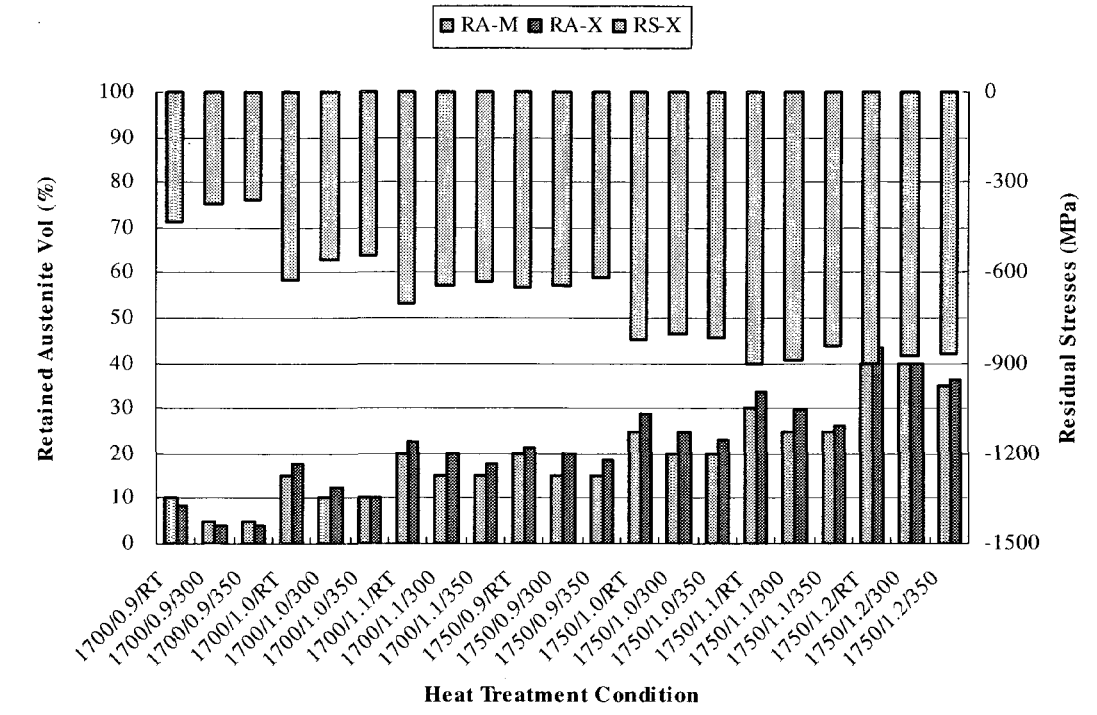

(a)

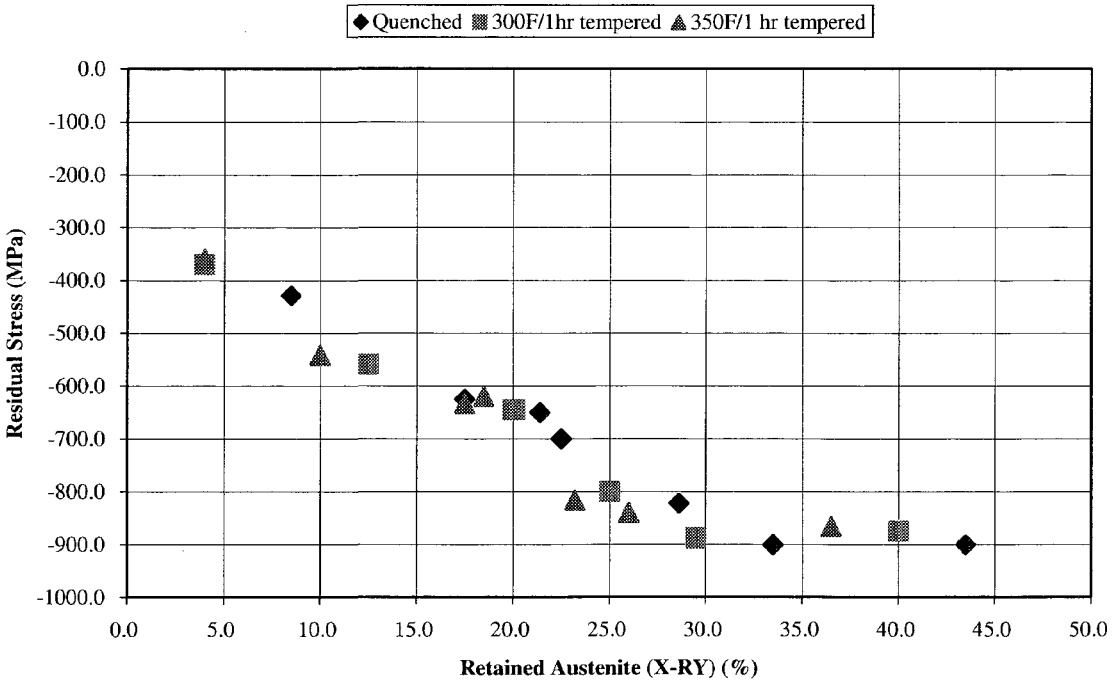

(b)

Fig. 4.6 Retained austenite vs. residual stresses. (a) the relationships between retained austenite, residual stress and carburizing temperature and carbon potential. (b) the relationship between retained austenite and residual stress after quenching, quenching and tempering at 300°F or 350°F for 1hour.

Table 4.3 OD distortion vs. retained austenite and residual stress after quenching

OD Distortion (%)		Heat Treatment	RA-M (%)		RA-X (%)		RS-X (MPa)	
Value	Rank		Value	Rank	Value	Rank	Value	Rank
0.071	1	1700/0.9/RT	10	[redacted]	8.5	[redacted]	-429.0	[redacted]
0.079	2	1700/1.0/RT	15	[redacted]	17.5	[redacted]	-625.5	[redacted]
0.096	3	1750/0.9/RT	20	[redacted]	21.4	[redacted]	-650.5	[redacted]
0.101	4	1750/1.1/RT	30	[redacted]	33.5	[redacted]	-901.0	[redacted]
0.102	5	1750/1.2/RT	40	[redacted]	43.5	[redacted]	-900.5	[redacted]
0.123	6	1750/1.0/RT	25	[redacted]	28.6	[redacted]	-822.5	[redacted]
0.146	7	1700/1.1/RT	20	[redacted]	22.5	[redacted]	-700.5	[redacted]

Table 4.4 Gap width distortion vs. retained austenite and residual stress after quenching

Gap Distortion (%)		Heat Treatment	RA-M (%)		RA-X (%)		RS-X (MPa)	
Value	Rank		Value	Rank	Value	Rank	Value	Rank
1.75	1	1700/0.9/RT	10	[redacted]	8.5	[redacted]	-429.0	[redacted]
1.98	2	1700/1.0/RT	15	[redacted]	17.5	[redacted]	-625.5	[redacted]
2.25	3	1750/0.9/RT	20	[redacted]	21.4	[redacted]	-650.5	[redacted]
2.54	4	1700/1.1/RT	20	[redacted]	22.5	[redacted]	-700.5	[redacted]
2.98	5	1750/1.0/RT	25	[redacted]	28.6	[redacted]	-822.5	[redacted]
3.10	6	1750/1.1/RT	30	[redacted]	33.5	[redacted]	-901.0	[redacted]
3.12	7	1750/1.2/RT	40	[redacted]	43.5	[redacted]	-900.5	[redacted]

Table 4.5 Flatness distortion vs. retained austenite and residual stress after quenching

Flatness Distortion (%)		Heat Treatment	RA-M (%)		RA-X (%)		RS-X (MPa)	
Value	Rank		Value	Rank	Value	Rank	Value	Rank
20.5	1	1700/0.9/RT	10	[redacted]	8.5	[redacted]	-429.0	[redacted]
31.4	2	1700/1.0/RT	15	[redacted]	17.5	[redacted]	-625.5	[redacted]
42.3	3	1700/1.1/RT	20	[redacted]	22.5	[redacted]	-700.5	[redacted]
62.9	4	1750/0.9/RT	20	[redacted]	21.4	[redacted]	-650.5	[redacted]
110.1	5	1750/1.0/RT	25	[redacted]	28.6	[redacted]	-822.5	[redacted]
125.2	6	1750/1.1/RT	30	[redacted]	33.5	[redacted]	-901.0	[redacted]
188.5	7	1750/1.2/RT	40	[redacted]	43.5	[redacted]	-900.5	[redacted]

Table 4.6 OD distortion vs. retained austenite and residual stress after 300°F/1hr tempering.

(a) Retained austenite is measured using an optical metallographic technique.

OD Distortion (%)		Heat Treatment	RA-M (%)		RS-X (MPa)	
Value	Rank		Value	Rank	Value	Rank
0.010	1	1750/1.1/300	25	▬▬▬▬▬	-888.0	▬▬▬▬▬▬
0.027	2	1700/0.9/300	5	▬	-370.0	▬
0.027	2	1750/0.9/300	15	▬▬▬	-645.5	▬▬▬
0.030	3	1700/1.1/300	15	▬▬▬	-645.5	▬▬▬
0.033	4	1700/1.0/300	10	▬▬	-559.5	▬▬
0.041	5	1750/1.0/300	20	▬▬▬▬	-800.5	▬▬▬▬
0.042	6	1750/1.2/300	40	▬▬▬▬▬▬▬	-874.5	▬▬▬▬▬

(b) Retained austenite is measured using a x-ray diffraction technique.

OD Distortion (%)		Heat Treatment	RA-X (%)		RS-X (MPa)	
Value	Rank		Value	Rank	Value	Rank
0.010	1	1750/1.1/300	29.5	▬▬▬▬▬▬▬	-888.0	▬▬▬▬▬▬▬
0.027	2	1700/0.9/300	4.0	▬	-370.0	▬
0.027	2	1750/0.9/300	20.0	▬▬▬	-645.5	▬▬▬
0.030	3	1700/1.1/300	20.1	▬▬▬▬	-645.5	▬▬▬▬
0.033	4	1700/1.0/300	12.5	▬▬	-559.5	▬▬
0.041	5	1750/1.0/300	25.0	▬▬▬▬▬	-800.5	▬▬▬▬
0.042	6	1750/1.2/300	40.0	▬▬▬▬▬▬▬▬	-874.5	▬▬▬▬▬

Table 4.7 Gap width distortion vs. retained austenite and residual stress after 300°F/1hr tempering.

(a) Retained austenite is measured using an optical metallographic technique.

Gap Distortion (%)		Heat Treatment	RA-M (%)		RS-X (MPa)	
Value	Rank		Value	Rank	Value	Rank
0.20	1	1700/0.9/300	5	▬	-370.0	▬
0.47	2	1750/0.9/300	15	▬▬▬	-645.5	▬▬▬
0.58	3	1750/1.0/300	20	▬▬▬▬	-800.5	▬▬▬▬
0.61	4	1700/1.0/300	10	▬▬	-559.5	▬▬
0.66	5	1700/1.1/300	15	▬▬▬	-645.5	▬▬▬
0.79	6	1750/1.1/300	25	▬▬▬▬▬	-888.0	▬▬▬▬▬▬
0.90	7	1750/1.2/300	40	▬▬▬▬▬▬▬	-874.5	▬▬▬▬▬

(b) Retained austenite is measured using a x-ray diffraction technique.

Gap Distortion (%)		Heat Treatment	RA-X (%)		RS-X (MPa)	
Value	Rank		Value	Rank	Value	Rank
0.20	1	1700/0.9/300	4.0	▬	-370.0	▬
0.47	2	1750/0.9/300	20.0	▬▬▬	-645.5	▬▬▬
0.58	3	1750/1.0/300	25.0	▬▬▬▬▬	-800.5	▬▬▬▬
0.61	4	1700/1.0/300	12.5	▬▬	-559.5	▬▬
0.66	5	1700/1.1/300	20.1	▬▬▬▬	-645.5	▬▬▬
0.79	6	1750/1.1/300	29.5	▬▬▬▬▬▬	-888.0	▬▬▬▬▬▬
0.90	7	1750/1.2/300	40.0	▬▬▬▬▬▬▬▬	-874.5	▬▬▬▬▬

Table 4.8 Flatness distortion vs. retained austenite and residual stress after 300°F/1hr tempering.

(a) Retained austenite is measured using an optical metallographic technique.

Flatness Distortion (%)		Heat Treatment	RA-M (%)		RS-X (MPa)	
Value	Rank		Value	Rank	Value	Rank
1.1	1	1750/0.9/300	15	■■■■	-645.5	■■■■
1.8	2	1750/1.1/300	25	■■■■■■	-888.0	■■■■■■■■
2.1	3	1700/1.1/300	15	■■■■	-645.5	■■■■
2.2	4	1700/1.0/300	10	■■■	-559.5	■■■
3.9	5	1700/0.9/300	5	■	-370.0	■
-8.3	6	1750/1.0/300	20	■■■■■	-800.5	■■■■■
26.2	7	1750/1.2/300	40	■■■■■■■■	-874.5	■■■■■■■

(b) Retained austenite is measured using a x-ray diffraction technique.

Flatness Distortion (%)		Heat Treatment	RA-X (%)		RS-X (MPa)	
Value	Rank		Value	Rank	Value	Rank
1.1	1	1750/0.9/300	20.0	■■■■	-645.5	■■■■
1.8	2	1750/1.1/300	29.5	■■■■■■■■	-888.0	■■■■■■■■
2.1	3	1700/1.1/300	20.1	■■■■■	-645.5	■■■■
2.2	4	1700/1.0/300	12.5	■■■	-559.5	■■■
3.9	5	1700/0.9/300	4.0	■	-370.0	■
-8.3	6	1750/1.0/300	25.0	■■■■■■	-800.5	■■■■■
26.2	7	1750/1.2/300	40.0	■■■■■■■■■	-874.5	■■■■■■■

Table 4.9 OD distortion vs. retained austenite and residual stress after 350°F/1hr tempering.

(a) Retained austenite is measured using an optical metallographic technique.

OD Distortion (%)		Heat Treatment	RA-M*(%)		RS-X* (MPa)	
Value	Rank		Value	Rank	Value	Rank
0.012	1	1750/0.9/350	15	[redacted]	-620.5	[redacted]
0.012	1	1750/1.1/350	25	[redacted]	-840.5	[redacted]
0.013	2	1750/1.0/350	20	[redacted]	-816.5	[redacted]
0.014	3	1700/1.0/350	10	[redacted]	-542.3	[redacted]
0.015	4	1700/1.1/350	15	[redacted]	-633.5	[redacted]
0.018	5	1750/1.2/350	35	[redacted]	-866.3	[redacted]
0.019	6	1700/0.9/350	5	[redacted]	-360.0	[redacted]

(b) Retained austenite is measured using a x-ray diffraction technique.

OD Distortion (%)		Heat Treatment	RA-X*(%)		RS-X* (MPa)	
Value	Rank		Value	Rank	Value	Rank
0.012	1	1750/0.9/350	18.5	[redacted]	-620.5	[redacted]
0.012	1	1750/1.1/350	26.0	[redacted]	-840.5	[redacted]
0.013	2	1750/1.0/350	23.2	[redacted]	-816.5	[redacted]
0.014	3	1700/1.0/350	10.0	[redacted]	-542.3	[redacted]
0.015	4	1700/1.1/350	17.5	[redacted]	-633.5	[redacted]
0.018	5	1750/1.2/350	36.5	[redacted]	-866.3	[redacted]
0.019	6	1700/0.9/350	4.0	[redacted]	-360.0	[redacted]

Table 4.10 Gap width distortion vs. retained austenite and residual stress after 350°F/1hr tempering.

(a) Retained austenite is measured using an optical metallographic technique.

Gap Distortion (%)		heat treatment	RA-M*(%)		RS-X* (MPa)	
Value	Rank		Value	Rank	Value	Rank
0.35	1	1700/0.9/350	5	▬	-360.0	▬
0.46	2	1750/0.9/350	15	▬▬▬	-620.5	▬▬▬
0.62	3	1700/1.0/350	10	▬▬	-542.3	▬▬
0.63	4	1750/1.0/350	20	▬▬▬▬	-816.5	▬▬▬▬▬
0.67	5	1700/1.1/350	15	▬▬▬	-633.5	▬▬▬▬
0.87	6	1750/1.1/350	25	▬▬▬▬▬	-840.5	▬▬▬▬▬▬
0.92	7	1750/1.2/350	35	▬▬▬▬▬▬	-866.3	▬▬▬▬▬▬▬

(b) Retained austenite is measured using a x-ray diffraction technique.

Gap Distortion (%)		heat treatment	RA-X*(%)		RS-X* (MPa)	
Value	Rank		Value	Rank	Value	Rank
0.35	1	1700/0.9/350	4.0	▬	-360.0	▬
0.46	2	1750/0.9/350	18.5	▬▬▬▬	-620.5	▬▬▬▬
0.62	3	1700/1.0/350	10.0	▬▬	-542.3	▬▬
0.63	4	1750/1.0/350	23.2	▬▬▬▬▬	-816.5	▬▬▬▬▬
0.67	5	1700/1.1/350	17.5	▬▬▬▬	-633.5	▬▬▬▬
0.87	6	1750/1.1/350	26.0	▬▬▬▬▬▬	-840.5	▬▬▬▬▬▬
0.92	7	1750/1.2/350	36.5	▬▬▬▬▬▬▬	-866.3	▬▬▬▬▬▬▬

Table 4.11 Flatness distortion vs. retained austenite and residual stress after 350°F/1hr tempering.

(a) Retained austenite is measured using an optical metallographic technique.

Flatness Distortion (%)		heat treatment	RA-M*(%)		RS-X* (MPa)	
Value	Rank		Value	Rank	Value	Rank
-0.6	1	1750/1.1/350	25	■■■■■■	-840.5	■■■■■■■■
1.2	2	1750/1.0/350	20	■■■■■	-816.5	■■■■■■■
2.3	3	1700/0.9/350	5	■	-360.0	■
3.3	4	1750/0.9/350	15	■■■■	-620.5	■■■■
4.7	5	1700/1.0/350	10	■■■	-542.3	■■■
4.8	6	1700/1.1/350	15	■■■■	-633.5	■■■■■
10.3	7	1750/1.2/350	35	■■■■■■■■	-866.3	■■■■■■■■■■

(b) Retained austenite is measured using a x-ray diffraction technique.

Flatness Distortion (%)		heat treatment	RA-X*(%)		RS-X* (MPa)	
Value	Rank		Value	Rank	Value	Rank
-0.6	1	1750/1.1/350	26.0	■■■■■■■■	-840.5	■■■■■■■■
1.2	2	1750/1.0/350	23.2	■■■■■■■	-816.5	■■■■■■■
2.3	3	1700/0.9/350	4.0	■	-360.0	■
3.3	4	1750/0.9/350	18.5	■■■■■	-620.5	■■■■
4.7	5	1700/1.0/350	10.0	■■■	-542.3	■■■
4.8	6	1700/1.1/350	17.5	■■■■	-633.5	■■■■■
10.3	7	1750/1.2/350	36.5	■■■■■■■■■	-866.3	■■■■■■■■■■

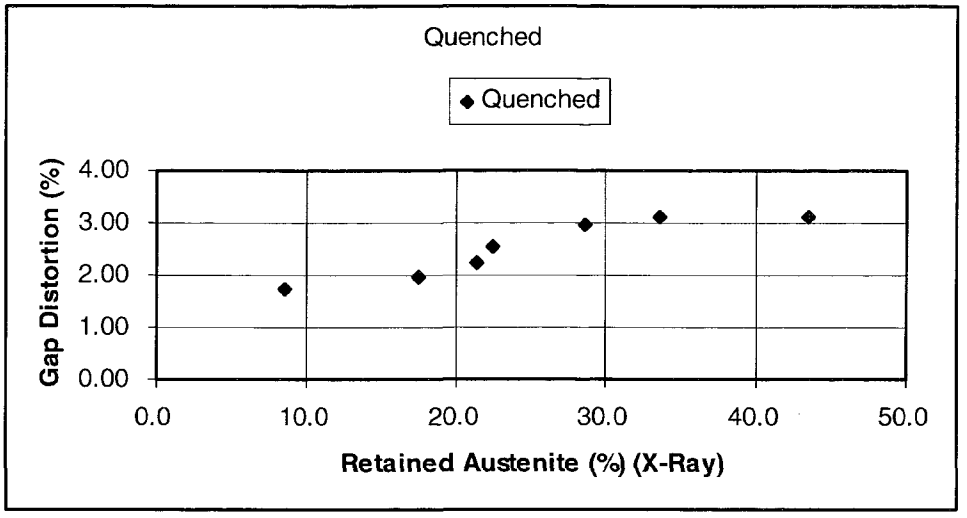

(a)

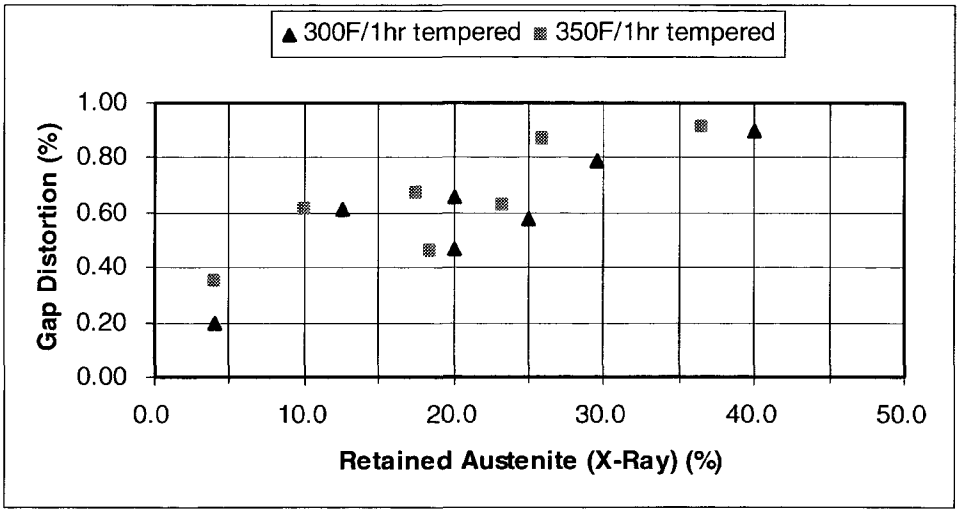

(b)

Fig. 4.7 Gap Distortion vs. Retained Austenite after quenching **(a)** and after quenching and tempering at 300°F or 350°F for 1 hour **(b)**.

Table 4.12 The lowest distortion vs. retained austenite and residual stress after quenching, quenching followed by 300°F/1hr tempering or 350°F/1hr tempering

Measuring Parameter	Distortion Absolute Value	Heat Treatment	RA-M (%)	RA-X (%)	RS-X (MPa)
OD	0.071	1700/0.9/RT	10	8.5	-429.0
	0.010	1750/1.1/300	25	29.5	-888.0
	0.012	1750/0.9/350	15	18.5	-620.5
	0.012	1750/1.1/350	25	26.0	-840.5
Gap Width	1.75	1700/0.9/RT	10	8.5	-429.0
	0.200	1700/0.9/300	5	4.0	-370.0
	0.350	1700/0.9/350	5	4.0	-360.0
Flatness	20.5	1700/0.9/RT	10	8.5	-429.0
	1.100	1750/0.9/300	15	20.0	-645.5
	0.600	1750/1.1/350	25	26.0	-840.5

4.4 Microstructure

Figs.4.8 (a) to 4.8 (u) shows optical photomicrographs of SAE 8620 C-ring specimens at all heat treated conditions. The dark material is martensite, while the surrounding light-colored material is austenite.

In all cases, the microstructure after 300°F tempering is not much different from the microstructure after 350°F tempering. Thus, changing the tempering temperature from 300°F to 350°F had little effect on the measured values for distortion, retained austenite and residual stress.

Figs. 4.9 (a) to 4.9 (l) are SEM photos of the Navy C-ring specimens carburized at the 1.0% carbon potential. For each specimen, two SEM photos are shown: one shows the microstructure of the case, the other shows the microstructure of the core area. The plate-like martensite is more readily seen in the core microstructure.

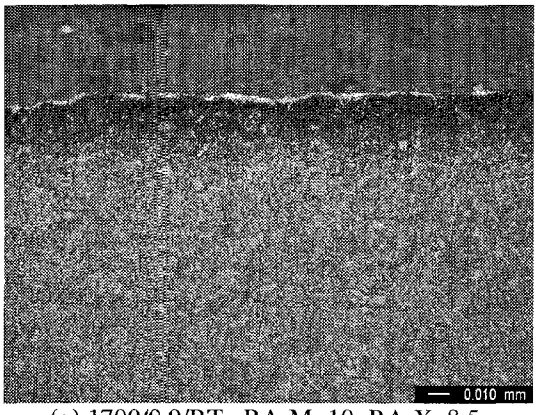

(a) 1700/0.9/RT. RA-M: 10; RA-X: 8.5.

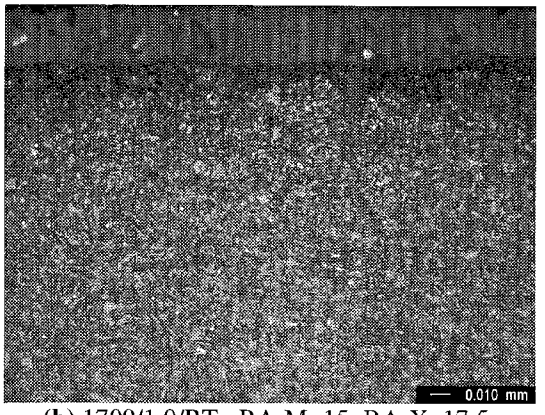

(b) 1700/1.0/RT. RA-M: 15; RA-X: 17.5.

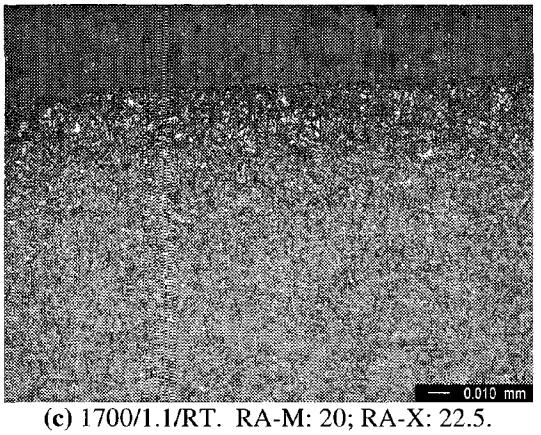

(c) 1700/1.1/RT. RA-M: 20; RA-X: 22.5.

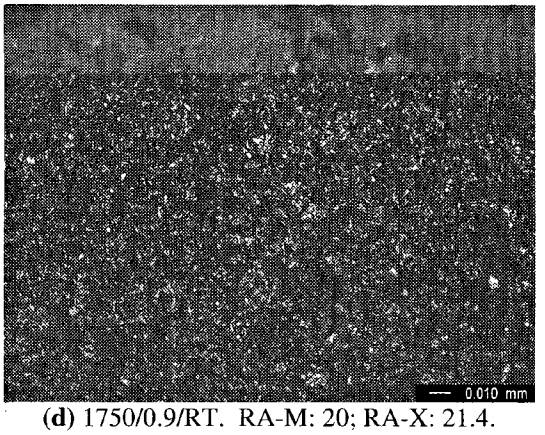

(d) 1750/0.9/RT. RA-M: 20; RA-X: 21.4.

Fig. 4.8 Photomicrographs of SAE 8620 C-ring specimens for all heat treatment conditions. The dark material is martensite, while the surrounding light-coloured material is austenite. **(a)** carburized at 1700°F for 6 hours at 0.9% carbon potential, quenched; **(b)** carburized at 1700°F for 6 hours at 1.0% carbon potential, quenched; **(c)** carburized at 1700°F for 6 hours at 1.1% carbon potential, quenched; **(d)** carburized at 1750°F for 4 hours at 0.9% carbon potential, quenched.

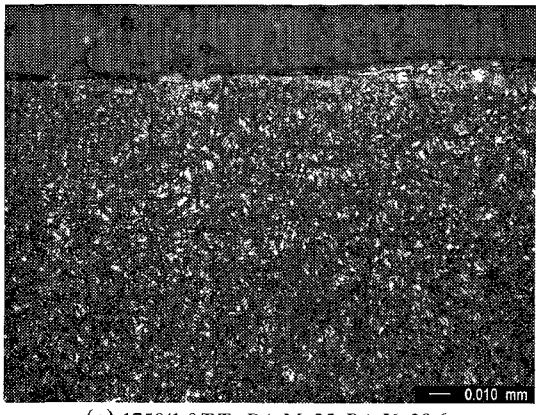

(e) 1750/1.0/RT. RA-M: 25; RA-X: 28.6.

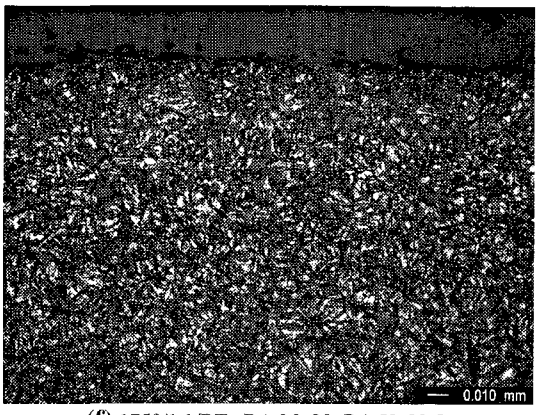

(f) 1750/1.1/RT. RA-M: 30; RA-X: 33.5.

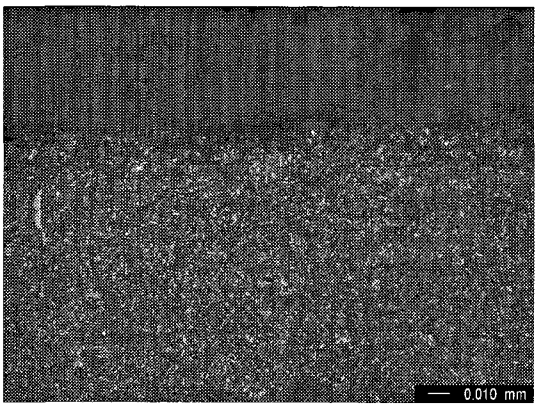

(g) 1700/0.9/300. RA-M: 5; RA-X: 4.0.

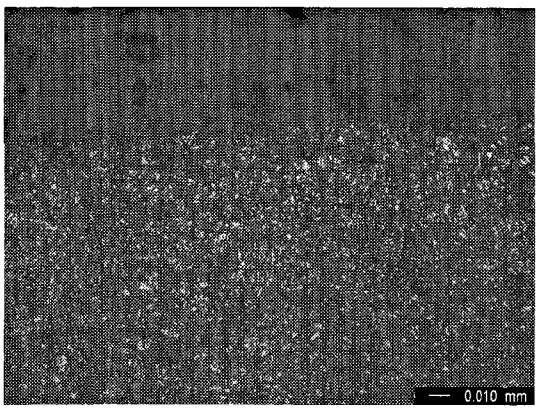

(h) 1700/1.0/300. RA-M: 10; RA-X: 12.5.

Fig. 4.8 Photomicrographs of SAE 8620 C-ring specimens for all heat treatment conditions. The dark material is martensite, while the surrounding light-coloured material is austenite. **(e)** carburized at 1750°F for 4 hours at 1.0% carbon potential, quenched; **(f)** carburized at 1750°F for 4 hours at 1.1% carbon potential, quenched; **(g)** carburized at 1700°F for 6 hours at 0.9% carbon potential, tempered at 300°F for 1 hour; **(h)** carburized at 1700°F for 6 hours at 1.0% carbon potential, tempered at 300°F for 1 hour.

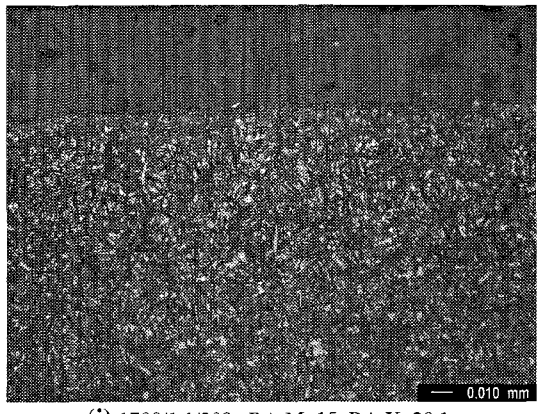

(i) 1700/1.1/300. RA-M: 15; RA-X: 20.1.

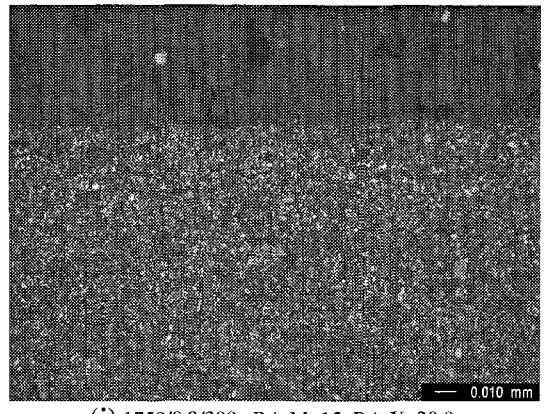

(j) 1750/0.9/300. RA-M: 15; RA-X: 20.0.

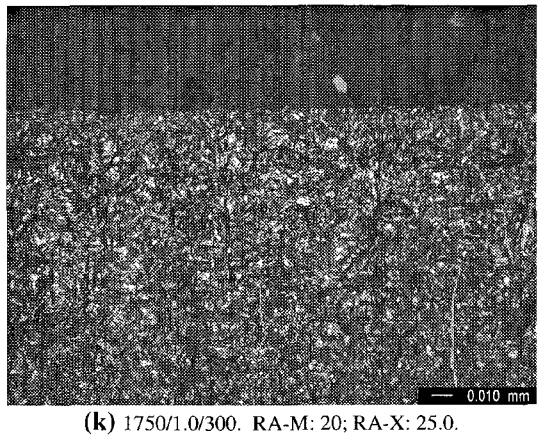

(k) 1750/1.0/300. RA-M: 20; RA-X: 25.0.

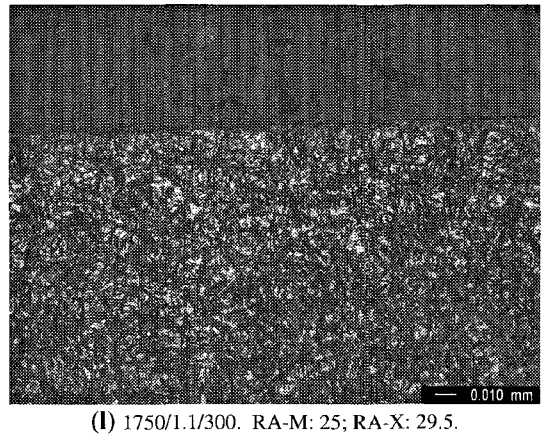

(l) 1750/1.1/300. RA-M: 25; RA-X: 29.5.

Fig. 4.8 Photomicrographs of SAE 8620 C-ring specimens for all heat treatment conditions. The dark material is martensite, while the surrounding light-coloured material is austenite. **(i)** carburized at 1700°F for 6 hours at 1.1% carbon potential, tempered at 300°F for 1 hour; **(j)** carburized at 1750°F for 4 hours at 0.9% carbon potential, tempered at 300°F for 1 hour; **(k)** carburized at 1750°F for 4 hours at 1.0% carbon potential, tempered at 300°F for 1 hour; **(l)** carburized at 1750°F for 4 hours at 1.1% carbon potential, tempered at 300°F for 1 hour.

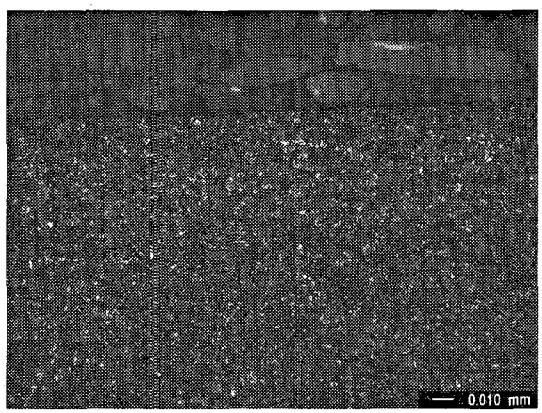

(m) 1700/0.9/350. RA-M: 5; RA-X: 4.0.

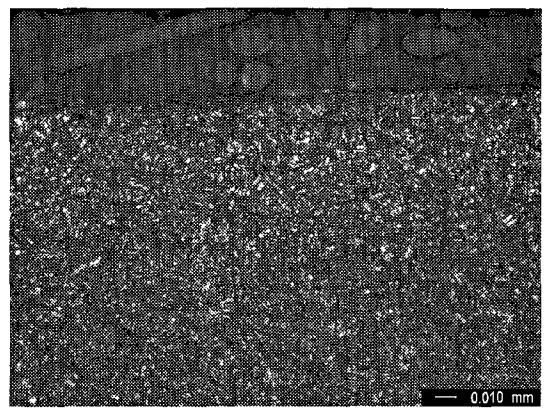

(n) 1700/1.0/350. RA-M: 10; RA-X: 10.0.

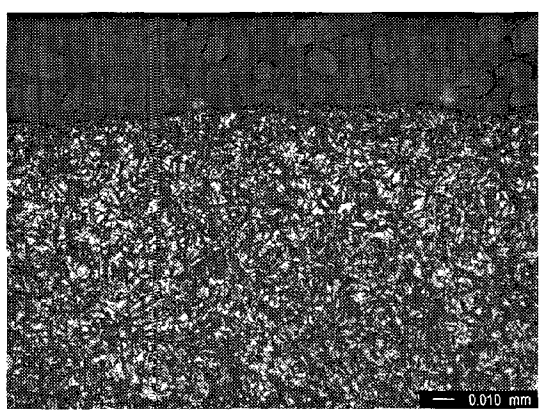

(o) 1700/1.1/350. RA-M: 15; RA-X: 17.5.

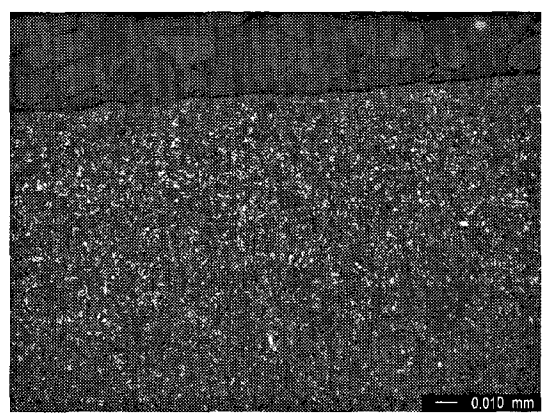

(p) 1750/0.9/350. RA-M: 15; RA-X: 18.5.

Fig. 4.8 Photomicrographs of SAE 8620 C-ring specimens for all heat treatment conditions. The dark material is martensite, while the surrounding light-coloured material is austenite. **(m)** carburized at 1700°F for 6 hours at 0.9% carbon potential, tempered at 350°F for 1 hour; **(n)** carburized at 1700°F for 6 hours at 1.0% carbon potential, tempered at 350°F for 1 hour; **(o)** carburized at 1700°F for 6 hours at 1.1% carbon potential, tempered at 350°F for 1 hour; **(p)** carburized at 1750°F for 4 hours at 0.9% carbon potential, tempered at 350°F for 1 hour.

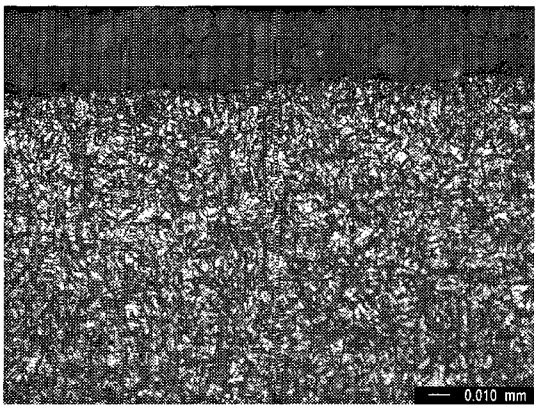

(q) 1750/1.0/350. RA-M: 20; RA-X: 23.2.

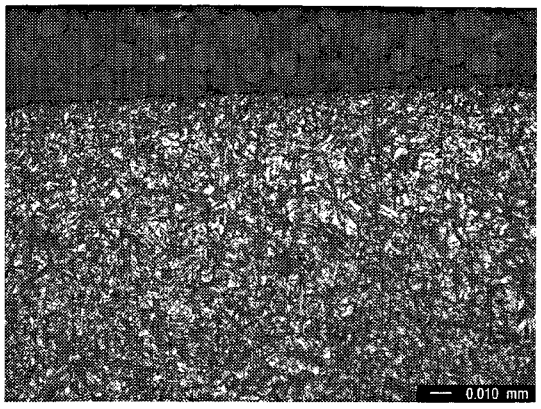

(r) 1750/1.1/350. RA-M: 25; RA-X: 26.0.

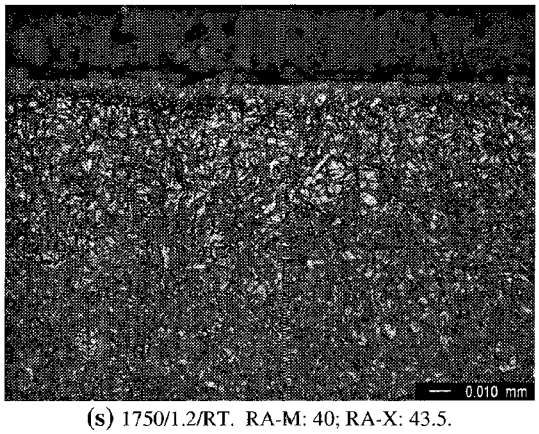

(s) 1750/1.2/RT. RA-M: 40; RA-X: 43.5.

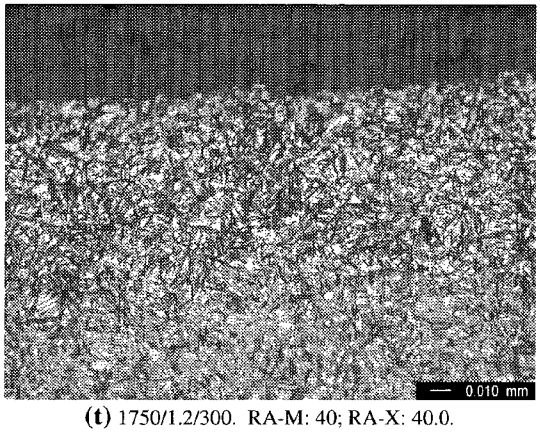

(t) 1750/1.2/300. RA-M: 40; RA-X: 40.0.

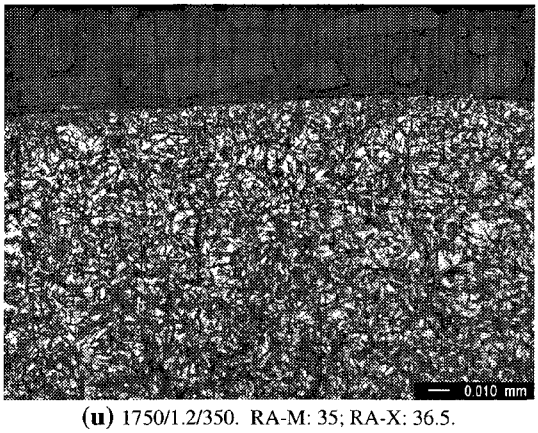

(u) 1750/1.2/350. RA-M: 35; RA-X: 36.5.

Fig. 4.8 Photomicrographs of SAE 8620 C-ring specimens for all heat treatment conditions. The dark material is martensite, while the surrounding light-coloured material is austenite. **(q)** carburized at 1750°F for 4 hours at 1.0% carbon potential, tempered at 350°F for 1 hour; **(r)** carburized at 1750°F for 4 hours at 1.1% carbon potential, tempered at 350°F for 1 hour; **(s)** carburized at 1750°F for 4 hours at 1.2% carbon potential, quenched; **(t)** carburized at 1750°F for 4 hours at 1.2% carbon potential, tempered at 300°F for 1 hour; **(u)** carburized at 1750°F for 4 hours at 1.2% carbon potential, tempered at 350°F for 1 hour.

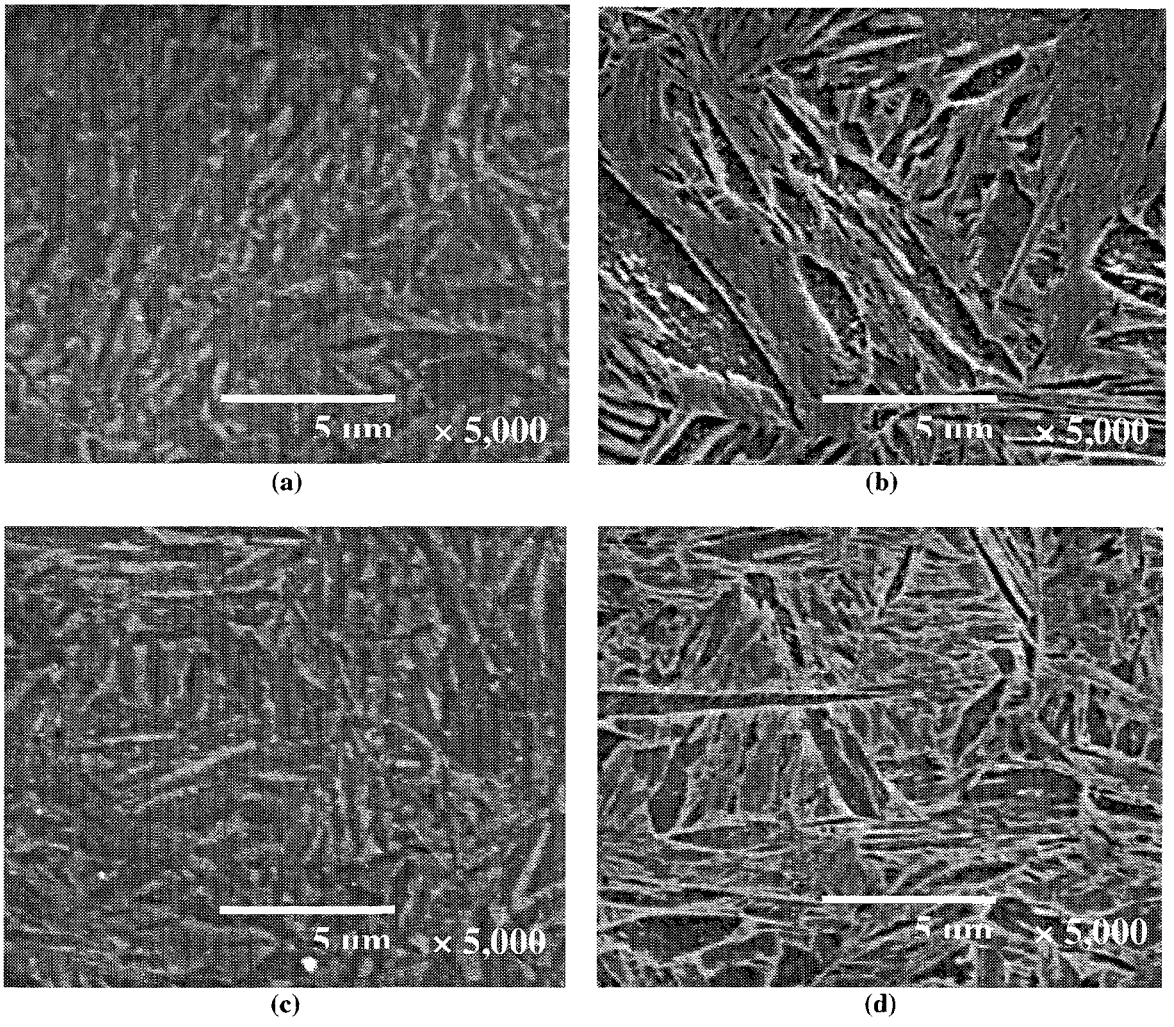

Fig. 4.9 SEM Micrographs of selected SAE 8620 C-ring specimens. All carburized at 1.0% carbon potential. **(a) / (b)** case / core micrograph of the specimen carburized at 1700°F for 6 hours, oil quenched; **(c) / (d)** case / core micrograph of the specimen carburized at 1700°F for 6 hours, oil quenched and tempered at 300°F for 1 hour.

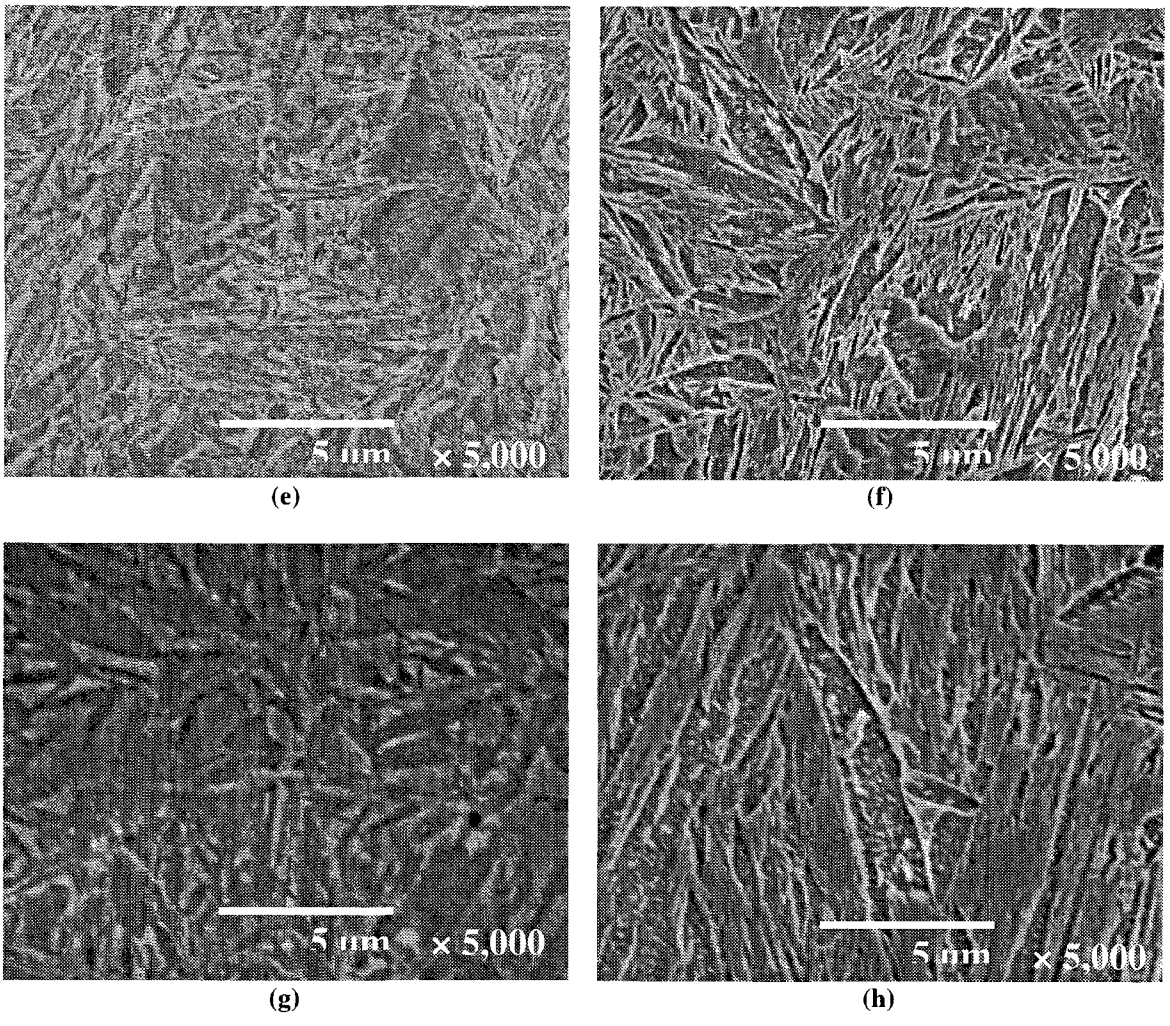

Fig. 4.9 SEM Micrographs of selected SAE 8620 C-ring specimens. All carburized at 1.0% carbon potential. **(e) / (f)** case / core micrograph of the specimen carburized at 1700°F for 6 hours, oil quenched and tempered at 350°F for 1 hour; **(g) / (h)** case / core micrograph of the specimen carburized at 1750°F for 4 hours, oil quenched.

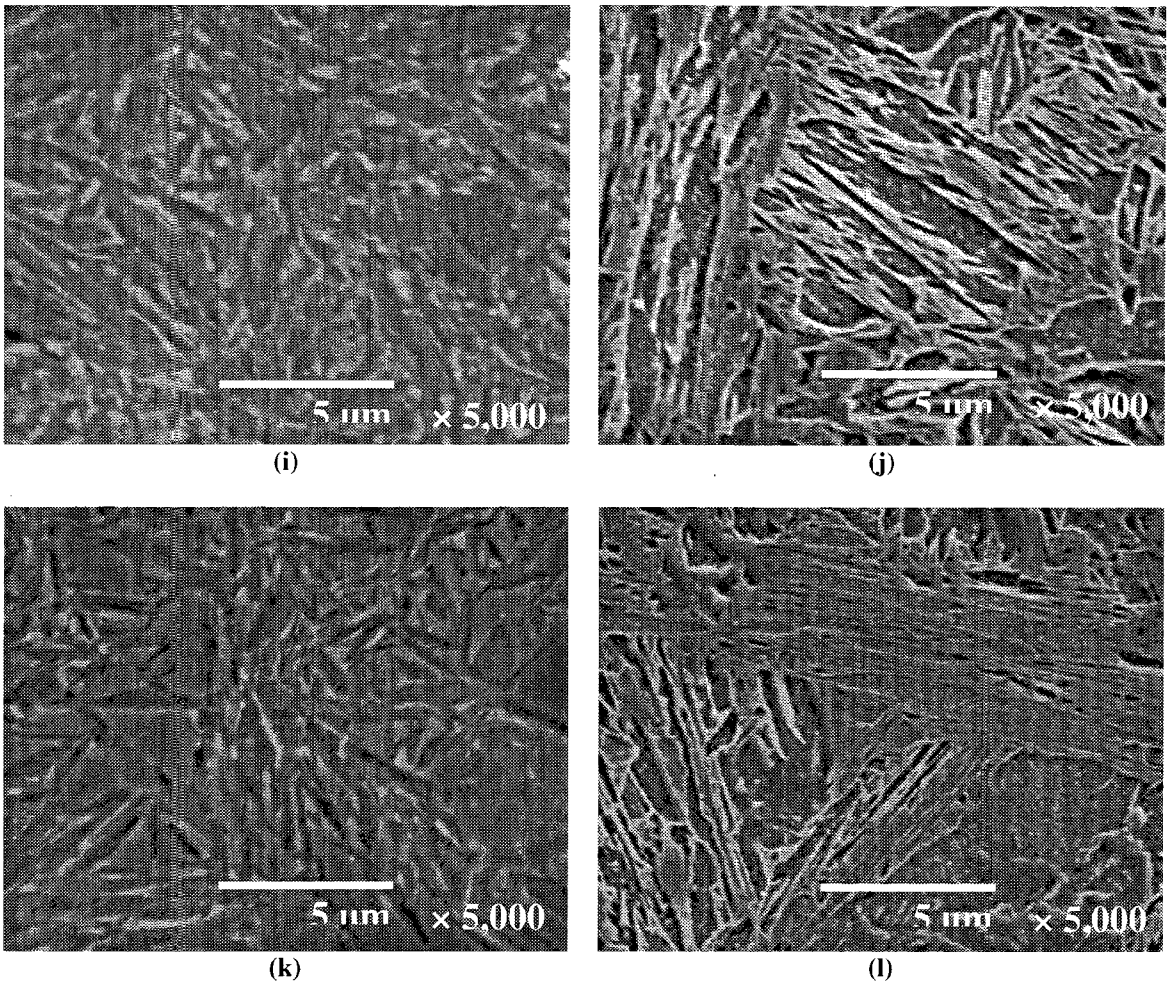

Fig. 4.9 SEM Micrographs of selected SAE 8620 C-ring specimens. All carburized at 1.0% carbon potential. **(i) / (j)** case / core micrograph of the specimen carburized at 1750°F for 4 hours, oil quenched and tempered at 300°F for 1 hour; **(k) / (l)** case / core micrograph of the specimen carburized at 1750°F for 4 hours, oil quenched and tempered at 350°F for 1 hour.

CHAPTER 5 THE EFFECT OF RETAINED AUSTENITE ON ID, THICKNESS, CYLINDRICITY AND ROUNDNESS DISTORTION OF SAE 8620 STEEL

In this chapter, the relationships between the heat treatment process parameters and the distortion parameters for ID, thickness, cylindricity and roundness are discussed. The optimum retained austenite and residual stress for the reduction of these four distortion parameters are detailed.

The distortion values for ID, thickness, cylindricity and roundness of the C-ring samples are summarized in Tables 5.1, 5.2, 5.3 and 5.4 respectively. The relationship between the ID distortion and process cycle is shown in Figure 5.1. Figure 5.2 shows the thickness distortion vs. process cycle. Figure 5.3 shows the cylindricity distortion vs. process cycle and Figure 5.4 shows the roundness distortion vs. process cycle.

From Figs 5.1, 5.2, 5.3 and 5.4, we can see that there is distortion as measured by these four parameters after carburizing and quenching / tempering. The ID, Fig. 5.1 and the thickness, Fig. 5.2, both increase. This is also due to the phase, and associated volume, change from austenite to martensite. From Figs 5.1, 5.2, 5.3 and 5.4, it can be seen that, in general, tempering reduces the distortion problem to some degree. Through relieving the internal stresses within the retained austenite, tempering helps eliminate the elastic deformation.

From Fig. 5.1 we can see the optimum heat treatment condition to reduce the ID distortion is 1750/1.2/300, i.e. carburized at 1750°F for 4 hours at 1.2% carbon potential, oil quenched and then tempered at 300°F for 1 hour. In this situation, the retained austenite content is 36.5%, Table 4.2, and the residual stress is -866.3MPa, Table 4.2. For the thickness distortion, Fig. 5.2, the optimum heat treatment condition is 1750/1.1/350,

i.e. carburized at 1750°F for 4 hours at 1.1% carbon potential, oil quenched and then tempered at 350°F for 1 hour. The retained austenite is 26.0%, Table 4.2, and the residual stress is –840.5MPa, Table 4.2. For the cylindricity distortion, Fig. 5.3, and the roundness distortion, Fig. 5.4, the optimum heat treatment condition is 1700/0.9/300, i.e. carburized at 1700°F for 6 hours at 0.9% carbon potential, oil quenched and then tempered at 300°F for 1 hour. The retained austenite is 4.0%, Table 4.2, and the residual stress is –370.0MPa, Table 4.2.

Figs. 5.5 and 5.6 are example plots for cylindricity and roundness, respectively. From Fig. 5.5 we can see that the deviation points (for cylindricity) for three inside cycles change their positions on quenching but then remain at the same location after tempering. As for the flatness distortion, the locations of largest deviation in the cylindricity measurements do not, in general, remain in the same location after tempering. From Fig. 5.6 we can see that the behaviour for roundness is similar to that for cylindricity, in that in most cases the positions of highest deviation from roundness change their positions during tempering.

Table 5.1 ID Distortion values of Navy-C ring specimens induced by heat treatments.

Cycle No.	Carburizing Temperature(°F) /Carbon Potential (%) /Tempering Temperature (°F)	ID Distortion			
		ID-1	ID-2	ID-3	Average
C1	1700/0.9/RT	0.0701	-0.0206	0.0620	0.0372
	1700/0.9/300	0.0862	-0.0794	0.0535	0.0201
	1700/0.9/350	0.0793	-0.0152	0.0670	0.0437
C2	1700/1.0/RT	0.2156	0.0984	0.1452	0.1531
	1700/1.0/300	0.2210	0.1041	0.1556	0.1602
	1700/1.0/350	0.1416	0.0104	0.0784	0.0768
C3	1700/1.1/RT	0.1502	-0.0256	0.0554	0.0600
	1700/1.1/300	0.0934	-0.0629	-0.0111	0.0065
	1700/1.1/350	0.1316	-0.0379	0.0199	0.0379
C4	1750/0.9/RT	0.1221	0.0133	0.1059	0.0804
	1750/0.9/300	0.0852	-0.0462	0.0083	0.0158
	1750/0.9/350	0.1071	0.0177	0.1218	0.0822
C5	1750/1.0/RT	0.1145	-0.0051	0.0101	0.0398
	1750/1.0/300	0.1123	-0.0564	-0.0003	0.0185
	1750/1.0/350	0.1039	-0.0525	0.0098	0.0204
C6	1750/1.1/RT	0.0536	-0.1175	-0.0694	-0.0444
	1750/1.1/300	0.0697	-0.0934	-0.0344	-0.0194
	1750/1.1/350	0.1053	-0.0298	0.0554	0.0436
C7	1750/1.2/RT	0.1715	0.0095	0.0888	0.0899
	1750/1.2/300	0.0846	-0.0804	-0.0136	-0.0031
	1750/1.2/350	0.1781	0.0174	0.0945	0.0967

Table 5.2 Thickness Distortion values of Navy-C ring specimens induced by heat treatments.

Cycle No.	Carburizing Temperature(°F) /Carbon Potential (%) /Tempering Temperature (°F)	Thickness Distortion			
		Thick-1	Thick-2	Thick-3	Average
	1700/0.9/RT	0.2117	0.1897	0.1955	0.1990
	1700/0.9/300	0.1517	0.1950	0.1180	0.1549
C1	1700/0.9/350	0.2049	0.1813	0.1908	0.1923
	1700/1.0/RT	0.3353	0.2755	0.1784	0.2631
	1700/1.0/300	0.1100	0.1850	0.1823	0.1591
C2	1700/1.0/350	0.1630	0.2011	0.1362	0.1668
	1700/1.1/RT	0.1931	0.2135	0.2140	0.2069
	1700/1.1/300	0.1116	0.1870	0.2205	0.1730
C3	1700/1.1/350	0.1965	0.2217	0.2177	0.2120
	1750/0.9/RT	0.1861	0.2882	0.2569	0.2437
	1750/0.9/300	0.1688	0.2656	0.2249	0.2198
C4	1750/0.9/350	0.1988	0.2354	0.1534	0.1959
	1750/1.0/RT	0.3878	0.4258	0.3690	0.3942
	1750/1.0/300	0.2390	0.2383	0.1602	0.2125
C5	1750/1.0/350	0.1856	0.2393	0.1691	0.1980
	1750/1.1/RT	0.3065	0.3202	0.2731	0.2999
	1750/1.1/300	0.2410	0.2666	0.2181	0.2419
C6	1750/1.1/350	0.1271	0.1902	0.0558	0.1244
	1750/1.2/RT	0.1607	0.2671	0.2404	0.2227
	1750/1.2/300	0.1367	0.2423	0.1861	0.1884
C7	1750/1.2/350	0.1776	0.1962	0.1270	0.1669

Table 5.3 Cylindricity Distortion values of Navy-C ring specimens induced by heat treatments.

Cycle No.	Carburizing Temperature(°F) /Carbon Potential (%) /Tempering Temperature (°F)	Cylindricity
C1	1700/0.9/RT	0.0600
	1700/0.9/300	0.0030
	1700/0.9/350	0.0564
C2	1700/1.0/RT	0.0593
	1700/1.0/300	0.0273
	1700/1.0/350	0.0594
C3	1700/1.1/RT	0.0331
	1700/1.1/300	0.0313
	1700/1.1/350	0.0287
C4	1750/0.9/RT	0.0536
	1750/0.9/300	0.0526
	1750/0.9/350	0.0184
C5	1750/1.0/RT	0.0975
	1750/1.0/300	0.0963
	1750/1.0/350	0.0342
C6	1750/1.1/RT	0.0246
	1750/1.1/300	0.0212
	1750/1.1/350	0.0233
C7	1750/1.2/RT	0.0348
	1750/1.2/300	0.0229
	1750/1.2/350	0.0352

Table 5.4 Roundness Distortion values of Navy-C ring specimens induced by heat treatments.

Cycle No.	Carburizing Temperature(°F) /Carbon Potential (%) /Tempering Temperature (°F)	Roundness			
		RD-1	RD-2	RD-3	Average
C1	1700/0.9/RT	-0.0003	0.0264	0.0205	0.0155
	1700/0.9/300	0.0080	0.0115	-0.0199	-0.0001
	1700/0.9/350	0.0000	0.0258	0.0196	0.0151
C2	1700/1.0/RT	-0.0007	0.0102	-0.0184	-0.0030
	1700/1.0/300	0.0009	0.0088	-0.0043	0.0018
	1700/1.0/350	-0.0014	0.0078	-0.0176	-0.0037
C3	1700/1.1/RT	0.0141	0.0172	0.0093	0.0135
	1700/1.1/300	0.0121	0.0161	0.0077	0.0120
	1700/1.1/350	0.0028	0.0162	0.0039	0.0076
C4	1750/0.9/RT	-0.0047	0.0101	0.0033	0.0029
	1750/0.9/300	-0.0046	0.0117	0.0034	0.0035
	1750/0.9/350	0.0012	0.0083	-0.0036	0.0020
C5	1750/1.0/RT	0.0501	0.0278	0.0513	0.0431
	1750/1.0/300	0.0183	0.0271	0.0217	0.0224
	1750/1.0/350	-0.0020	0.0050	-0.0052	-0.0007
C6	1750/1.1/RT	0.0128	0.0299	0.0159	0.0195
	1750/1.1/300	-0.0015	0.0161	0.0016	0.0054
	1750/1.1/350	0.0126	0.0305	0.0157	0.0196
C7	1750/1.2/RT	-0.0293	-0.0007	-0.0027	-0.0109
	1750/1.2/300	0.0103	0.0132	0.0040	0.0092
	1750/1.2/350	-0.0309	-0.0009	-0.0019	-0.0112

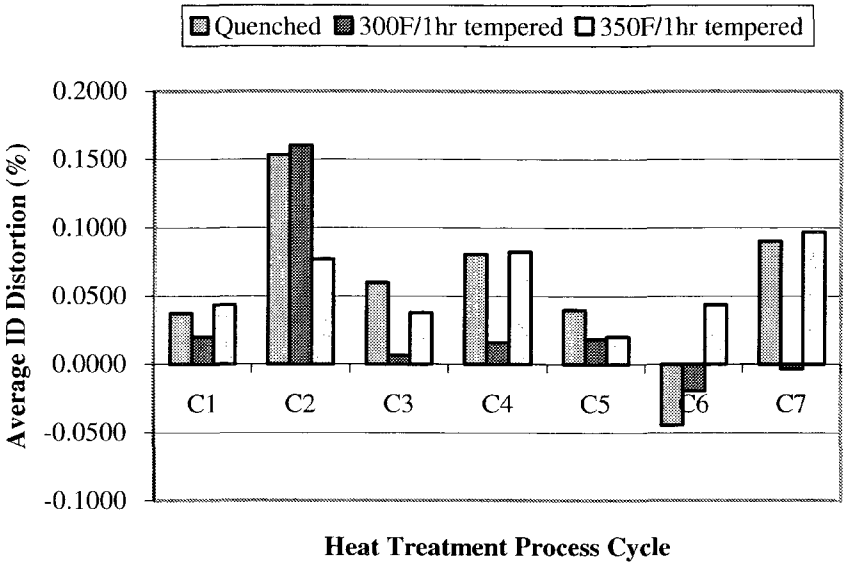

Fig. 5.1 ID distortion vs. heat treatment process cycle.

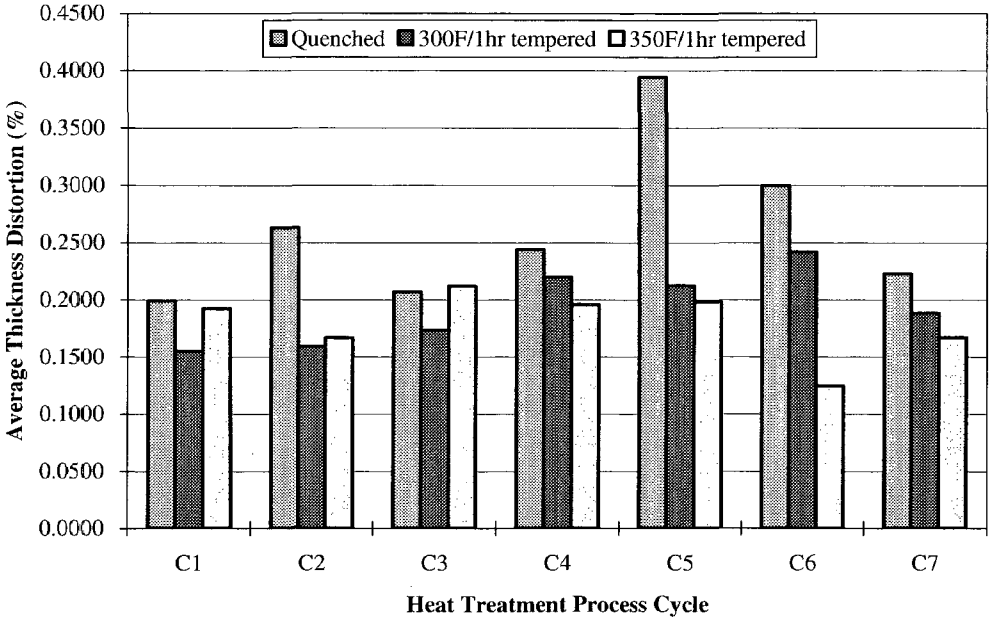

Fig. 5.2 Thickness distortion vs. heat treatment process cycle.

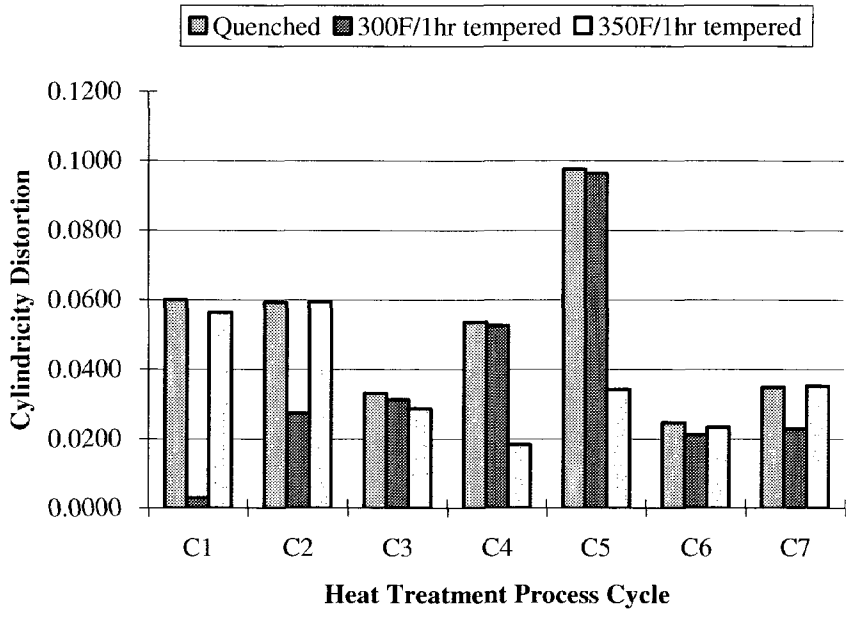

Fig. 5.3 Cylindricity distortion vs. heat treatment process cycle.

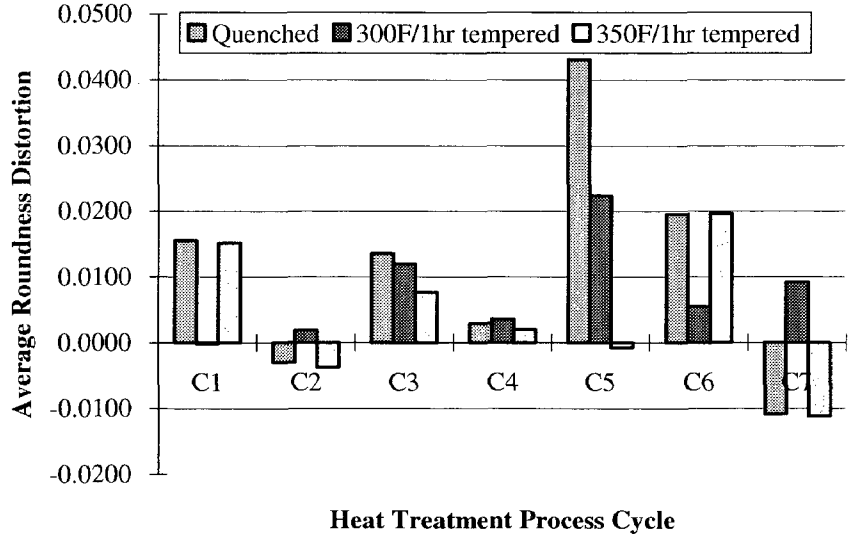

Fig.5.4 Roundess distortion vs. heat treatment process cycle.

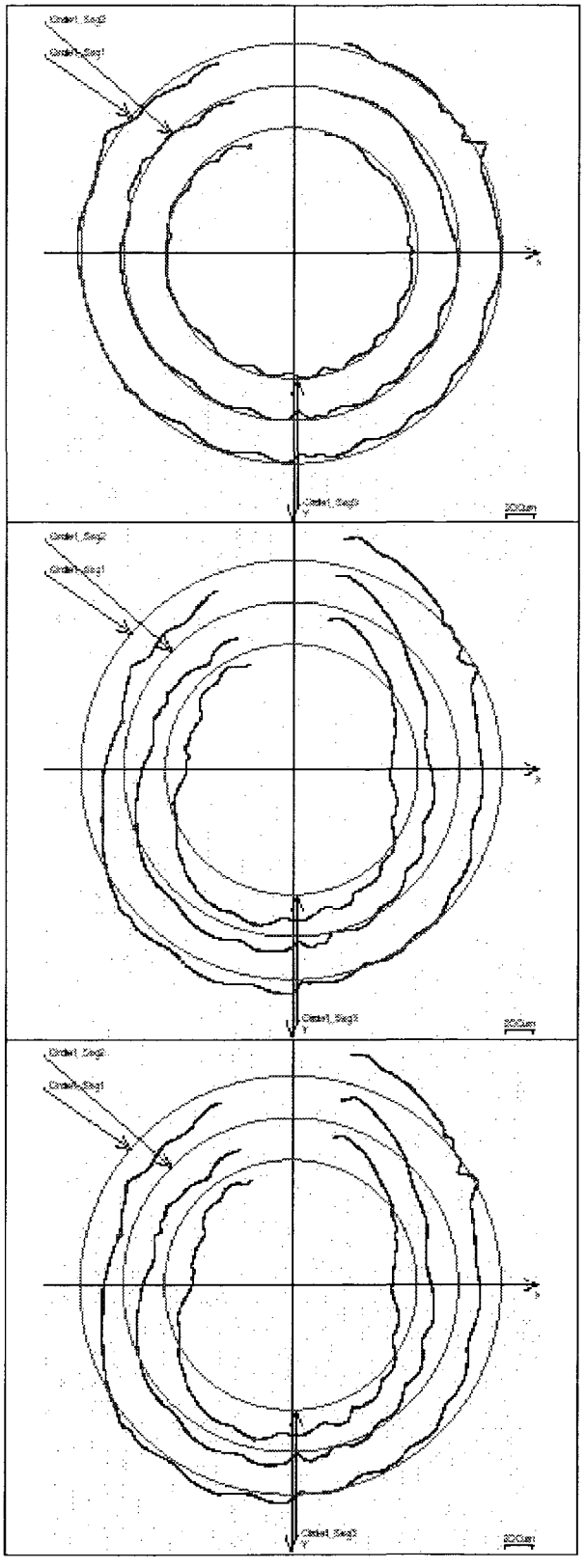

as-machined

1700F/1.1/RT

1700F/1.1/300

Figs. 5.5 Cylindricity distortion of specimens at heat treatment process cycle C3 (1700/1.1)

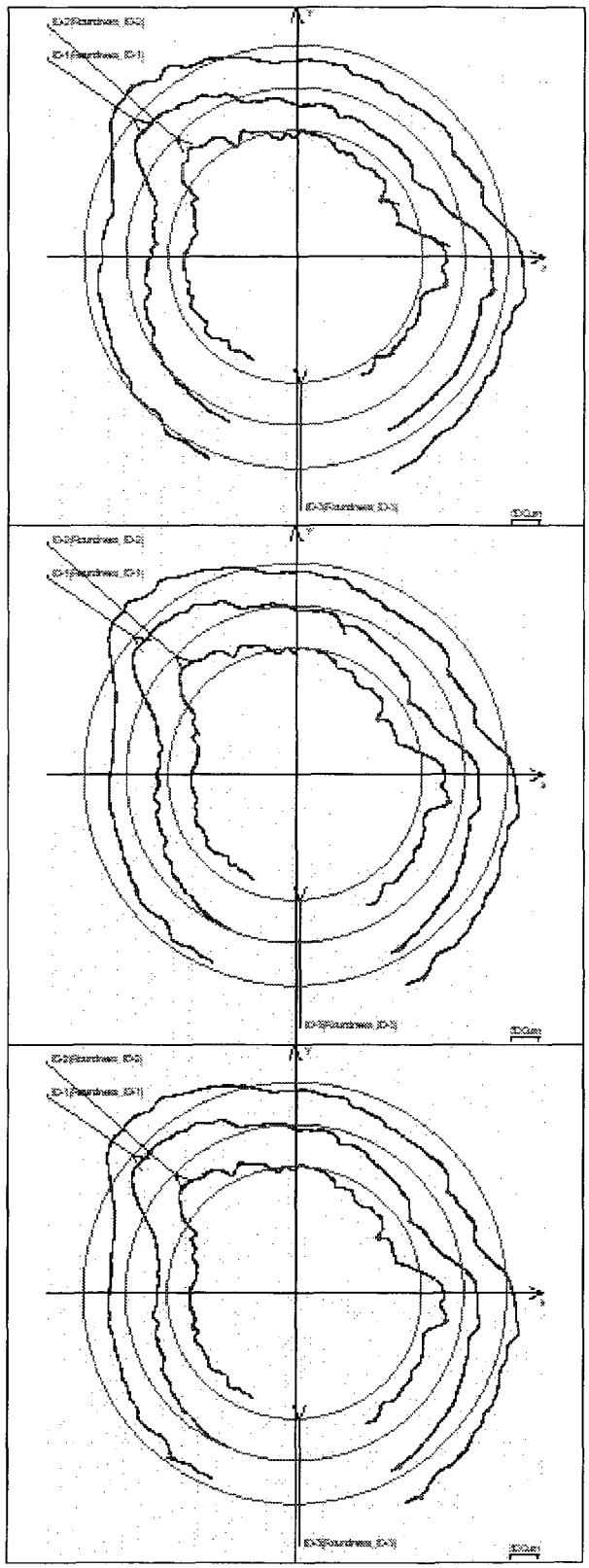

as-machined

1700F/1.1/RT

1700F/1.1/300

Figs. 5.6 Roundness distortion of specimens at heat treatment process cycle C3 (1700/1.1)

CHAPTER 6 HARDNESS PROFILES AND CARBON CONTENT

6.1 Hardness Profiles

Table 6.1, Figure 6.1 and Figure 6.2 (a) to (g) show the measured hardness profile results from the surface to the core in all of the as-quenched samples, i.e. not tempered. Figs 6.2 (a) to (g) are the individual profiles. From Figs 6.1 and 6.2(a) to (g) we can see that all the quenched C-ring samples have very similar hardness profiles. The peak hardness occurs at a distance from the surface of 0 ~ 0.01 inches. When the first indentation was placed at the harder martensite, the hardness was highest at the surface, as in the following specimens: 1700/0.9/RT, 1700/1.1/RT, 1750/0.9/RT, 1750/1.0/RT and 1750/1.1/RT. When the first indentation was placed at the softer retained austenite, or at the interface of the martensite and the retained austenite, the surface hardness was not the highest hardness, as in the following specimens: 1700/1.0/RT and 1750/1.2/RT. With increasing distance from the surface the amount of both retained austenite and carbon becomes smaller. Thus, the measured hardness reaches a maximum at a distance of about 0 to 0.01 inches from the surface and then decreases with increasing distance from the surface.

The effective case depths to HRC 50 of all quenched specimens are given in Table 6.2. The effective case depth varied between 0.051 to 0.060 inches. For the same carbon potential, the effective case depth increased slightly with increasing carburizing temperature.

Table 6.3 and Figure 6.3 show the surface hardness values for each heat treatment condition. It can be seen that tempering the as-quenched specimens decreases the

hardness at the surface. However, changing the tempering temperature from 300°F to 350°F has little effect on surface hardness.

6.2 Carbon Contents and Other Elemental Analysis as determined by OES

The elemental analyses at the surface as determined by OES are given in Table 6.4 for selected samples.

It is readily seen that the carbon content at the surface increases with increasing carburizing temperature and carbon potential. Since the amount of retained austenite also increases with the increasing carburizing temperature and carbon potential, it appears that, as expected, the amount of retained austenite increases with increasing carbon content.

Based on the data in Tables 6.2 and 6.4, Figure 6.4 has been constructed, showing the carbon content at the surface vs. effective case depth to HRC 50 for heat treatment processes, 1700/0.9/RT, 1700/1.0/RT and 1700/1.1/RT. From Fig. 6.4 we can see that there is no systematic relationship between the carbon content at the surface and the effective case depth to HRC 50.

Based on the data in Tables 6.3 and 6.4, Figure 6.5 has been constructed to show the relationship between carbon content at the surface and hardness at the surface. For the 1700F/6h carburized condition we can see that hardness at the surface increases with increasing carbon content at the surface. However, for the 1750F/4h carburized condition, the hardness at the surface decreases with increasing carbon content at the surface. It is well known that increasing the carbon content produces a harder martensite but it also increases the amount of the softer retained austenite. The hardness at surface will be a balance between that of the harder martensite and the softer retained austenite. For the 1700F/6h carburized condition, the effect of the harder martensite that is produced, more than compensates for the softer retained austenite. Thus, the hardness increases with the

increasing carbon content. For the 1750/4h carburized condition, the larger amount of the softer retained austenite more than offsets the effects of the harder martensite, and the hardness decreases with increasing carbon content.

The relationship between amount of retained austenite and the (surface) carbon content is shown in Figure 6.6, which is based on the data in Tables 4.2 and 6.4. We can readily see that the amount of retained austenite increases with increasing (surface) carbon content for both carburizing temperatures.

Table 6.1 Hardness profile of all quenched C-ring specimens (not tempered)

Distance from surface (inch)	1700/0.9/RT	1700/1.0/RT	1700/1.1/RT	1750/0.9/RT	1750/1.0/RT	1750/1.1/RT	1750/1.2/RT
	Hardness (HRC) (converted from micro)						
0.000	63.5	65.2	65.0	65.5	66.0	65.5	65.2
0.005	63.0	65.4	64.0	65.0	65.8	65.0	65.6
0.010	62.5	65.2	63.0	65.0	65.6	65.5	65.2
0.015	61.0	63.7	63.0	65.0	65.0	62.7	65.3
0.020	60.0	61.6	62.0	64.0	64.1	61.9	64.1
0.025	59.5	60.2	61.0	63.0	62.4	62.8	63.8
0.030	59.0	58.7	61.0	62.0	60.5	61.6	62.5
0.035	56.0	56.6	59.0	60.0	57.9	58.9	59.3
0.040	54.0	54.1	56.0	57.0	55.2	55.7	58.0
0.045	53.0	52.1	54.0	55.0	53.4	53.7	55.3
0.050	52.0	50.2	52.0	52.0	52.3	51.5	52.9
0.055	49.0	49.4	50.0	51.0	49.9	50.1	51.5
0.060	47.5	49.1	49.0	50.0	49.0	48.6	50.0
0.065	47.0	48.6	48.0	49.0	48.2	47.8	49.9
0.070	47.0	48.6	47.0	48.0	48.0	47.8	49.3
0.075	46.5	48.2	47.0	46.0	47.2	47.3	48.2
0.080	46.0	47.8	47.0	46.0	47.9	47.3	48.0
0.085	45.0	46.5	46.0	45.0	47.6	48.0	47.9
0.090	45.5	45.2	45.0	45.0	47.4	47.1	46.8
0.095	43.5	43.2	44.0	45.5	47.8	46.9	45.2
0.100	42.0	41.0	42.0	43.0	47.2	47.1	44.3

Table 6.2 Heat treatment process vs. effective case depth to HRC 50

Cycle No.	Carburizing Temp. (°F) /Carbon Potential (%) /Tempering Temp. (°F)	Effective Case Depth to HRC 50 (inch)
C1	1700/0.9/RT	0.0533
C2	1700/1.0/RT	0.0513
C3	1700/1.1/RT	0.0550
C4	1750/0.9/RT	0.0600
C5	1750/1.0/RT	0.0548
C6	1750/1.1/RT	0.0554
C7	1750/1.2/RT	0.0600

Table 6.3 The surface hardness (HRC) of C-ring specimens at all heat treatment conditions.

Cycle	Quenched	300 °F	350 °F
C1	64.0	63.0	60.5
C2	65.0	63.5	62.0
C3	66.0	64.0	62.0
C4	65.0	63.0	61.5
C5	65.0	63.0	61.5
C6	64.0	63.0	61.5
C7	64.0	63.0	61.0

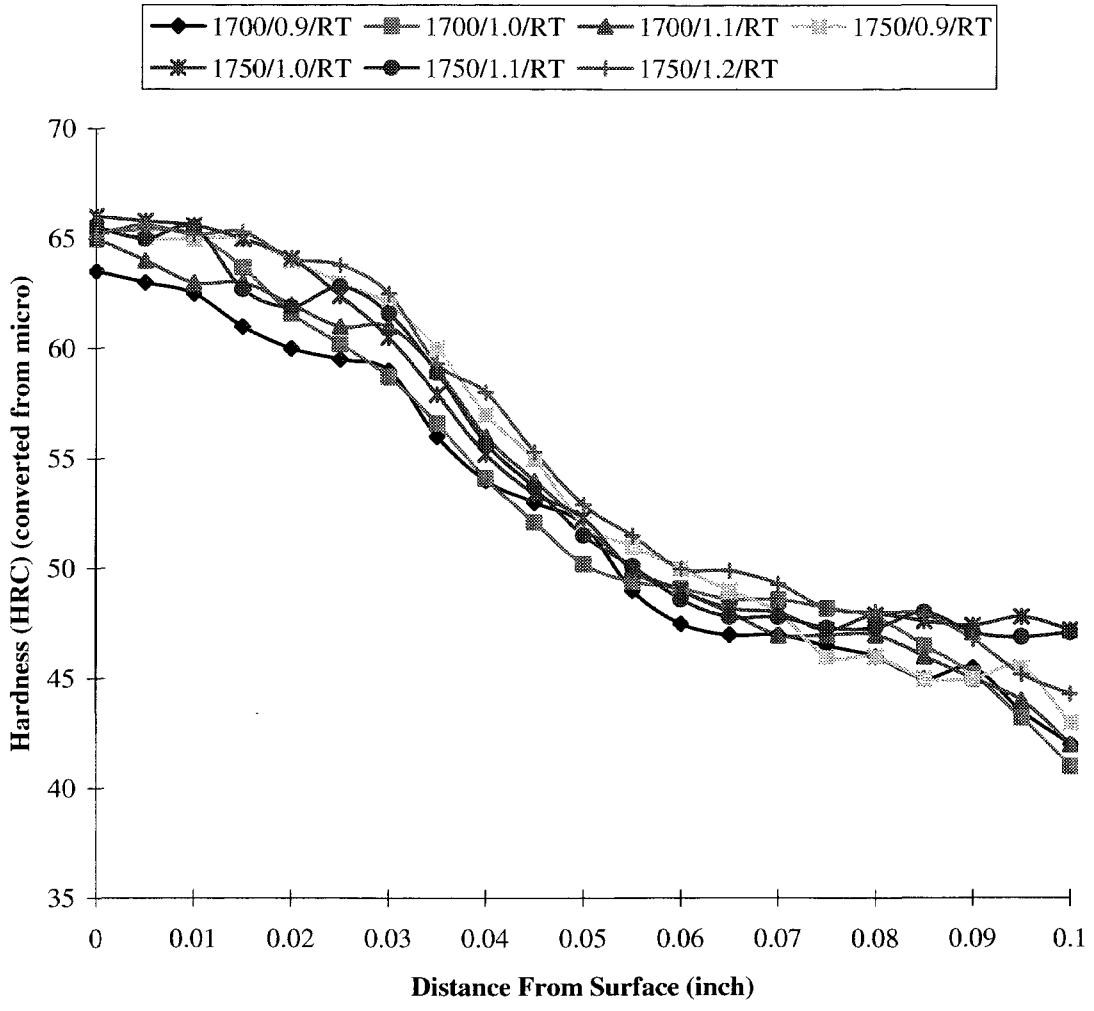

Fig. 6.1 Hardness profile of all quenched C-ring specimens.

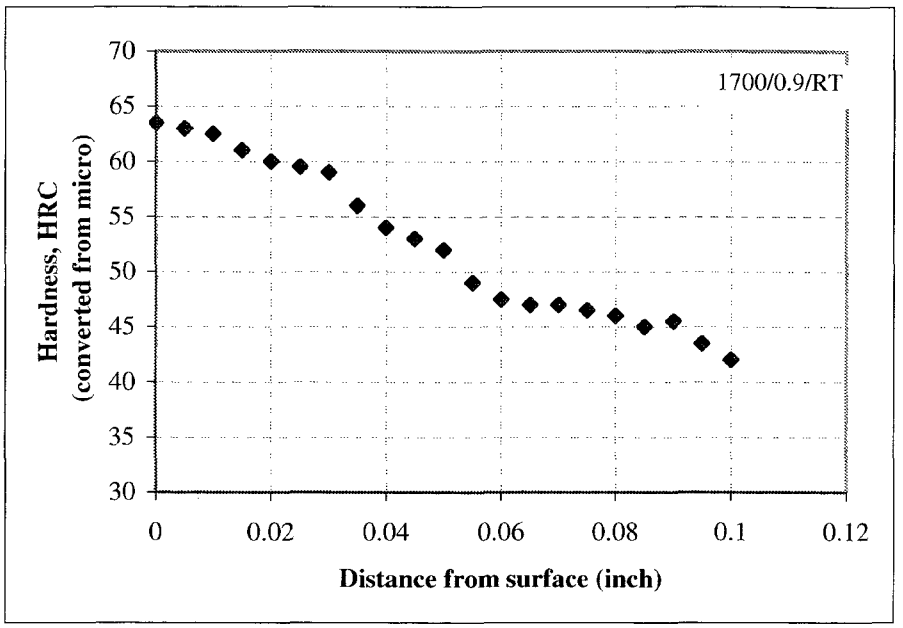

(a)

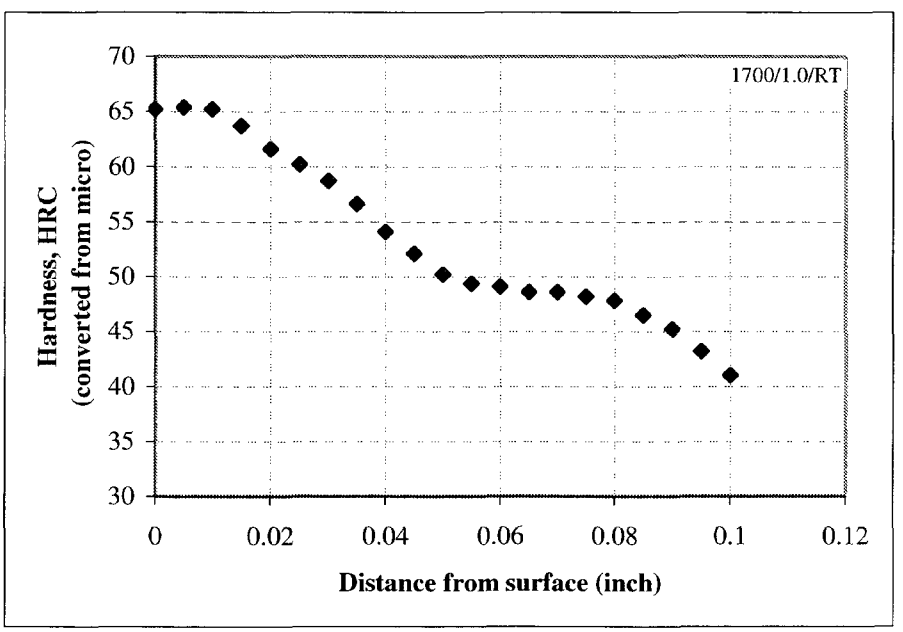

(b)

Fig.6.2 Hardness profiles of C-ring sample. **(a)** Carburized at 1700°F for 6 hours at 0.9% carbon potential and then oil quenched. **(b)** Carburized at 1700°F for 6 hours at 1.0% carbon potential and then oil quenched.

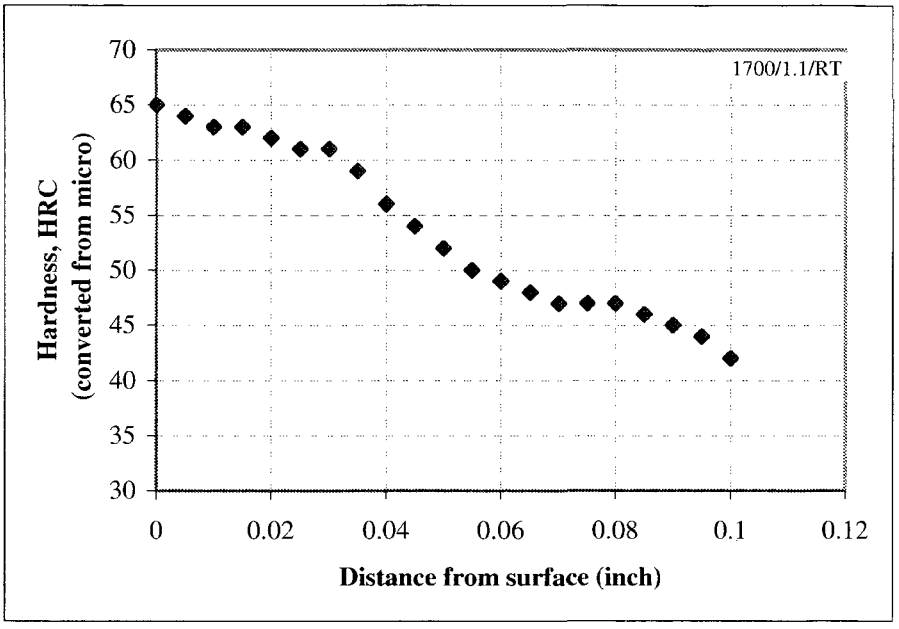

(c)

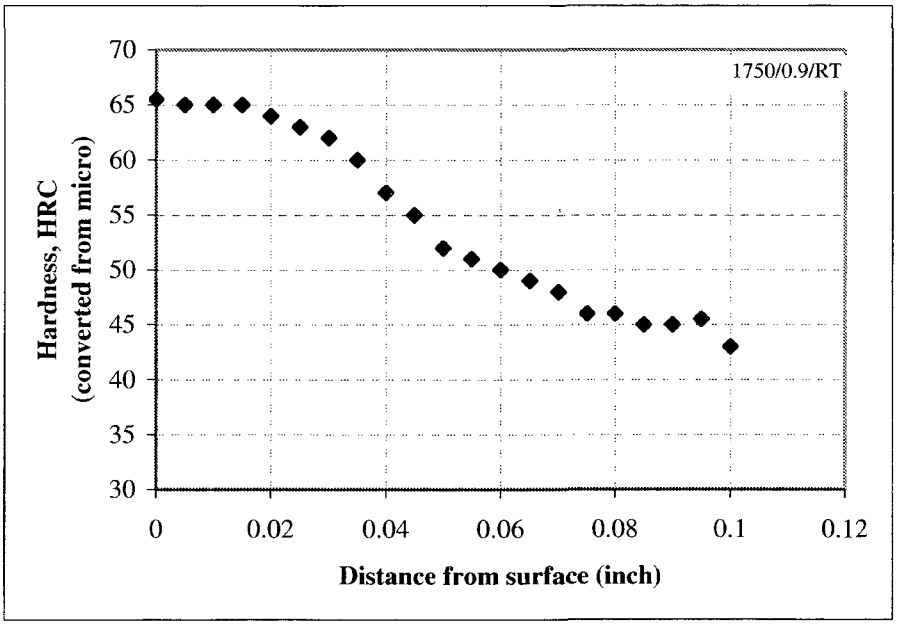

(d)

Fig.6.2 Hardness profiles of C-ring sample. **(c)** Carburized at 1700°F for 6 hours at 1.1% carbon potential and then oil quenched. **(d)** Carburized at 1750°F for 4 hours at 0.9% carbon potential and then oil quenched.

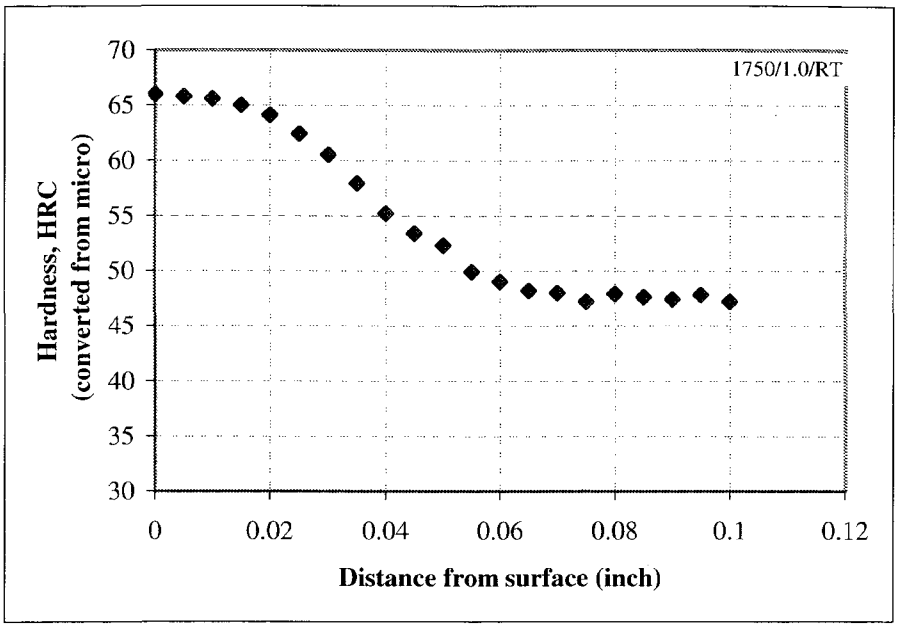

(e)

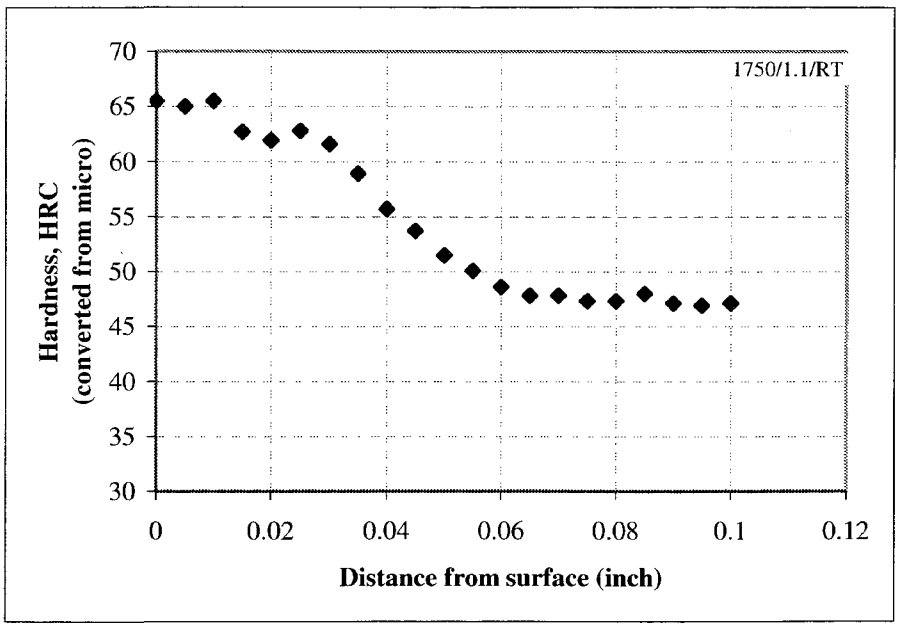

(f)

Fig.6.2 Hardness profiles of C-ring sample. **(e)** Carburized at 1750°F for 4 hours at 1.0% carbon potential and then oil quenched. **(f)** Carburized at 1750°F for 4 hours at 1.1% carbon potential and then oil quenched.

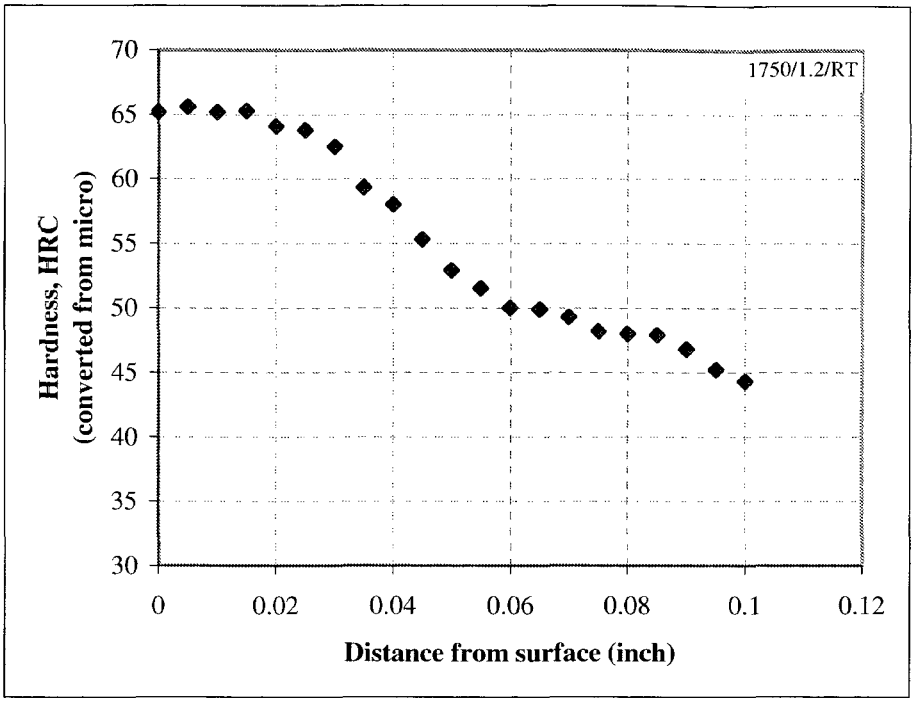

(g)

Fig.6.2 Hardness profiles of C-ring sample. **(g)** carburized at 1750˚F for 4 hours at 1.2% carbon potential and then oil quenched.

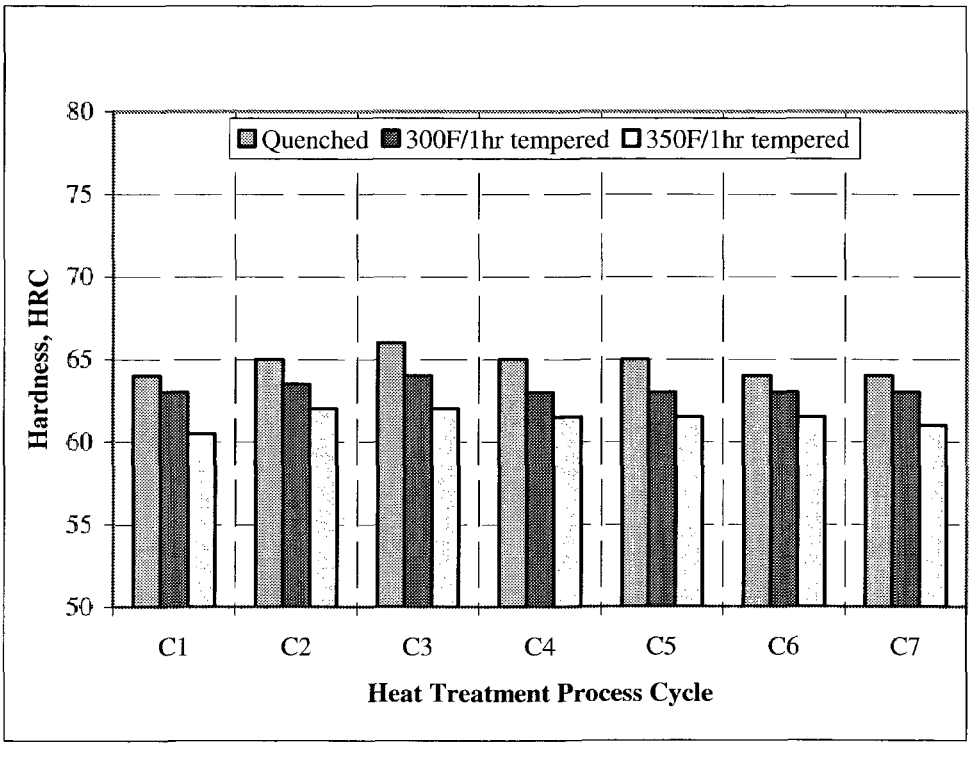

Fig. 6.3 Surface hardness of C-ring samples vs. heat treatment process cycle.

Table 6.4 Carbon contents at the surface of C-ring samples after heat treatment.

Element	Carburizing Temperature(°F) / Carbon Potential (%) /Tempering Temperature (°F)						
	1700/0.9/RT	1700/1.0/RT	1700/1.1/RT	1750/0.9/RT	1750/1.0/300	1750/1.1/300	1750/1.2/350
C	0.6700	0.8200	0.8600	0.7700	0.8400	0.8700	1.0000
Mn	0.7900	0.7300	0.6900	0.7000	0.8300	0.8400	0.7800
P	0.0140	0.0180	0.0160	0.0150	0.0140	0.0150	0.0160
S	0.0260	0.0210	0.0200	0.0200	0.0250	0.0280	0.0230
Si	0.2100	0.2000	0.2000	0.2000	0.2100	0.2200	0.2100
Cr	0.4700	0.4300	0.3900	0.4000	0.4800	0.4900	0.4500
Ni	0.5100	0.5000	0.5000	0.5000	0.5000	0.5000	0.5000
Mo	0.1800	0.1800	0.1800	0.1800	0.1800	0.1800	0.1800
Cu	0.2000	0.2000	0.2000	0.2000	0.2000	0.2100	0.2000
Al	0.0250	0.0250	0.0250	0.0250	0.0250	0.0250	0.0250
V	0.0040	0.0030	0.0030	0.0030	0.0040	0.0040	0.0040
Cb	ND	ND	ND	ND	ND	ND	ND
Ti	0.0030	0.0030	0.0030	0.0030	0.0030	0.0030	0.0030
Zr	ND	ND	ND	ND	ND	ND	ND
Co	0.0100	0.0100	0.0100	0.0100	0.0100	0.0100	0.0100
Sn	0.0100	0.0100	0.0100	0.0100	0.0100	0.0100	0.0100
B	0.0001	0.0001	0.0001	0.0001	0.0001	0.0001	0.0001
Pb	ND	ND	ND	ND	ND	ND	ND
Ca	0.0014	0.0011	0.0012	0.0014	0.0011	0.0012	0.0011
W	ND	ND	ND	ND	ND	ND	ND

ND = None Detected

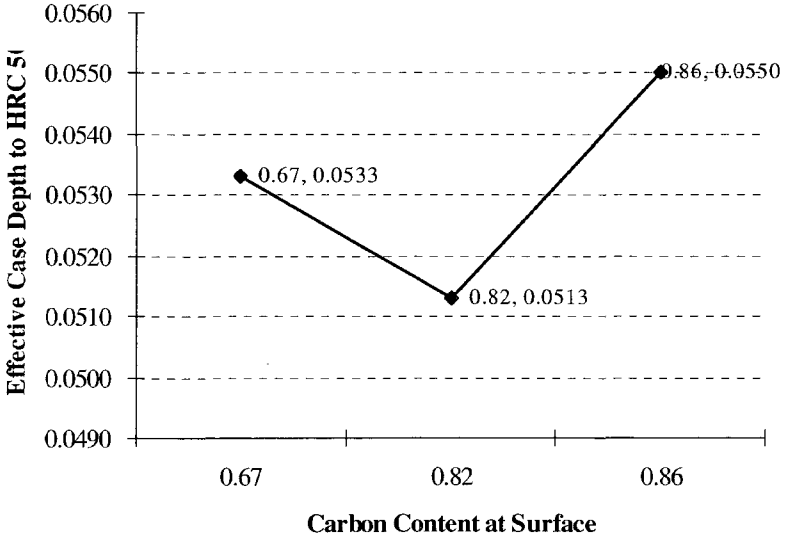

Fig. 6.4 Carbon content at surface vs. effective case depth to HRC 50

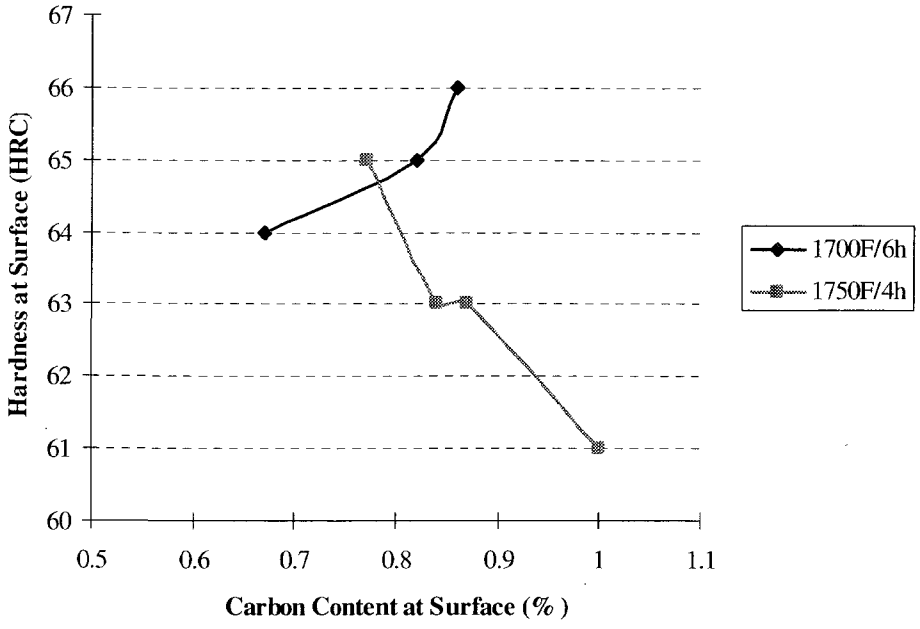

Fig. 6.5 Carbon content at surface vs. hardness at surface

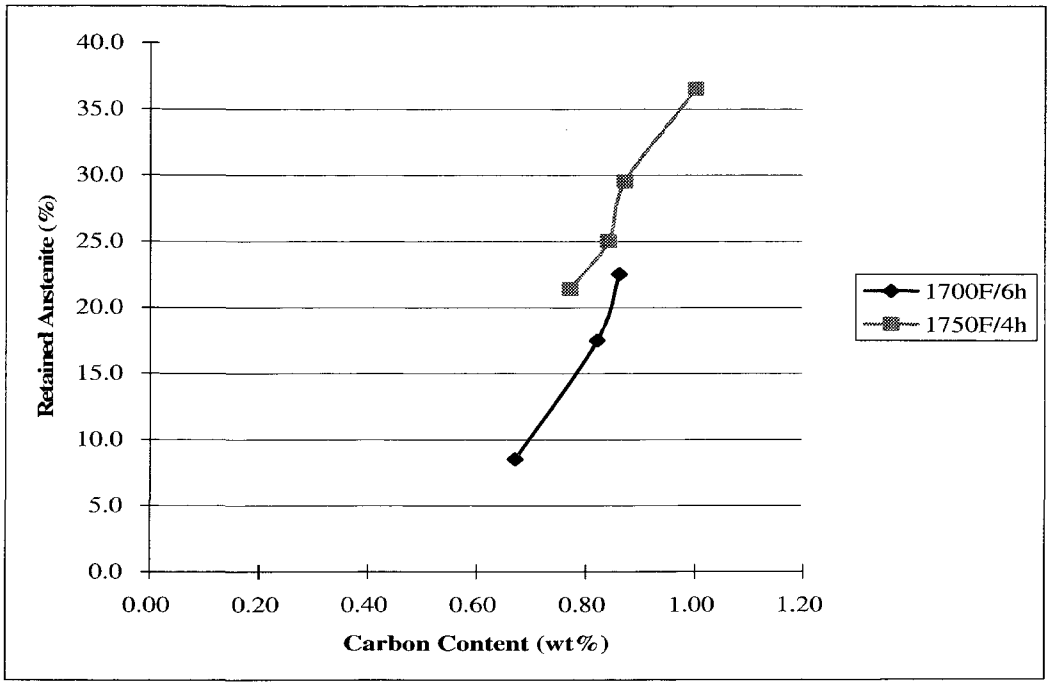

Fig. 6.6 The relationship between carbon content and retained austenite

CHAPTER 7 CONCLUSIONS AND RECOMMENDATIONS FOR FUTURE WORK

7.1 Conclusions

This study has examined the effects of retained austenite, residual stress and other metallurgical parameters on the distortion of a carburized SAE 8620 steel. The dimensional changes of specially designed Navy C-ring specimens were investigated after heat treatment at a series of 21 different heat treatment conditions.

Based on the distortion measurements for 3 key parameters, namely, OD (outside diameter), gap width and flatness, the main conclusions are as follows:

1. The amount of retained austenite and the residual stress increase with increasing carburizing temperature and carbon potential. For heat treatment process cycles C1, C2, C3, i.e. specimens that were carburized at 1700F/6h, both the amount of retained austenite and the residual stress increase with increasing carbon potential from 0.9% to 1.1%. The same behaviour was found for heat treatment process cycles C4, C5, C6 and C7, i.e. specimens that were carburized at 1750F/4h. The amount of retained austenite increases with increasing carbon content. For the same carbon potential, the amount of retained austenite and level of residual stress at the 1750°F carburizing temperature are higher than for the 1700°F carburizing temperature. This observation reflects the effect of austenitizing temperature on the amount of retained austenite and the residual stress level.
2. The amount of retained austenite and the level of residual stress both decrease with increasing tempering temperature from 300 to 350F. However, the changes are not large.

3. Distortion is influenced both by the amount of retained austenite and the magnitude of the residual stress. After quenching, the distortion as measured by changes in gap width and flatness, becomes more severe with increasing levels of retained austenite / residual stress. A combination of 8.5% austenite and -429.0MPa residual stress, produces the lowest values for distortion. The distortion increases with the increasing amount of retained austenite and level of residual stress, reaching a maximum for the sample with 43.5% retained austenite and -900.5MPa residual stress. The OD distortion shows similar, but not identical behaviour to the gap width and flatness distortion.
4. After tempering, the relationship between the retained austenite / residual stress levels and the distortion of the OD, gap width and flatness is not as well defined as for the quenched specimens. The lowest OD distortion occurs for the specimen 1750/1.1/300 (carburized at 1750°F for 4 hours at 1.1% carbon potential, oil quenched and then quenched at 300°F for 1 hour), which contains 29.5% retained austenite and a -888.0MPa residual stress. For the gap width distortion the lowest distortion is for the 1700/0.9/300 specimen (carburized at 1700°F for 6 hours at 0.9% carbon potential, oil quenched and then tempered at 300°F for 1 hour), with only 4.0% retained austenite and a -370.0MPa residual stress. For the flatness distortion, the lowest distortion is for the 1750/1.1/350 specimen (carburized at 1750°F for 4 hours at 1.1% carbon potential, oil quenched and tempered at 350°F for 1 hour), with 26.0% retained austenite and a -840.5MPa residual stress. Therefore, it is necessary to know which distortion parameter(s) is the most important in the actual application so as to design the proper heat treatment process to produce the desired retained austenite and residual stress levels.

5. Based on the average distortion data (OD, ID & Flatness) for the tempered specimens, which is the condition in which this steel is typically used, the optimum amount of retained austenite was about 25% (25% using optical metallographic technique; 26% using X-ray diffraction technique). The heat treatment condition was 1750/1.1/350 (carburized at 1750°F for 4 hours at 1.1% carbon potential, oil quenched and then tempered at 350°F for 1 hour) where the residual stress value was -840.5 MPa. However, as with conclusion 4, it should be emphasised that in any practical industrial application, there would be a need to consider the type of distortion that we were attempting to minimize, size (OD, ID, Thickness or Gap Width) or shape (flatness, roundness or cylindricity). The "optimum" retained austenite content of 25% is based on minimizing the average distortion, as measured by a combination of size and shape distortion parameters, for the limited number (21) of heat treatment process cycles examined in this study.
6. Quenched C-ring specimens all have very similar hardness profiles: the peak hardness occurs at a distance from the surface of 0 ~ 0.01 inches. With increasing distance from the surface, the hardness decreases, reflecting the balance between the harder martensite and the softer retained austenite. The effective case depths to HRC 50 are in the range of 0.05 to 0.06 inches. After tempering, the hardness at the surface decreases. However, changing the tempering temperature from 300°F to 350°F has little effect on hardness.
7. The carbon content at the surface increases with increasing carburizing temperature and carbon potential. Since the amount of retained austenite also increases with the increasing carburizing temperature and carbon potential, it appears that the amount of retained austenite increases with increasing carbon content at the surface.

8. In all cases, the microstructure after 300°F tempering is not obviously different from the microstructure after 350°F tempering. Thus, changing the tempering temperature from 300°F to 350°F has a little effect on the values of distortion, retained austenite and residual stress. On average, 350F tempering produces a 1.5 to 2.5 HRC reduction in hardness compared to 300F tempering.

Based on the distortion of ID (inside diameter), thickness, roundness and cylindricity the main results are as the follows:

1. After carburizing and quenching / tempering, there is distortion of all four parameters. The ID and thickness increase because the transformation of the retained austenite to martensite is associated with a volume expansion. Generally, tempering reduces the level of distortion of ID, thickness, cylindricity and roundness, but to a lesser degree than the distortion of OD, gap width and flatness.
2. The optimum heat treatment condition for reduction of ID distortion is 1750/1.2/300, i.e. carburized at 1750°F for 4 hours at 1.2% carbon potential, oil quenched and then tempered at 300°F for 1 hour. For this heat treatment condition, the amount of retained austenite is 36.5%, and the residual stress is -866.3MPa. For the thickness distortion, the optimum heat treatment condition to reduce distortion is 1750/1.1/350, i.e. carburized at 1750°F for 4 hours at 1.1% carbon potential, oil quenched and then tempered at 350°F for 1 hour. The amount of retained austenite is 26.0%, and the residual stress is –840.5MPa. For both the cylindricity and roundness distortions, the optimum heat treatment condition is 1700/0.9/300, i.e. carburized at 1700°F for 6 hours at 0.9% carbon potential, oil quenched and then tempered at 300°F for 1 hour. The amount of retained austenite is 4.0%, and the residual stress is –370.0MPa. Again, it must be emphasised that these "optimum" heat treatment conditions are

defined based on both minimizing the distortion for an individual distortion parameter and the limited number of heat treatment process cycles examined.

7.2 Recommendations For Future Work

1. In this study the amount of retained austenite and the residual stress were only measured at the specimen surface. The distribution of the retained austenite and the residual stress through the thickness should be measured. This will give greater insights into the changes in the various distortion parameters.
2. In this study the quenching position of all specimens was horizontal. In future work, different quenching positions such as vertical-gap down, vertical-gap up and vertical -gap side should be investigated. The different start positions for quenching in the nonuniform-wall thickness specimens will lead to different cooling rates in different directions, which will influence the severity and direction of distortion.
3. The Navy-C ring specimen can provide information on two types of distortion parameters, namely, size distortion and shape distortion. In the production of automotive components with varying geometries, these two types of distortion parameters (size and shape) have varying influences on the final distortion of the component due to heat treatment. A factorial design series of experiments should be carried out to investigate the effect of various process and metallurgical parameters on particular size, or shape, distortion parameters.
4. Use a Finite Element Analysis (FEA) technique to simulate the microstructural distribution from the surface to the core. Based on the microstructural distribution, FEA can also be used to predict the hardness and residual stress distributions from the surface to the core.

APPENDIX

EXAMPLES OF THE CALCULATION OF DISTORTION USING DATA FROM CMM

The calculation processes for distortion are given in this Appendix. The original data were taken from the Navy C-ring Specimen 3D Measurement Report (Data File) of the PRISMO Coordinate Measuring Machine (CMM).

The distortion (%) can be determined using the following methods.

1. Distortion due to carburizing and quenching is equal to:
   [(actual dimension after carburizing and quenching – as-received actual dimension) × 100%] / (as-received actual dimension)

2. Distortion due to tempering is equal to:
   [(actual dimension after tempering –actual dimension after carburizing and quenching) × 100%] / (actual dimension after carburizing)

3. Distortion due to carburizing and tempering is equal to:
   [(actual dimension after tempering – as-received actual dimension) × 100%] / (as-received actual dimension)

For flatness, cylindricity and roundness, the distortion was also evaluated using an absolute value and the following equations.

A. Distortion due to carburizing is equal to:
   [(actual dimension after carburizing – as-received actual dimension)]

B. Distortion due to tempering is equal to:
   [(actual dimension after tempering –actual dimension after carburizing)]

C. Distortion due to carburizing and tempering is equal to:
   [(actual dimension after tempering – as-received actual dimension)]

The following three Figures (Figure A.1, A.2 & A.3) show distortion profiles of flatness, cylindricity & roundness of three Navy C-ring specimens carburized at 1750°F for 4 hours at 1.1% carbon potential followed by quenching and tempering at each of two

tempering temperatures (300°F and 350°F) for 1 hour. Tables A.1, A.2 and A.3 show distortion calculations for these three specimens.

Figure A.1 (a) Flatness profile of specimen 1750/1.1/RT before and after heat treatment.

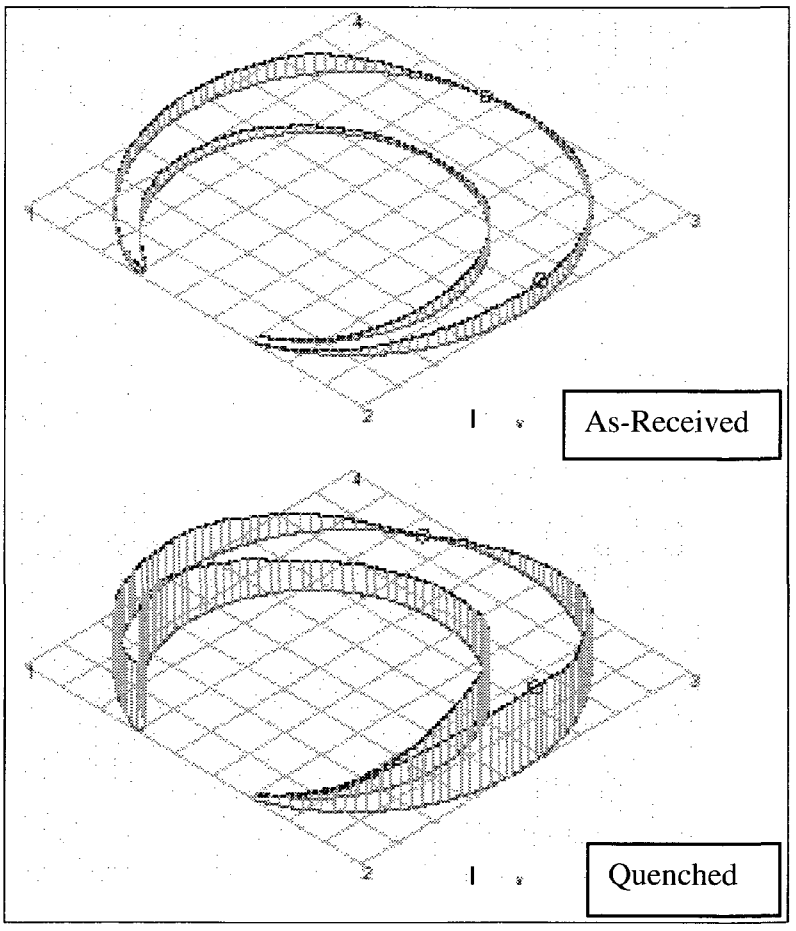

Figure A.1 (b) Cylindricity and roundness profiles of specimen 1750/1.1/RT before and after heat treatment.

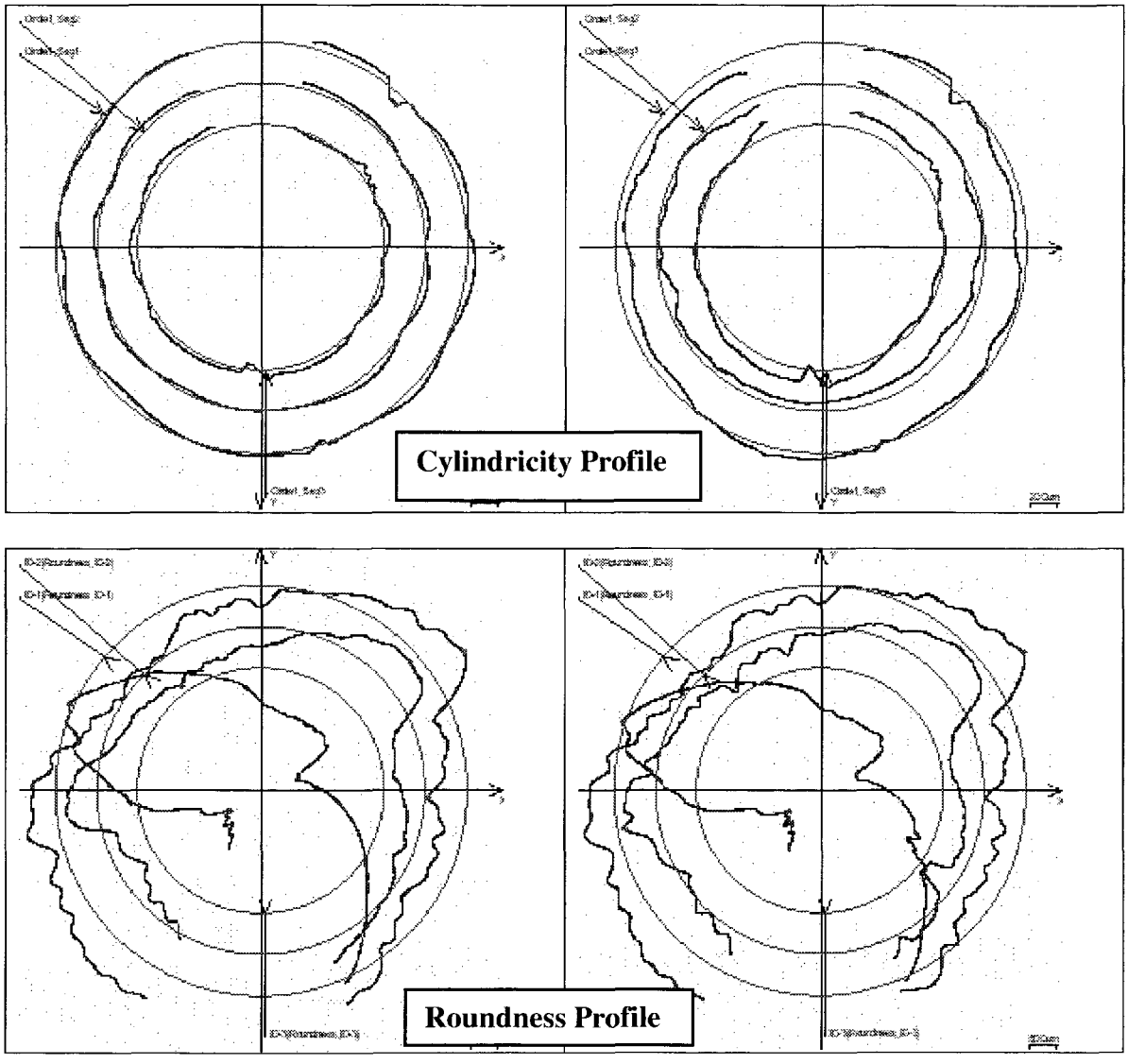

Table A.1 Distortion calculations for specimen 1750/1.1/RT

Condition	Actual	Nominal	Upper Tol.	Lower Tol.	Deviation	Distortion due to carburizing
as received	Flatness_Numbered Side				0.0111	–
	0.0111	0.0000	0.0000		0.0111	
carburized	Flatness_Numbered Side				0.025	125.2%
	0.025	0.0000	0.0000		0.025	
as received	Cylindricity_OD				0.0131	–
	0.0131	0.0000	0.0000		0.0131	
carburized	Cylindricity_OD				0.0242	0.0111
	0.0242	0.0000	0.0000		0.0242	
as received	Diameter_OD					–
	50.7451	50.7500	0.1000	-0.1000	-0.0049	
carburized	Diameter_OD					0.1009%
	50.7963	50.7500	0.1000	-0.1000	0.0463	
Roundness_ID-1						
as received	Roundness_ID-1				0.1447	–
	0.1447	0.0000	0.0000		0.1447	
carburized	Roundness_ID-1				0.1490	0.0043
	0.1490	0.0000	0.0000		0.1490	
Roundness_ID-2						
as received	Roundness_ID-2				0.1187	–
	0.1187	0.0000	0.0000		0.1187	
carburized	Roundness_ID-2				0.1299	0.0112
	0.1299	0.0000	0.0000		0.1299	
Roundness_ID-3						
as received	Roundness_ID-3				0.3232	–
	0.3232	0.0000	0.0000		0.3232	
carburized	Roundness_ID-3				0.3181	-0.0051
	0.3181	0.0000	0.0000		0.3181	

Table A.1 Distortion calculations for specimen 1750/1.1/RT (Continued)

Condition	Actual	Nominal	Upper Tol.	Lower Tol.	Deviation	Distortion due to carburizing
Diameter_ID-1						
as received	Diameter_ID-1					–
	31.4739	31.6000	0.1500	-0.1500	-0.1261	
carburized	Diameter_ID-1					0.0343%
	31.4847	31.6000	0.1500	-0.1500	-0.1153	
Diameter_ID-2						
as received	Diameter_ID-2					–
	31.6053	31.6000	0.1500	-0.1500	0.0053	
carburized	Diameter_ID-2					-0.0421%
	31.5920	31.6000	0.1500	-0.1500	-0.0080	
Diameter_ID-3						
as received	Diameter_ID-3				-0.0999	–
	31.3501	31.6000	0.1500	-0.1500	-0.2499	
carburized	Diameter_ID-3				-0.0878	0.0386%
	31.3622	31.6000	0.1500	-0.1500	-0.2378	
Thickness_1						
as received	Thickness_1				-0.2149	–
	18.4851	18.8000	0.1000	-0.1000	-0.3149	
carburized	Thickness_1				-0.1622	0.2851%
	18.5378	18.8000	0.1000	-0.1000	-0.2622	
Thickness_2						
as received	Thickness_2				0.1449	–
	19.0449	18.8000	0.1000	-0.1000	0.2449	
carburized	Thickness_2				0.1937	0.2562%
	19.0937	18.8000	0.1000	-0.1000	0.2937	
Thickness_3						
as received	Thickness_3				0.2833	–
	19.1833	18.8000	0.1000	-0.1000	0.3833	
carburized	Thickness_3				0.3167	0.1741%
	19.2167	18.8000	0.1000	-0.1000	0.4167	
Dis_Gap_Top						
as received	Dis_Gap_Top					–
	6.9438	7.0000	0.1000	-0.1000	-0.0562	
carburized	Dis_Gap_Top					3.11%
	7.1596	7.0000	0.1000	-0.1000	0.1596	
Dis_Gap_Bottom						
as received	Dis_Gap_Bottom					–
	6.9342	7.0000	0.1000	-0.1000	-0.0658	
carburized	Dis_Gap_Bottom					3.09%
	7.1486	7.0000	0.1000	-0.1000	0.1486	

Figure A.2 (a) Flatness profile of specimen 1750/1.1/300 before and after heat treatment.

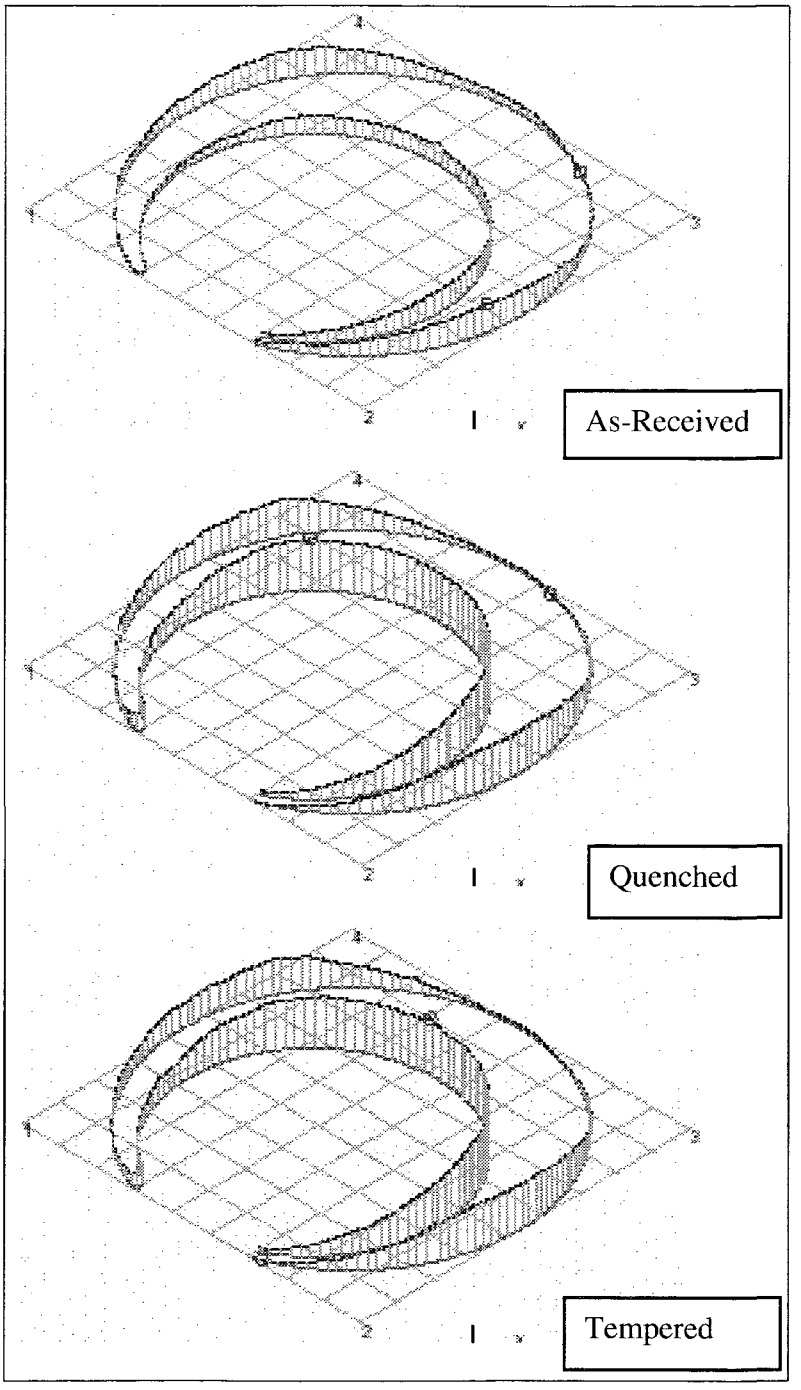

Figure A.2 (b) Cylindricity profile of specimen 1750/1.1/300 before and after heat treatment.

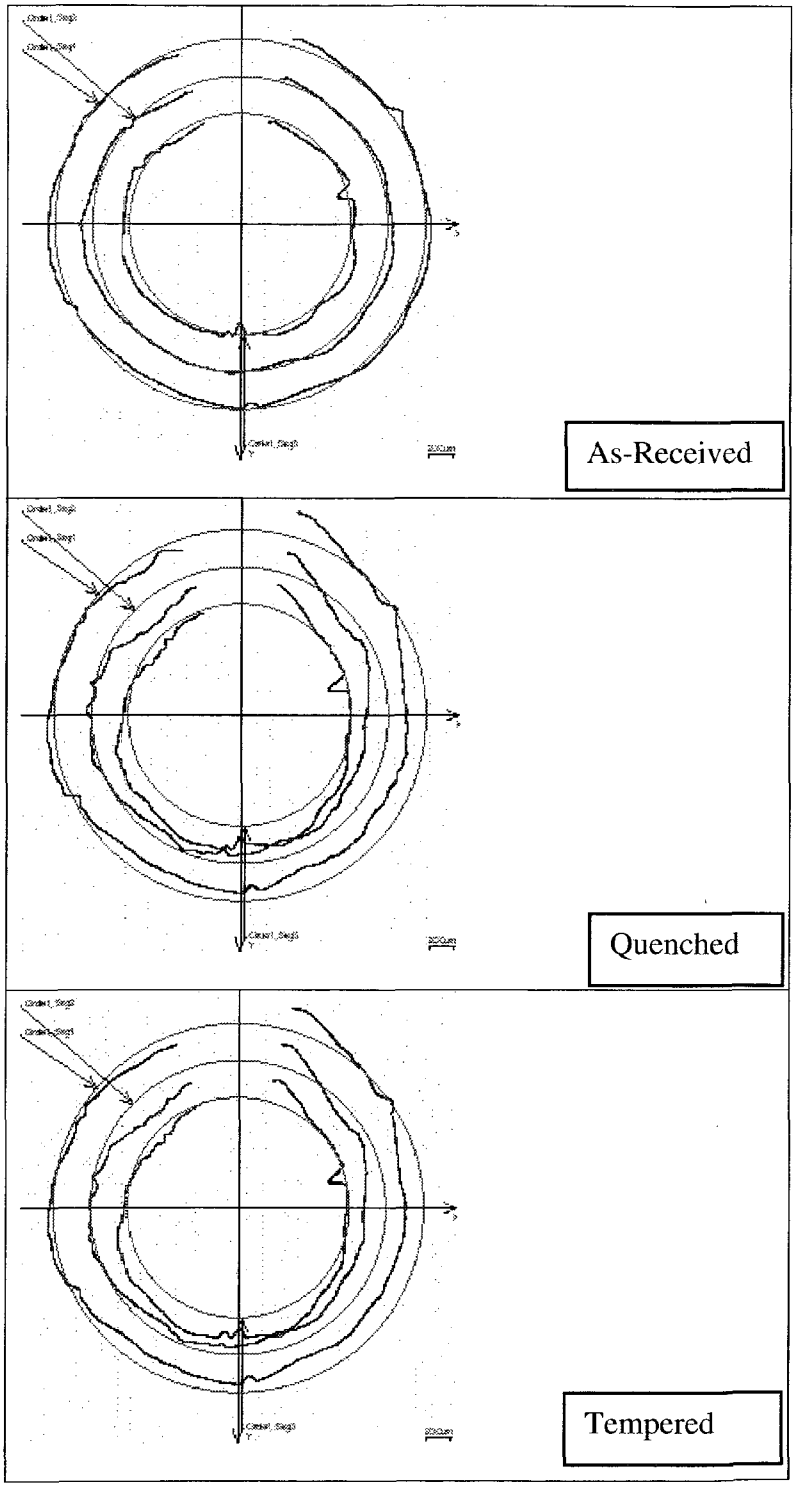

Figure A.2 (c) Roundness profile of specimen 1750/1.1/300 before and after heat treatment.

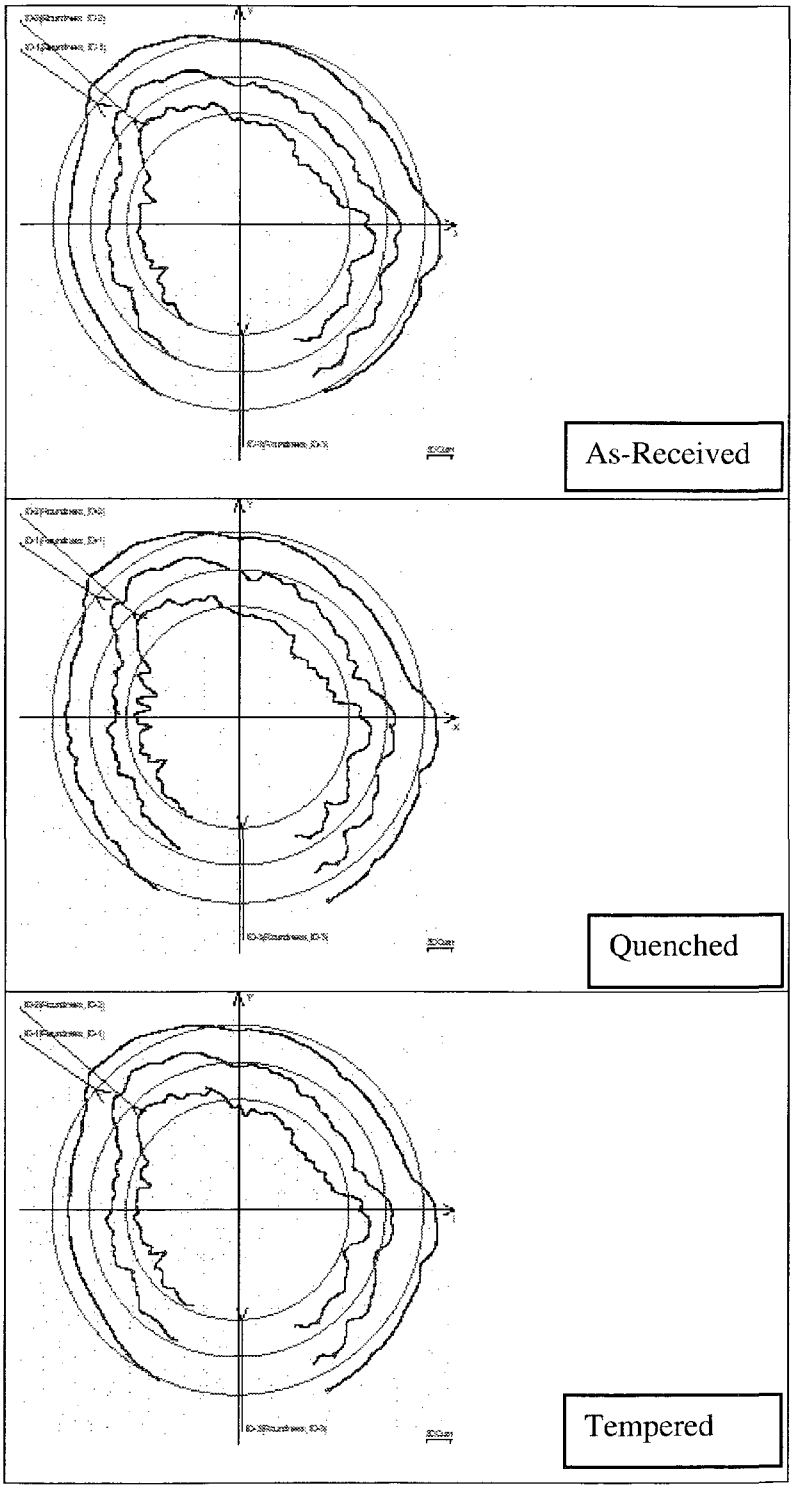

Table A.2 Distortion calculations for specimen 1750/1.1/300

Condition	Actual	Nominal	Upper Tol.	Lower Tol.	Deviation	Distortion due to carburizing	Distortion due to tempering	Distortion due to carburizing & tempering
as received	Flatness_ Numbered Side				0.0111	–	–	–
	0.0111	0.0000	0.0000		0.0111			
carburized	Flatness_ Numbered Side				0.025	125.2%	–	–
	0.025	0.0000	0.0000		0.025			
tempered	Flatness_ Numbered Side				0.0113	–	-54.8%	1.8%
	0.0113	0.0000	0.0000		0.0113			
as received	Cylindricity_OD				0.0177	–	–	–
	0.0177	0.0000	0.0000		0.0177			
carburized	Cylindricity_OD				0.0412	0.0235	–	–
	0.0412	0.0000	0.0000		0.0412			
tempered	Cylindricity_OD				0.0389	–	-0.0023	0.0212
	0.0389	0.0000	0.0000		0.0389			
as received	Diameter_ OD					–	–	–
	50.7451	50.7500	0.1000	-0.1000	-0.0049			
carburized	Diameter_ OD					0.101%	–	–
	50.7963	50.7500	0.1000	-0.1000	0.0463			
tempered	Diameter_ OD					–	-0.090%	0.010%
	50.7504	50.7500	0.1000	-0.1000	0.0004			

Table A.2 Distortion calculations for specimen 1750/1.1/300 (Continued)

Condition	Actual	Nominal	Upper Tol.	Lower Tol.	Deviation	Distortion due to carburizing	Distortion due to tempering	Distortion due to carburizing & tempering
Roundness_ID-1								
as received	Roundness _ID-1				0.0706	–	–	–
	0.0706	0.0000	0.0000		0.0706			
carburized	Roundness _ID-1				0.0765	0.0059	–	–
	0.0765	0.0000	0.0000		0.0765			
tempered	Roundness _ID-1				0.0691	–	-0.0074	-0.0015
	0.0691	0.0000	0.0000		0.0691			
Roundness_ID-2								
as received	Roundness _ID-2				0.0920	–	–	–
	0.0920	0.0000	0.0000		0.0920			
carburized	Roundness _ID-2				0.1127	0.0207	–	–
	0.1127	0.0000	0.0000		0.1127			
tempered	Roundness _ID-2				0.1081	–	-0.0046	0.0161
	0.1081	0.0000	0.0000		0.1081			
Roundness_ID-3								
as received	Roundness _ID-3				0.1084	–	–	–
	0.1084	0.0000	0.0000		0.1084			
carburized	Roundness _ID-3				0.1196	0.0112	–	–
	0.1196	0.0000	0.0000		0.1196			
tempered	Roundness _ID-3				0.1100	–	-0.0096	0.0016
	0.1100	0.0000	0.0000		0.1100			

Table A.2 Distortion calculations for specimen 1750/1.1/300 (Continued)

Condition	Actual	Nominal	Upper Tol.	Lower Tol.	Deviation	Distortion due to carburizing	Distortion due to tempering	Distortion due to carburizing & tempering
Diameter_ID-1								
as received	Diameter_ ID-1 31.5423	31.6000	0.1500	-0.1500	-0.0577	–	–	–
carburized	Diameter_ ID-1 31.5592	31.6000	0.1500	-0.1500	-0.0408	0.0536%	–	–
tempered	Diameter_ ID-1 31.5643	31.6000	0.1500	-0.1500	-0.0357	–	0.0162%	0.0697%
Diameter_ID-2								
as received	Diameter_ ID-2 31.5688	31.6000	0.1500	-0.1500	-0.0312	–	–	–
carburized	Diameter_ ID-2 31.5317	31.6000	0.1500	-0.1500	-0.0683	-0.1175%	–	–
tempered	Diameter_ ID-2 31.5393	31.6000	0.1500	-0.1500	-0.0607	–	0.0241%	-0.0934%
Diameter_ID-3								
as received	Diameter_ ID-3 31.4290	31.6000	0.1500	-0.1500	-0.0210 -0.1710	–	–	–
carburized	Diameter_ ID-3 31.4072	31.6000	0.1500	-0.1500	-0.0428 -0.1928	-0.0694%	–	–
tempered	Diameter_ ID-3 31.4182	31.6000	0.1500	-0.1500	-0.0318 -0.1818	–	0.0350%	-0.0344%

Table A.2 Distortion calculations for specimen 1750/1.1/300 (Continued)

Condition	Actual	Nominal	Upper Tol.	Lower Tol.	Deviation	Distortion due to carburizing	Distortion due to tempering	Distortion due to carburizing & tempering
Thickness_1								
as received	Thickness_1				0.0244	–	–	–
	18.9244	18.8000	0.1000	-0.1000	0.1244			
carburized	Thickness_1				0.0824	0.3065%	–	–
	18.9824	18.8000	0.1000	-0.1000	0.1824			
tempered	Thickness_1				0.0700	–	-0.0653%	0.2410%
	18.9700	18.8000	0.1000	-0.1000	0.1700			
Thickness_2								
as received	Thickness_2				0.1192	–	–	–
	19.0192	18.8000	0.1000	-0.1000	0.2192			
carburized	Thickness_2				0.1801	0.3202%	–	–
	19.0801	18.8000	0.1000	-0.1000	0.2801			
tempered	Thickness_2				0.1699	–	-0.0535%	0.2666%
	19.0699	18.8000	0.1000	-0.1000	0.2699			
Thickness_3								
as received	Thickness_3					–	–	–
	18.8911	18.8000	0.1000	-0.1000	0.0911			
carburized	Thickness_3				0.0427	0.2731%	–	–
	18.9427	18.8000	0.1000	-0.1000	0.1427			
tempered	Thickness_3				0.0323	–	-0.0549%	0.2181%
	18.9323	18.8000	0.1000	-0.1000	0.1323			

Table A.2 Distortion calculations for specimen 1750/1.1/300 (Continued)

Condition	Actual	Nominal	Upper Tol.	Lower Tol.	Deviation	Distortion due to carburizing	Distortion due to tempering	Distortion due to carburizing & tempering
Dis_Gap_Top								
as received	Dis_Gap_ Top 6.9438	7.0000	0.1000	-0.1000	-0.0562	–	–	–
carburized	Dis_Gap_ Top 7.1596	7.0000	0.1000	-0.1000	0.1596	3.11%	–	–
tempered	Dis_Gap_ Top 7.0002	7.0000	0.1000	-0.1000	0.0002	–	-2.23%	0.81%
Dis_Gap_Bottom								
as received	Dis_Gap_ Bottom 6.9342	7.0000	0.1000	-0.1000	-0.0658	–	–	–
carburized	Dis_Gap_ Bottom 7.1486	7.0000	0.1000	-0.1000	0.1486	3.09%	–	–
tempered	Dis_Gap_ Bottom 6.9876	7.0000	0.1000	-0.1000	-0.0124	–	-2.25%	0.77%

Figure A.3 (a) Flatness profile of specimen 1750/1.1/350 before and after heat treatment.

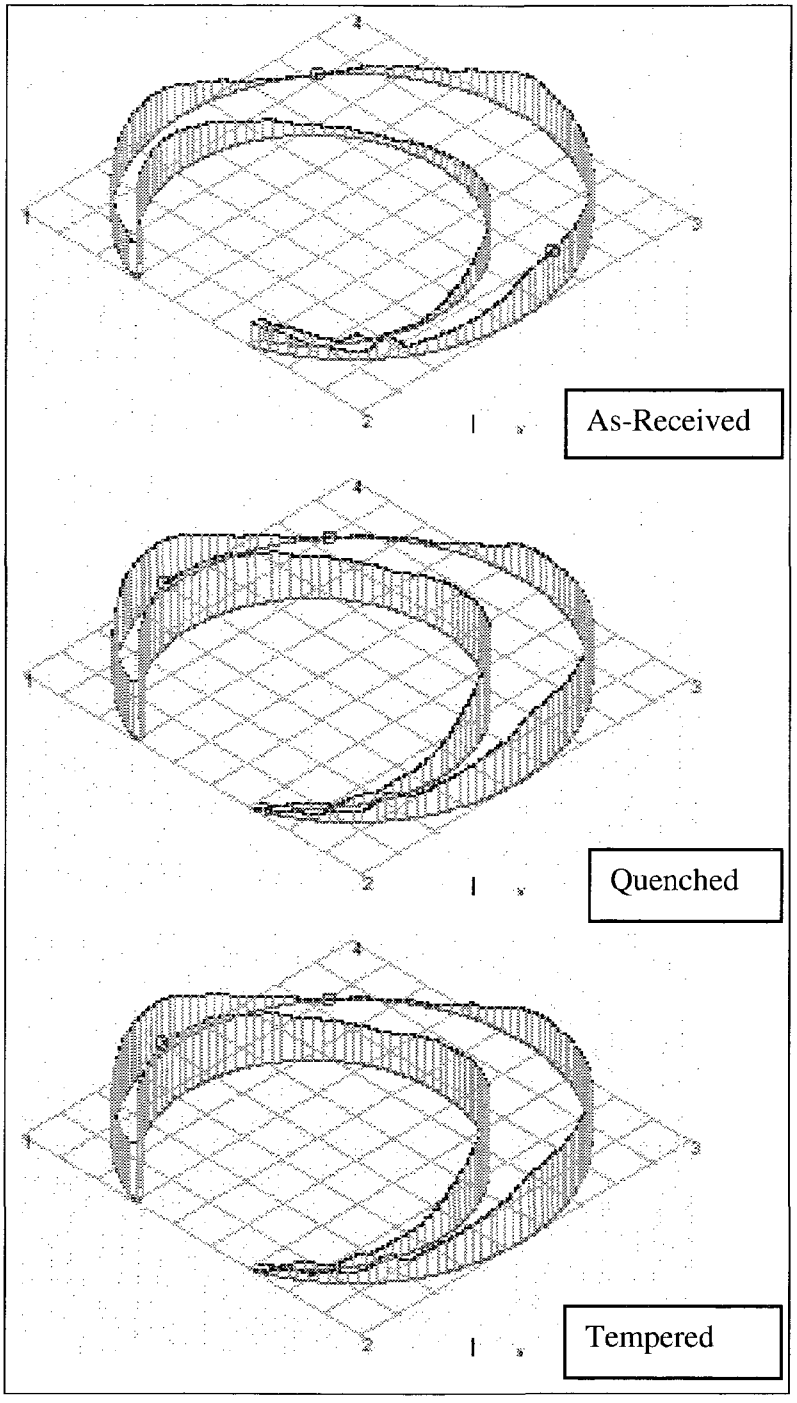

Figure A.3 (b) Cylindricity profile of specimen 1750/1.1/350 before and after heat treatment.

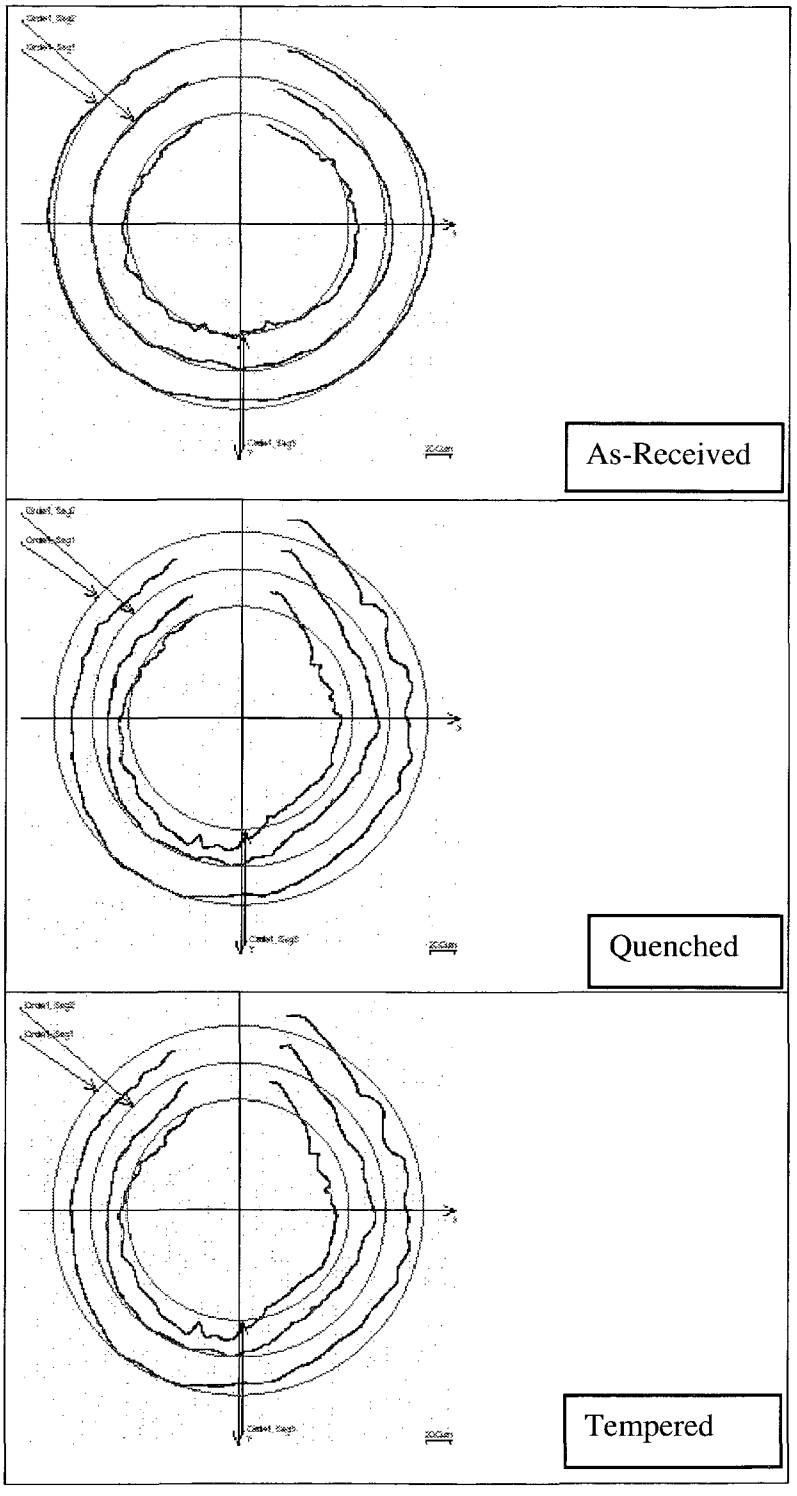

Figure A.3 (c) Roundness profile of specimen 1750/1.1/350 before and after heat treatment.

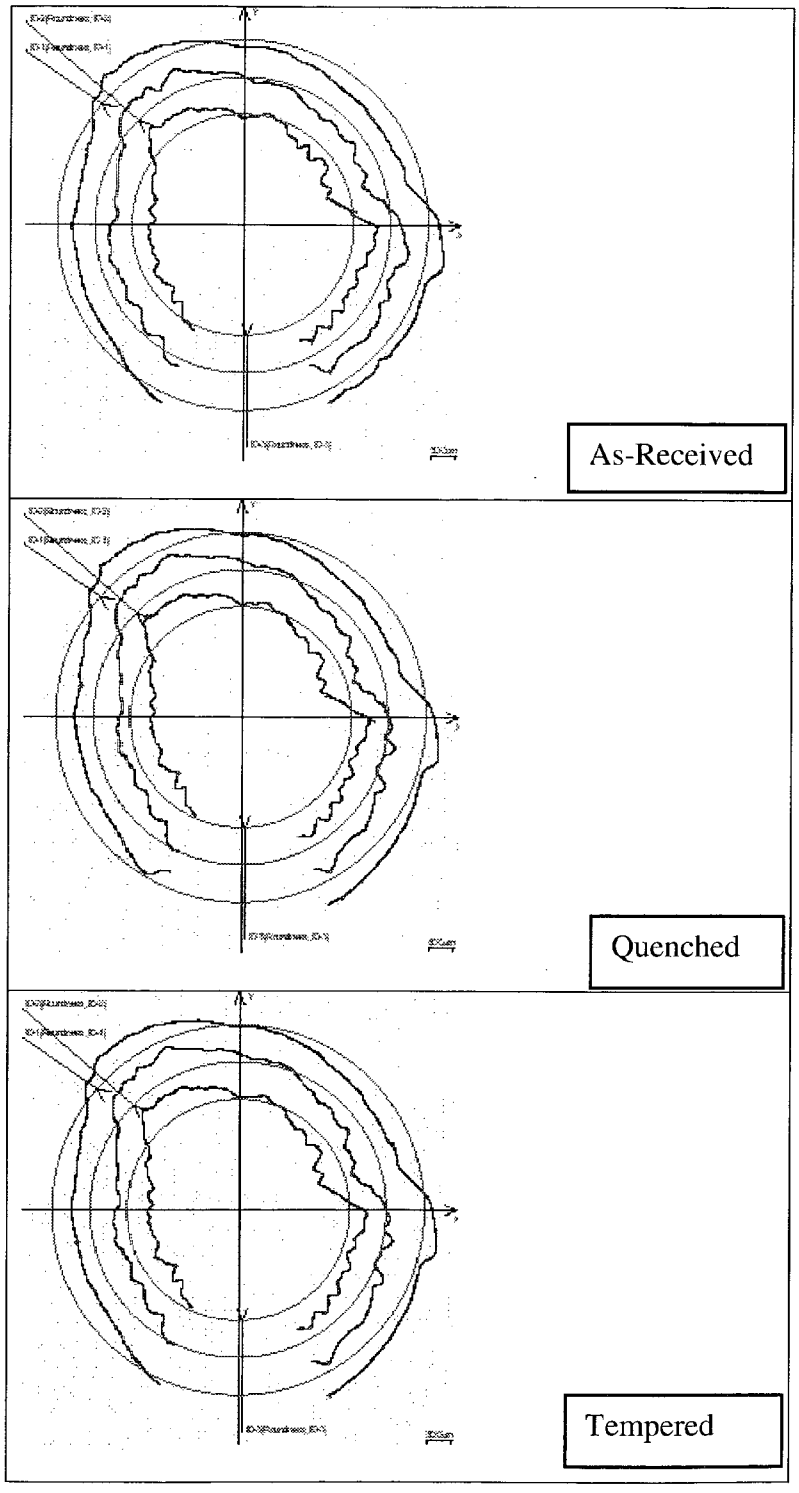

Table A.3 Distortion calculations for specimen 1750/1.1/350

Condition	Actual	Nominal	Upper Tol.	Lower Tol.	Deviation	Distortion due to carburizing	Distortion due to tempering	Distortion due to carburizing & tempering
as received	Flatness_ Numbered Side				0.0166	–	–	–
	0.0166	0.0000	0.0000		0.0166			
carburized	Flatness_ Numbered Side				0.0385	131.9%	–	–
	0.0385	0.0000	0.0000		0.0385			
tempered	Flatness_ Numbered Side				0.0165	–	-57.1%	-0.6%
	0.0165	0.0000	0.0000		0.0165			
as received	Cylindricity_OD				0.0163	–	–	–
	0.0163	0.0000	0.0000		0.0163			
carburized	Cylindricity_OD				0.0409	0.0246	–	–
	0.0409	0.0000	0.0000		0.0409			
tempered	Cylindricity_OD				0.0396	–	-0.0013	0.0233
	0.0396	0.0000	0.0000		0.0396			
as received	Diameter_ OD					–	–	–
	50.7451	50.7500	0.1000	-0.1000	-0.0049			
carburized	Diameter_ OD					0.114%	–	–
	50.8029	50.7500	0.1000	-0.1000	0.0529			
tempered	Diameter_ OD					–	-0.101%	0.012%
	50.7514	50.7500	0.1000	-0.1000	0.0014			

Table A.3 Distortion calculations for specimen 1750/1.1/350 (Continued)

Condition	Actual	Nominal	Upper Tol.	Lower Tol.	Deviation	Distortion due to carburizing	Distortion due to tempering	Distortion due to carburizing & tempering
Roundness_ID-1								
as received	Roundness_ID-1 0.0762	0.0000	0.0000		0.0762 0.0762	–	–	–
carburized	Roundness_ID-1 0.0890	0.0000	0.0000		0.0890 0.0890	0.0128	–	–
tempered	Roundness_ID-1 0.0888	0.0000	0.0000		0.0888 0.0888	–	-0.0002	0.0126
Roundness_ID-2								
as received	Roundness_ID-2 0.0919	0.0000	0.0000		0.0919 0.0919	–	–	–
carburized	Roundness_ID-2 0.1218	0.0000	0.0000		0.1218 0.1218	0.0299	–	–
tempered	Roundness_ID-2 0.1224	0.0000	0.0000		0.1224 0.1224	–	0.0006	0.0305
Roundness_ID-3								
as received	Roundness_ID-3 0.0951	0.0000	0.0000		0.0951 0.0951	–	–	–
carburized	Roundness_ID-3 0.1110	0.0000	0.0000		0.1110 0.1110	0.0159	–	–
tempered	Roundness_ID-3 0.1108	0.0000	0.0000		0.1108 0.1108	–	-0.0002	0.0157

Table A.3 Distortion calculations for specimen 1750/1.1/350 (Continued)

Condition	Actual	Nominal	Upper Tol.	Lower Tol.	Deviation	Distortion due to carburizing	Distortion due to tempering	Distortion due to carburizing & tempering
Diameter_ID-1								
as received	Diameter_ ID-1 31.5141	31.6000	0.1500	-0.1500	-0.0859	–	–	–
carburized	Diameter_ ID-1 31.5433	31.6000	0.1500	-0.1500	-0.0567	0.0927%	–	–
tempered	Diameter_ ID-1 31.5473	31.6000	0.1500	-0.1500	-0.0527	–	0.0127%	0.1053%
Diameter_ID-2								
as received	Diameter _ID-2 31.5613	31.6000	0.1500	-0.1500	-0.0387	–	–	–
carburized	Diameter _ID-2 31.5488	31.6000	0.1500	-0.1500	-0.0512	-0.0396%	–	–
tempered	Diameter _ID-2 31.5519	31.6000	0.1500	-0.1500	-0.0481	–	0.0098%	-0.0298%
Diameter_ID-3								
as received	Diameter _ID-3 31.3940	31.6000	0.1500	-0.1500	-0.0560 -0.2060	–	–	–
carburized	Diameter _ID-3 31.4093	31.6000	0.1500	-0.1500	-0.0407 -0.1907	0.0487%	–	–
tempered	Diameter _ID-3 31.4114	31.6000	0.1500	-0.1500	-0.0386 -0.1886	–	0.0067%	0.0554%

Table A.3 Distortion calculations for specimen 1750/1.1/350 (Continued)

Condition	Actual	Nominal	Upper Tol.	Lower Tol.	Deviation	Distortion due to carburizing	Distortion due to tempering	Distortion due to carburizing & tempering
Thickness_1								
as received	Thickness_1 18.7281	18.8000	0.1000	-0.1000	-0.0719	–	–	–
carburized	Thickness_1 18.7849	18.8000	0.1000	-0.1000	-0.0151	0.3033%	–	–
tempered	Thickness_1 18.7519	18.8000	0.1000	-0.1000	-0.0481	–	-0.1757%	0.1271%
Thickness_2								
as received	Thickness_2 18.7127	18.8000	0.1000	-0.1000	-0.0873	–	–	–
carburized	Thickness_2 18.7820	18.8000	0.1000	-0.1000	-0.0180	0.3703%	–	–
tempered	Thickness_2 18.7483	18.8000	0.1000	-0.1000	-0.0517	–	-0.1794%	0.1902%
Thickness_3								
as received	Thickness_3 18.8149	18.8000	0.1000	-0.1000	0.0149	–	–	–
carburized	Thickness_3 18.8572	18.8000	0.1000	-0.1000	0.0572	0.2248%	–	–
tempered	Thickness_3 18.8254	18.8000	0.1000	-0.1000	0.0254	–	-0.1686%	0.0558%

Table A.3 Distortion calculations for specimen 1750/1.1/350 (Continued)

Condition	Actual	Nominal	Upper Tol.	Lower Tol.	Deviation	Distortion due to carburizing	Distortion due to tempering	Distortion due to carburizing & tempering
Dis_Gap_Top								
as received	Dis_Gap_Top 7.0107	7.0000	0.1000	-0.1000	0.0107	–	–	–
carburized	Dis_Gap_Top 7.2305	7.0000	0.1000	-0.1000	0.2305	3.14%	–	–
tempered	Dis_Gap_Top 7.0704	7.0000	0.1000	-0.1000	0.0704	–	-2.21%	0.85%
Dis_Gap_Bottom								
as received	Dis_Gap_Bottom 6.7707	7.0000	0.1000	-0.1000	-0.2293	–	–	–
carburized	Dis_Gap_Bottom 6.9801	7.0000	0.1000	-0.1000	-0.0199	3.09%	–	–
tempered	Dis_Gap_Bottom 6.8302	7.0000	0.1000	-0.1000	-0.1698	–	-2.15%	0.88%

REFERENCES

[1] E. Nakamura and Y. Hayashi, the Influence of Quench Condition on Distortion of Oil Quenching, 20th ASM Heat Treating Society Conference, St. Louis, MO, USA, 9-12 Oct. 2000, ASM International, Materials Park, OH (2001), 713-718.

[2] J. Volkmuth, U. Sjoblom, J. Slycke and A. Thuvander, Effect of Uneven Residual Stresses on Dimensional Changes and Variations of Through Hardening Bearing Steel Rings, 20th ASM Heat Treating Society Conference, St. Louis, MO, USA, 9-12 Oct. 2000, ASM International, Materials Park, OH (2001), 455-460.

[3] G. F. Vander Voort, Volume Editor, ASM Handbook, Metallography and Microstructures, ASM, Materials Park, Ohio Vol. 9 (2004), 627-631.

[4] AISI 8620 (Carburizing Grade Alloy Steel), Crucible Specialty Metals Div., Colt Industries, (1982), 4.

[5] V. Rudnev, D. Loveless, R. Cook and M. Black, Handbook of Induction Heating, Marcel Dekker, Inc., (2003), 18.

[6] H. E. McGannon (Editor), the Making, Shaping and Treating of Steel, Ninth Edition, United States Steel, Herbick & Held, Pittsburgh, Pennsylvania, USA (1971), 1238-1239.

[7] Principles of Heat Treatment, Western Ontario Chapter, American Society For Metals (ASM) (1969),183-189.

[8] J. R. Davis, Gas Carburizing, Surface Hardening of Steels: Understanding the Basics, ASM International, Materials Park, OH (2002), 17-89.

[9] Gas Carburizing, ASM, Metals Park, Ohio (1964), 47-137.

[10] M. Bauccio, ASM Metals Reference Book, 3rd Edition, ASM International, Materials Park, (2001), 286-309.

[11] C. F. Jatczak, Retained Austenite and Its Measurement by X-Ray Diffraction, SAE Technical Paper No. 800426, Pennsylvania (1980), 1-19.

[12] R. L. Banerjee, Effect of Room-Temperature Aging on Low-Temperature Transformation of Retained Austenite, J. Heat Treat., Vol. 3, no. 4 (1984), 353-355.

[13] Cryogenics Gives an Edge to Tooling Manufacturers, Materials Australia, Vol. 38, No. 3 (2005), 22.

[14] P. Gordon, M. Cohen and R. S. Rose, Kinetics of Austenite Decomposition in High Speed Steel, Trans. ASM, Vol. 31, no.1 (1943), 161-198.

[15] A. Rose and H. P. Hougardy, Transformation Characteristics and Hardenability of Carburizing Steels, Transformation and Hardenability in Steel, Climax Molybdenum Co. of Michigan, USA, Symposium (1967), 155-167.

[16] M. Cohen, Retained Austenite, ASM, Metal Progress, Vol. 54, no. 6 (1948), 823-826.

[17] D. P. Koistinen and R. E. Marburger, A General Equation for Austenite – Martensite Transformation in Pure Carbon Steels, Acta Met., Vol. 7 (1959), 59.

[18] C. F. Jatczak, Graphitic Cold Work Tool Steels, ASM Paper No: C72-25.2 (1972), 1-5.

[19] R. W. Gregorutti, J. L. Sarutti and J. Sikora, Microstructural Stability of Austempered Ductile Iron after Sub-Zero Cooling, Materials Science and Technology. Vol. 19, no. 6 (2003), 831-835.

[20] A. P. Gulyaev, Cold Treatment of Steel, Metal Science and Heat Treatment, Vol. 40, no. 11-12 (1999), 449-455.

[21] F. Hoffmann, Residual Austenite, Measurement and Influencing; Effect on Mechanical Properties, Journal of Materials (Netherlands), Vol. 4 (1997), 31-34.

[22] J. Grosch and O.Schwarz, Retained Austenite and Residual Stress Distribution in Deep Cooled Carburized Microstructures, 1995 Carburizing and Nitriding With Atmospheres, ASM International, Materials Park, OH (1995), 71-76.

[23] I-T diagrams (Isothermal Transformation of Austenite in a Wide Variety of Steels), United States Steel (USS), 3rd Edition (1980), 109.

[24] G. Parrish, Influence of Microstructure on Properties of Case Carburized Components, Part 4 – Retained Austenite, ASM, Metals Park, OH (1980), 61-89.

[25] B. S. Lement, B. L. Averbach and M. Cohen, Microstructural Changes on Tempering Iron-Carbon Alloys, American Society for Metals Meeting, Oct 19-23 1953, ASM -- Preprint 25 (1953), 1-27.

[26] I. R. Sare and B. K. Arnold, the Influence of Heat Treatment on the High-Stress Abrasion Resistance and Fracture Toughness of Alloy White Cast Irons, Metall. Mater. Trans. A (USA), Vol. 26A, no. 7 (1995), 1785-1793.

[27] O. Zmeskal and M. Cohen, the Tempering of Two High Carbon – High Chromium Steels, Trans. ASM, Vol. 31, no. 2 (1943), 380-408.

[28] H. Berns, M. Karlsohn, F. Schmalt and W. Trajahn, Increasing the Hardness of Stainless Martensitic Steels, Journal of Materials (Germany), Vol. 59, no. 2 (2004), 87-97.

[29] J. J. Spice, D. K. Matlock and G. Fett, Optimized Carburized Steel Fatigue Performance As Accessed with Gear and Modified Brugger Fatigue Tests, SAE Transactions: Journal of Materials & Manufacturing, Vol. 111, no. 2002 (2003), 589-597.

[30] S. C. Lee and W. Y. Ho, Effect of Surface Hardening on Fracture Toughness of Carburized Steel, Metallurgical Transactions A (Physical Metallurgy and Materials Science), Vol. 20A, no. 3 (1989), 519-525.

[31] E. S. Machlin and M. Cohen, Burst Phenomenon in Martensitic Transformation, Journal of Metals, Vol. 3, no. 9, AIME (1951), 746-754.

[32] H. R. Woherle, H. R. Clough, and G. S. Ansell, A Thermal Stabilization of Austenite, ASM Trans. Quart, Vol. 59, no. 4 (1996), 784-803.

[33] B. Edmondson, Thermal Stabilization of Austenite in 10% Ni, 1%C Steel, Acta Metallurgica, Vol. 5, no. 4 (1957), 208-215.

[34] E. J. Klimek, Metallographic Method for Measuring Retained Austenite, Heat Treat, Vol. 9, no. 10 (1977),16-22.

[35] B. L. Averbach and M. Cohen, X-Ray Determination of Retained Austenite by Integrated Intensities, Trans, AIME, vol.176 (1948), 401.

[36] S. Paciornik, A. R. Martins, J. B. De Campos, F. A. R. Serra and P. Manso, Color Image Segmentation to Measure Residual Austenite, 14th International Congress on Electron Microscopy, Cancun, Mexico, 31 Aug.-4 Sept. 1998, Institute of Physics Publishing, UK (1998), 165-166.

[37] S. R. Pati and M. Cohen, Nucleation of the Isothermal Martensitic Transformation, Acta Met., Vol. 17, no. 3 (1969), 189-199.

[38] L. Chang, Phase Transformations in Thin Films of Titanium Nickel Thermoelastic Alloys, Dissertation Abstracts International,Vol. 54, no. 5 (1993), 256.

[39] R. L. Miller, Volume Fraction Analysis of Phases in Texture Alloys, ASM Trans. Quart, Vol. 61, no. 3 (1968), 592-597.

[40] H. C. Child, Residual Stress in Heat-Treated Components, Heat Treatment of Metals, no. 8 (1981), 89-94.

[41] W. E. Littmann, An X-Ray Spectrometer Determination of Retained Austenite in Steel, MS Thesis, MIT (1952), 1-69.

[42] H. R. Erard, Technique for Measuring Low Percentages of Retained Austenite Using Filtered X-Ray Radiation and An X-Ray Diffractometer, Advances in X-Ray Analysis, Vol. 7 (1963), 256-264.

[43] R. Lindgren, Measuring Retained Austenite by X-ray Techniques, Metal Progress, Vol. 87, no. 4 (1965), 102-104.

[44] R. L. Miller, Rapid X-ray Method for Determination of Retained Austenite, Trans. ASM, Vol. 57, no. 4 (1964), 892-899.

[45] J. Durnin and K. A. Ridal, Determination of Retained Austenite in Steel by X-ray Diffraction, Journal of Iron and Steel Institute, Vol. 206, no.1 (1968), 60-67.

[46]. K. E. Beu, Modifications of X-ray Method for Measurement of Retained Austenite Concentrations in Hardened Steels, Journal of Metals, Vol. 4, no.12 (1952), 1327-1328.

[47] M. James, J. B. Cohen, A Portable X-ray Analyzer for Residual Stresses, Journal of Testing & Evaluation, Vol. 6, no. 2 (1978), 91-97.

[48] B. D. Cullity, Elements of X-ray Diffraction, Addison-Wesley Reading, Massachusetts (1956), 2-35.

[49] A Taylor, X-ray Metallography, John Wiley & Sons, New York (1961), 18-26.

[50] H. P. Klug and L. E. Alexander, X-ray Diffraction Procedures for Polycrystalline and Amorphous Materials, J. Wiley & Sons, New York (1970), 11-13.

[51] M. J. Dickson, Significance of Texture Parameters in Phase Analysis by X-Ray Diffraction, J Applied Crystallography, Vol.2, no. 4 (1969), 76-80.

[52]. A. K. Sinha, Defects and Distortion in Heat-Treated Parts, ASM Handbook, Heat Treating, ASM International, Materials Park, OH, Vol. 4 (1991), 601-619.

[53] T. Hanabusa and H. Fujiwara, Evaluation of Macro and Micro Residual Stresses by X-Ray Stress Measurement, Thirty-Second Japan Congress on Materials Research, Society of Materials Science, Kyoto, Japan (1989), 27-36.

[54] G. E. Dieter, Engineering Design, A Materials and Processing Approach, McGraw-Hill Book Company (1987),169.

[55] R. W. K. Honeycombe and H. K. D. H. Bhadeshia, Steels: Microstructure and Properties, Edward Arnold, London, UK, Second Edition (1995), 255.

[56] B. S. Lement, Distortion in Tool Steel, ASM, Metals Park, OH (1959), 38.

[57] T. J. Baker and W. D. Harrison, Overheating and Burning in Steel Castings, Metals Technology, Vol. 2, no. 5 (1975), 201-205.

[58] P. Rangaswamy, C. P. Scherer and M. A. M. Bourke, Experimental Measurements and Numerical Simulation of Stress and Microstructure in Carburized 5120 Steel Disks, Materials Science and Engineering A (Switzerland), Vol. 298, no. 1-2 (2001), 158-165.

[59] L. Salonen, Internal Stresses in the Carbonized Layers of An Unalloyed and of A Mo-Cr Alloyed Steel after Various Heat Treatments, Acta Polytech. Scand. Ser., Vol 109 (1972), 7-26.

[60] B. Hildenwall and T. Ericsson, Prediction of Residual Stresses in Case-Hardening Steels, Hardenability Concepts With Applications to Steel, Metallurgical Society AIME, Warrendale (1978), 579-606.

[61] M. Motoyama, R. E. Ricklefs, and J. A. Larson, the Effect of Carburizing Variables on Residual Stresses in Hardened Chromium Steel, SAE Technical Paper Series 750050, Society of Automotive Engineers (1975), 1-22.

[62] J. A Burnett, Prediction of Stresses Generated During the Heat Treating of Case Carburized Parts, Residual Stress for Designers and Metallurgists, ASM, Metals Park, OH (1981), 51-69.

[63] P. S. Prevey, X-Ray Diffraction Procedures for Residual Stress Measurement, Lambda Research Inc., Cincinnati, Ohio (1977), 1-15.

[64] A. W. Bowen, X-Ray Diffraction, Microstructural Characterisation, E. Metcalfe, the Institute of Metals (UK) (1988), 227-302.

[65] F. Hoffmann, J. Dong, T. Lubben and P. Mayr, Formation of Distortion During Heat Treatment Processes, Journal of Materials (Germany), Vol. 92, no. 3 (2001), 242-245.

[66] G. E. Hollox and R. T. Von Bergn, Distortion in the Heat Treatment of Bearings, Heat Treatment of Metals, Wolfson Heat Treatment Centre, UK, Vol. 5, no. 2 (1978), 27-31.

[67] T. Bell, Survey of the Heat Treatment of Engineering Components, Metals Society, Iron and Steel Institute, London (1973), 69-72.

[68] K. W. Chambers, Aspects of Quality Control in Heat Treatment, Heat Treatment of Metals, Iron and Steel Institute (1966), 94-95.

[69] B. Edenhofer, W. Grafen and J. Muller-Ziller, Handling of Distortion Problems in Industrial Heat Treatment, Journal of Materials (Germany), Vol. 58, no. 6 (2003), 328-335.

[70] R. Lucic, Crystallography of Martensitic Transformations, Journal of Materials (Belgrade). Vol. 35, no. 2 (1980), 227-234.

[71] C. E. Bates, Predicting Properties and Minimizing Residual Stress in Quenched Steel Parts, Heat Treat, Vol. 6, no. 1 (1988), 27-45.

[72] P. G. Greenwood and R. H. Johnson, the Deformation of Metals under Small Stresses during Phase Transformation, Proc. Roy. Soc., Vol. A283 (1965), 403.

[73] R. Shang and J. P. Ma, Improved Heat Treatment Process for Enhancing Contact Precision of Gears, Heat Treatment of Metals (China), Vol. 4 (2001), 41-42.

[74] H. Altena, P. Jurci and P. Stola, Gas and Oil Quenching Effects on Gear Distortion, Industrial Heating, Vol. 71, no. 3 (2004), 45-48.

[75] F. Vivas and J. A. Tardio, the Influence of Quenching Oil, Its Temperature and Agitation, on Distortion in Carburised and Hardened F-1522 Steel, Deform. Met., no. 111, (1985), 31-47.

[76] H. Webster and W. J. Jr. Laird, Martempering of Steel, ASM Handbook, Heat Treating, ASM International, Materials Park, OH, Vol. 4 (1991), 137-151.

[77] D. J. Yoon, M. H. Lee, J. K. Jin, S. H. Kang and T. H. Nam, Microstructure and Rolling Contact Fatigue Life of Austenitic Nitro-Carburized STB 2 High Carbon Chromium Bearing Steel, Metals and Materials, Vol. 6, no. 5 (2000), 429-433.

[78] F. T. Krotine, G. M. F. Mc, L. J. Ebert and A.R. Troiano, Influence of Case Properties and Retained Austenite on the Behavior of Carburized Components, ASM Trans. Quart, Vol. 62 (1969), 829-838.

[79] M. W. Bai, Z. Chen and Z. Zhou, the Effects of Gas Carbonitrided Structure on the Contact Fatigue, Heat Treatment of Metals (China), no. 7 (1992), 8-13.

[80] Z. R. Liu, Y. D. Wei and C. Y. Wang, Effects of Rare Earth Element (RE) on the Carburizing and Carbo-Nitriding Processes of 20CrMnTi Steel and Their Production Application, Heat Treatment of Metals (China) , no. 10 (1987), 17-24.

[81] T. Kinami and T. Kimura, Development of Bearing Steels for Special Environment, Electric Furnace Steel, Vol. 75, no. 1(2004), 65-68.

[82] V. F. Da Silva, L. F. Canale, D. Spinelli, W. W. Bose-Filho and O. R. Crnkovic, Influence of Retained Austenite on Short Fatigue Crack Growth and Wear Resistance of Case Carburized Steel, Journal of Materials Engineering and Performance (USA), Vol. 8, no. 5 (1999), 543-548.

[83] K. Evanson, G. Krauss, D. Medlin and M. J. Patel, Bending Fatigue Behavior of Vacuum Carburized AISI 8620 Steel, 1995 Carburizing and Nitriding With Atmospheres, Cleveland, Ohio, USA, 6-8 Dec., 1995, ASM International, Materials Park, OH (1995), 61-69.

[84] H. J. Kim and Y. G. Kweon, High Cycle Fatigue Behavior of Gas-Carburized Medium Carbon Cr-Mo Steel, Metallurgical and Materials Transactions A (USA), Vol. 27A, no. 9 (1996), 2557-2564.

[85] H. T. S. Ogata, A. S. C. M. D'Oliveira and P. S. C. P. Da Silva, Determination of Residual Stresses in Carburized, Quenched and Tempered AISI 8620 Steel, Proceedings of the 6th European Conference on Residual Stresses, Coimbra, Portugal, 10-12 July 2002, Materials Science Forum (Switzerland), Vol. 404-407 (2002), 197-204.

[86] S. C. Lee and W. Y. Ho, the Effects of Surface Hardening on Fracture Toughness of Carburized Steel, Metall. Trans. A, Vol. 20A, no. 3 (1989), 519-525.

[87] L. Chen and Q. Chen, Tracking Observation on Subsurface Cracking in GCr15 Bearing Steel under Rolling Contact Fatigue, Acta Metallurgica Sinica (China), Vol. 27, no. 5 (1991), A377-A381.

[88] R. H. Richman and R. W. Landgraf, Some Effects of Retained Austenite on Fatigue Resistance of Carburized Steel, Met. Trans., Vol. 6A (1975), 955-964.

[89] G. Krauss, Microstructures and Properties of Carburized Steels, ASM Handbook, Heat Treating, ASM International, Materials Park, OH, Vol. 4 (1991), 363-375.

[90] H. Tanaka, T. Kobayashi, F. Nakasato and M.Uno, Effects of Alloying Elements and Shot Peening on Impact Fatigue Strength of Carburized Steels, Journal of the Iron and Steel Institute, Vol. 79, no. 1 (1993), 90-97.

[91] G. Y. Lai, W. E. Wood, R. A. Clark, V. F. Zackay and E. R. Parker, Effect of Austenitizing Temperature on the Microstructure and Mechanical Properties of As-Quenched 4340 Steel, Met. Trans., Vol. 5, no. 7 (1974), 1663-1670.

[92] D. Bhandakarar, V. F. Zackay and E. R. Parker, Stability and Mechanical Properties of Some Metastable Austenitic Steels, Met. Trans., Vol. 3, no.10 (1972), 2619-2631.

[93] E. R. Parker, Interrelations of Compositions, Transformation Kinetics, Morphology and Mechanical Properties of Alloy Steels, Met. Trans. A, Vol. 8A, no. 7 (1977), 1025-1042.

[94] C. T. Kwok, K. I. Leong, F. T. Cheng and H. C. Man, Microstructural and Corrosion Characteristics of Laser Surface-Melted Plastics Mold Steels, Materials Science and Engineering A, Vol. 357, no. 1-2 (2003), 94-103.

[95] S. G. Fletcher, B. L. Averbach and M. Cohen, the Dimensional Stability of Steel, Part 1, ASM Meeting, Oct 16-20, 1944, ASM--Preprints 27 (1944), 1-22.

[96] S. G. Fletcher, B. L. Averbach and M. Cohen, the Dimensional Stability of Steel, Part 2, ASM Meeting, Oct 18-24, 1947, ASM -- Preprint 7 (1947), 1-18.

[97] G. Liebmann and H. Luck, Influence of Silicon in Tool Steels on the Isothermal Stabilization of Residual Austenite, Journal of Materials (Germany), Vol. 27, no. 10 (1982), 371-373.

[98] J. J. McCarthy, Air-Hardening Tool Steel Grades Facilitate Size Change Reproduction, American Metal Market, Vol. 88, no. 28 (1980), 33-34.

[99] W. Reitz and J. Pendray, Cryoprocessing of Materials: A Review of Current Status, Materials and Manufacturing Processes (USA), Marcel Dekker Journals, Vol. 16, no. 6 (2001), 829-840.

[100] E. M. Grinberg, S. I. Arkhangel'skij and I. V. Tikhonova, Dimensional Stability and Strength of Multiphase Metastable Materials, Journal of Materials (Russia), Vol. 5 (1998), 12-16.

[101] H. Vetters and J. M. Schissler, the Amount of Retained Austenite on Machining Parameters of Austempered Spheroidal Cast-Iron, Journal of Materials (France), Vol. 319 (2001), 24-26.

[102] H. Fujio and K. Yamada, Influence of Hardenability of Material on Gear Distortions Caused by Hardening: II Through-Hardening of Spur Gears Made of Low-Alloyed Steels, Bull. Jpn. Soc. Mech. Eng., Vol. 28, no. 244 (1985), 2414-2421.

[103] N. N. Prokhorov, N. N. Shabalina and V. S. Drizhkov, Analysis of the Effect of the Strain Ageing of Alloys During Welding on the Deformation of Welded Components, Welding Production, Vol. 22, no. 7 (1975), 7-8.

[104] S. Lee, Residual Stress in a Swage Autofrettaged Steel Cylinder with Semi-Circular Mid-Wall Channels, Army Armament Research Development and Engineering Center (USA) (1998), 1-20.

[105] R. D'Agostino and F. Fracassi, Optical Emission Spectroscopy for Diagnostic of Plasma Polymer Deposition Processes, Proceedings of the ACS Division of Polymeric Materials Science and Engineering, Apr. 1990, Boston, MA, USA, Polymeric Materials Science and Engineering, Vol. 62 (1990), 150-151.

[106] D. M. Anthony, Engineering Metrology, Pergamon Press, Oxford, England, UK (1986), 91-101.

[107] K. Katsurada, K. Goho, K. Mitsui and A. Hayashi, Cylindricity Measurement of Parallel Rollers Based on A V-block Method, Transactions of the Japan Society of Mechanical Engineers, Part C, Vol. 69, no. 11 (2003), 3124-3129.

[108] S. Y. Chou and C. W. Sun, Assessing Cylindricity for Oblique Cylindrical Features, International Journal of Machine Tools and Manufacture, Vol. 40, no. 3 (2000), 327-341.

[109] F. T. Farago, Handbook of Dimensional Measurement, Industrial Press Inc., New York (1968), 336.

VITA AUCTORIS

Haitao He was born in 1970 in Heilongjiang, China. She went on to the Jilin University of Technology in 1990 and obtained a B.Sc in Mechanical in 1994. She is currently a candidate for the Master of Applied Science degree in Engineering Materials at the University of Windsor and hopes to graduate in Fall 2005.

PRESENTATIONS & PUBLICATIONS RESULTING FROM THIS THESIS

1. Lily He and Derek O. Northwood, "The Effect of Retained Austenite on Distortion of Carburized SAE 8620 Steel", 2nd International Conference on Heat Treatment and Surface Engineering in Automotive Applications, Riva del Garda, Italy, 20-22 June 2005. To be published in Proceedings, 13pp, Associazione Italiana Di Metallurgia, Milan, Italy.